AD-A080 443 CINCINNATI UNIV OH DEPT OF AEROSPACE ENGINEERING AND--ETC F/G 20/4
CALCULATION OF OPTIMAL COORDINATES FOR TWO-DIMENSIONAL INCOMPRE--ETC(U)
JUL 79 R T DAVIS, R K ROUT N00014-76-C-0359
UNCLASSIFIED AFL-79-7-47 NL

1 OF 2
AD A080443

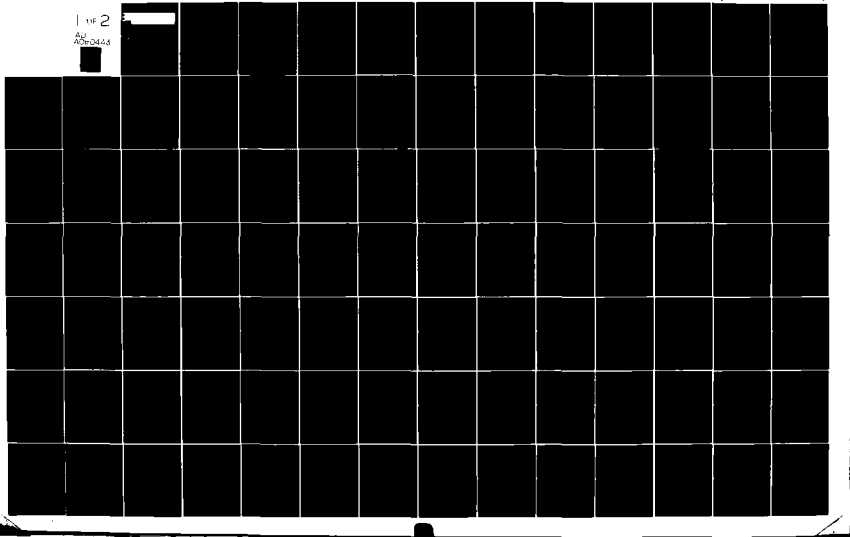

REPORT NO. AFL 79-7-47

AD A080443

CALCULATION OF OPTIMAL COORDINATES FOR TWO-DIMENSIONAL INCOMPRESSIBLE FLOW

R.T. DAVIS AND R.K. ROUT

LEVEL II

Approved for public release; distribution unlimited.

This research was supported by the Naval Sea Systems Command General Hydromechanics Research Program administered by the David W. Taylor Naval Ship Research and Development Center under Contract N00014-76-C-0359 and the Office of Naval Research under Contract N00014-76-C-0364.

July 1979

80 2 036

SECURITY CLASSIFICATION OF THIS PAGE (When Data Entered)

REPORT DOCUMENTATION PAGE

READ INSTRUCTIONS BEFORE COMPLETING FORM

1. REPORT NUMBER: AFL-79-7-47	2. GOVT ACCESSION NO. / 3. RECIPIENT'S CATALOG NUMBER
4. TITLE (and Subtitle): CALCULATION OF OPTIMAL COORDINATES FOR TWO-DIMENSIONAL INCOMPRESSIBLE FLOW	5. TYPE OF REPORT & PERIOD COVERED: Final 1979 / 6. PERFORMING ORG. REPORT NUMBER
7. AUTHOR(s): R. T. Davis & R. K. Rout	8. CONTRACT OR GRANT NUMBER(s): N00014-76-C-0359, N00014-76-C-0364
9. PERFORMING ORGANIZATION NAME AND ADDRESS: Department of Aerospace Engineering and Applied Mechanics, University of Cincinnati	10. PROGRAM ELEMENT, PROJECT, TASK AREA & WORK UNIT NUMBERS: 61153N R02301, SR 023 01 01
11. CONTROLLING OFFICE NAME AND ADDRESS: David W. Taylor Naval Ship Research and Development Center (Code 1505), Bethesda, Md 20084	12. REPORT DATE: July 1979 / 13. NUMBER OF PAGES: 126
14. MONITORING AGENCY NAME & ADDRESS (if different from Controlling Office): Office of Naval Research, 800 N. Quincy St, Arlington, Va 22217	15. SECURITY CLASS. (of this report): UNCALSSIFIED / 15a. DECLASSIFICATION/DOWNGRADING SCHEDULE

16. DISTRIBUTION STATEMENT (of this Report)

APPROVED FOR PUBLIC RELEASE; DISTRIBUTION UNLIMITED

(16) SR02301

17. DISTRIBUTION STATEMENT (of the abstract entered in Block 20, if different from Report)

(17) SR0230101

18. SUPPLEMENTARY NOTES

Sponsored by the Naval Sea Systems Command General Hydromechanics Research (GHR) Program administered by the David W. Taylor Naval Ship R&D Center, Code 1505, Bethesda, Md 20084, and the Office of Naval Research

19. KEY WORDS (Continue on reverse side if necessary and identify by block number)

Two-dimensional laminar flow
GHR Program
Two-Dimensional Incompressible Flow

20. ABSTRACT (Continue on reverse side if necessary and identify by block number)

Two Dimensional steady symmetric incompressible laminar flow past a class of blunt and sharp nosed bodies is investigated in optimal coordinates. The analysis is carried out for different problem parameters and the folution is specialized for the cases of the parabola, and a semi-infinite thin flat plate and the flow against a vertical wall.

The problem is formulated by mapping the body from a Cartesian plant into a conformal plane by applying a Schwarz-Christoffel transformation. This

DD FORM 1 JAN 73 1473 EDITION OF 1 NOV 65 IS OBSOLETE S/N 0102-LF-014-6601

UNCLASSIFIED

SECURITY CLASSIFICATION OF THIS PAGE (When Data Entered)

type of transformation maps the flow field into a stagnation point flow in th conformal plane. The governing differential equations are developed in an optimal coordinate system such that the viscous solutions contain the first-order inviscid solution as well as the folution for flow due to displacement thickness. This type of formulation of the viscous flow problem in optimal coordinates results in a coupled set of flow and coordinate equations. A boundary-layer and parabolized Navier-Stokes analysis is used for the solution procedure in the present optimal coordinate system.

Optimal coordinates are computed according to the classical first-order boundary-layer approximation as well as with a prarbolized version of streamfunction vorticity form of the full Navier-Stokes equations. A boundary-layer type forward marching numerical scheme is employed to solve the flow equations in optimal coordinates. An alternating direction implicity (ADI) schemem is used to solve the coordinate equations.

The analysis is carried out for two example problems, a semi-infinite thick plate and a semi-infinite blunted wedge. The solutions are obtained for different body geometries (bluntness parameters) in both examples. Results for skin friction, displacement thickness, pressure gradient parameter and optimal coordinates, for different problem parameters, are presented for unseparated flow cases. Physical quantities such as surface pressure gradient distribution, skin friction and displacement thickness for cases of flow past the parabola, the thin flat plate and flot against a vertical wall are compared with existing numerical and analytical results.

CALCULATION OF OPTIMAL COORDINATES FOR TWO-DIMENSIONAL INCOMPRESSIBLE FLOW

R.T. Davis* and R.K. Rout**

Aerospace Engineering and Applied Mechanics Department
University of Cincinnati
Cincinnati, Ohio 45221

This research was supported by the Naval Sea Systems Command General Hydromechanics Research Program administered by the David W. Taylor Naval Ship Research and Development Center under Contract N00014-76-C-0359 and the Office of Naval Research under Contract N00014-76-C-0364.

---

* Professor.

** Research Assistant.

ABSTRACT

Two dimensional steady symmetric incompressible laminar flow past a class of blunt and sharp nosed bodies is investigated in optimal coordinates. The analysis is carried out for different problem parameters and the solution is specialized for the cases of the parabola, a semi-infinite thin flat plate and the flow against a vertical wall.

The problem is formulated by mapping the body from a Cartesian plane into a conformal plane by applying a Schwarz-Christoffel transformation. This type of transformation maps the flow field into a stagnation point flow in the conformal plane. The governing differential equations are developed in an optimal coordinate system such that the viscous solutions contain the first-order inviscid solution as well as the solution for flow due to displacement thickness. This type of formulation of the viscous flow problem in optimal coordinates results in a coupled set of flow and coordinate equations. A boundary-layer and parabolized Navier-Stokes analysis is used for the solution procedure in the present optimal coordinate system.

Optimal coordinates are computed according to the classical first-order boundary-layer approximation as well as with a parabolized version of streamfunction vorticity form of the full Navier-Stokes equations. A boundary-layer type forward marching numerical scheme is employed to solve the flow equations in optimal coordinates. An alternating direction implicit (ADI) scheme is used to solve the coordinate equation.

The analysis is carried out for two example problems, a semi-infinite thick plate and a semi-infinite blunted wedge. The solutions are obtained

next page

for different body geometries (bluntness parameters) in both examples. Results for skin friction, displacement thickness, pressure gradient parameter and optimal coordinates, for different problem parameters, are presented for unseparated flow cases. Physical quantities such as surface pressure gradient distribution, skin friction and displacement thickness for cases of flow past the parabola, the thin flat plate and flow against a vertical wall are compared with existing numerical and analytical results.

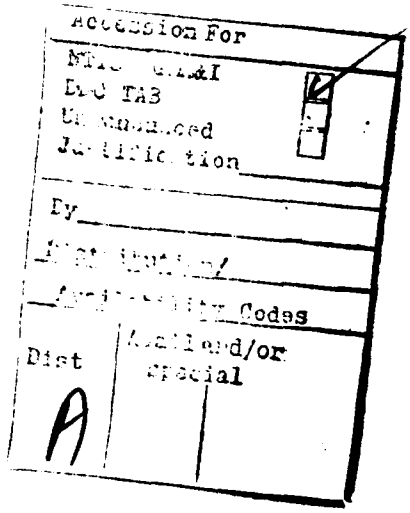

TABLE OF CONTENTS

LIST OF FIGURES

SYMBOLS

A	constant used in the stretching of the independent variable ξ
a	radius of curvature at the stagnation point
α	shape parameter for blunted plate
β	Falkner-Skan pressure gradient parameter
β_i	pressure gradient parameter
b	normalised width of the thick plate in conformal plane
C	transformed displacement constant
δ	semi-wedge angle at downstream infinity
δ_e	displacement thickness
η	optimal coordinate component
f	streamfunction
g	vorticity function
H	inverse scale factor
H_r	scale factor of transformation from optimal to conformal plane
h	scale factor of transformation from physical to conformal plane
$\bar{h}$	modified streamfunction
K	constant of integration used in Equation(2.57b)
L	width of the semi-infinite thick plate perpendicular to the main stream
$\ell(p)$	displacement function in conformal coordinate
$\bar{\ell}$	displacement function in optimal coordinates
n	exponent used in the transformation relation (4.1)

N	normal independent variable in computational plane
ΔN	step size in N direction
q_w	value of the conformal coordinate q at the wall
$\bar{q}_w$	normalised value of q_w , $\bar{q}_w = q_{/a}{}^{1/2}$
Re	Reynolds number based on the nose radius of curvature
Re_L	body shape parameter related to the thickness of the plate, $Re_L = 2U_r L/\pi\nu$
S	streamwise coordinate in computational plane
ΔS	step size in S direction
t	coordinate function
t_w	coordinate function at the surface of the body
u	streamwise velocity component
U_∞	freestream velocity
U_r	reference velocity
V	normal velocity component
v	fictitious time
Δv	time step
x	component of the Cartesian coordinates
y	component of the Cartesian coordinates
z	physical coordinate
ζ	conformal coordinate
ξ	optimal coordinate component

Subscripts

in	inviscid quantity
m	grid point in S direction
n	grid point in N direction
S	differentiation with respect to S
N	differentiation with respect to N
ξ	differentiation with respect to ξ
η	differentiation with respect to η
∞	freestream condition
w	wall condition
o	stagnation condition

Superscripts

-	normalised quantity
*	first sweep of Alternating Direction Implicit (ADI) scheme
n	time level preceding star(*) level
n+1	second sweep of Alternating Direction (ADI) scheme
'	total differentiation with respect to ξ

I. INTRODUCTION

A suitable choice of a coordinate system can simplify the complexity of a problem especially one involving non-linear partial differential equations. In some cases the proper choice of independent and dependent variables reduces the original partial differential equation to an ordinary differential equation, i.e. if similarity conditions exist. The Falkner-Skan similarity variables are an example of such a case where the boundary-layer equations reduce to an ordinary differential equation called the Falkner-Skan equation. Due to the simplicity of ordinary differential equations, the numerical solution of ordinary differential equations can be found more accurately and with less effort, in general, than the numerical solution of the original partial differential equations.

In many singular perturbation problems, which show a boundary-layer like behavior, the coordinate system chosen for the problem may play an important role in describing the flow appropriately. In other words, the solution of boundary-layer type flows may depend on the coordinate system chosen. This fact did not receive a systematic investigation until Kaplun[1] introduced the idea of optimal coordinates which according to Kaplun removes the singularity due to the boundary-layer approximation and renders the boundary-layer solution uniformly valid in the entire flow field for high Reynolds number flow.

The idea of optimal coordinates, although first mentioned by Kaplun is also mentioned in the works of Latta[2], Friedrichs[3], Weyl[4] and Segel[5]. The dependence of the boundary-layer solution on the coordinate system is discussed by Van Dyke[19] for flow past a flat plate in Cartesian and parabolic coordinates. Some other applications of optimal coordinate theory have been given by Crespo da Silva and Davis[6].

Kaplun[1] shows that the inviscid high Reynolds number solution is independent of the coordinate system, since it is governed by a vector equation. However, he also shows that in a boundary-layer type analysis, while going from the viscous flow region to the inviscid flow, the boundary-layer solution produces different types of outer inviscid flows depending on which coordinate system has been chosen. The coordinate system which provides the outer flow including the displacement effect, to a given order, is an optimal coordinate system to that order. Therefore Kaplun's investigation of the dependence of the boundary-layer solution on the coordinate system leads to the possibility of developing the most appropriate coordinate system for carrying out high Reynolds number flow computations.

Since the introduction of the idea of optimal coordinates by Kaplun, several investigators have explored the application of optimal coordinate theory to obtain uniformly valid solutions for singular perturbation problems in fluid mechanics. A review of the literature related to optimal coordinates is presented by Legner[7]. Legner[7] shows that the application of Kaplun's idea is not limited to fluid mechanics problems, but also can successfully be applied to singular perturbation problems in other applied engineering areas. For example, Zauderer's[8] work on defraction problems involving multi-region transition and Segel's work on the vibration of convex cylinders in a uniform stream are worth mentioning.

An extension of Kaplun's correlation theorem was made by Van Dyke[9] who extended Kaplun's first-order theorem to second-order. This allows one to transform a second-order boundary-layer solution from one coordinate

system to another. A further development of Kaplun's work was presented by Legner[7] who extended the entire optimal coordinate theory to higher order. Subsequent generalization of Legner's approach to finding optimal coordinates was provided by Davis.[10]

The numerical determination fo coordinate systems for use with the boundary-layer or Navier-Stokes equations has been studied by several investigators, see for example, Thompson et al.[11,12,13] In these methods in order to generate a coordinate system, a criterion must be specified which the coordinate system should satisfy. Therefore, if we set our criterion for the coordinate system such that the boundary-layer solution in these sets of coordinates reproduce the inviscid solution including the displacement effect, the coordinates thus obtained will be optimal in the sense of Kaplun's definition. Davis[10] has discussed how the optimal coordinates can be generated numerically in a manner similar to that used by Thompson et al.[11] for non optimal coordinates.

The advantages of the use of the optimal coordinates with the boundary-layer and the Navier-Stokes equations for obtaining numerical as well as analytical solutions are ellaborated in the works of Davis[10] and Davis.[14] In the optimal coordinate study by Davis[10] it has been shown that for a plane symmetric flow, the use of the Legner condition and the assumption of the orthogonality condition for the coordinate system results in a set of conformal coordinates. These conformal coordinates, which in the sense of optimal coordinate theory are the best coordinates, are used in the numerical scheme of Davis[15] for viscous flow past the parabola, which becomes a flat plate as the nose radius of

curvature approaches zero. This coordinate system shows considerable improvement over other coordinate systems in the convergence and accuracy of the numerical solution. These coordinates were also successful in removing the leading edge singularity for the flow past the flat plate. However, the use of conformal coordinates in the case of flow past wedges (see Davis, U. Ghia and K. Ghia[16]), although showing good resolution and convergence in most of the flow field, fails to remove the leading edge singularity except for the special cases of semi-wedge angle equal to zero, (the flat plate case), and 90° (the vertical wall case). Davis[10] has further shown that it may be possible to generate a non-orthogonal optimal coordinate system which removes the leading edge singularity for the sharp wedge cases, by introducing the required arbitrariness into the generation of optimal coordinates.

The present numerical work will show that in optimal coordinates, parabolization of the Navier-Stokes equations renders a considerable simplification in the numerical treatment of the Navier-Stokes equations and at the same time, that it is possible to achieve good agreement between solutions to the parabolized equations and the full Navier-Stokes equations. Previous work on developing parabolized models for the same type of problems, but not in a fully optimal coordinate system, has been done by Davis,[15] U. Ghia and Davis,[17] and Werle and Bernstein.[18]

In the present analysis, a parabolic form of the Navier-Stokes equations is therefore developed in a generalized non-orthogonal optimal coordinate system. The purpose of this investigation is to determine if there is an advantage in using these optimal coordinates.

Analytical determination of the present optimal coordinate system is rather difficult, since in order to determine the present set of coordinates it is essential to solve for the flow due to displacement thickness. Only for a few simple cases of viscous flow is the analytical expression for the inviscid flow due to displacement thickness known. In most cases the solution to the inviscid flow due to displacement thickness, must be generated numerically. Therefore in the present analysis, a method is developed to numerically generate the optimal coordinates using a finite difference technique. The flow equations are solved utilizing a boundary-layer like forward marching technique and the coordinate equation is solved using a time dependent relaxation scheme. Two model problems are considered in order to demonstrate the application of the present analysis. It is shown through model problems that it is possible to numerically generate a set of optimal coordinates and that the solution obtained from the present calculations shows good agreement with the existing analytical and numerical results.

II. GENERATION OF OPTIMAL COORDINATES

It was mentioned in the Introduction that in order to determine optimal coordinates in a high Reynolds number flow problem, it is necessary to know apriori not only the first-order inviscid flow but also the flow due to displacement thickness. This implies that one should have the first-order boundary-layer solution at hand in order to determine optimal coordinates to first order. This information is available in the form of self-similar solutions for a few simple flows but in most cases one must resort to a numerical method in order to determine the boundary-layer solution. The inviscid flow due to the displacement effect is then determined from a separate analysis or numerical calculation.

In the subsequent section a brief description is presented on how to generate optimal coordinates numerically for a two dimensional incompressible symmetric flow. However, the analysis could be extended to unsymmetric, compressible, three dimensional, etc. flows as well, see Legner.[7]

For the present study we will assume that the form of the optimal coordinates chosen are such that they produce a separable solution for the inviscid flow to arbitrary order. These types of optimal coordinates are described and developed in detail by Davis.[10] However, a brief summary of Davis [10] analysis is presented in the following section for the sake of completeness.

In the Davis[10] analysis it is assumed that the independent variables are chosen such that a separable solution exists in the inviscid while

an unseparable solution is confined at most to the viscous region. In some special cases the viscous region may also be separable. Choice of such variables represent definite advantages in determining solutions analytically as well as numerically.

In order to obtain a set of optimal coordinates, hereafter denoted by a (ξ,η) coordinate system, the flow field in the physical (x,y) plane is mapped into a stagnation point type flow by a conformal transformation of the following form (see Figure 1):

$$z = f(p+iq) = f(\zeta) \quad . \tag{2.1}$$

The quantity $\zeta = p+iq$ represents the conformal plane and f is an analytic function. This type of mapping is used in order to simplify the boundary conditions which result from relating the optimal to the conformal system of coordinates. In addition there are certain other advantages to this type of mapping and these will be elaborated on in a later section.

The outer inviscid flow, which according to optimal coordinate theory, (see, Legner[7]) is independent of the coordinate system, is matched with the boundary-layer solution in the (ξ,η) coordinate system, by applying the asymptotic-matching principle, (see, Van Dyke[19]). In the present matching of two solutions it is assumed that the boundary-layer solution in the (ξ,η) optimal coordinate system is uniformly valid far from the body, i.e. in the transverse direction. This type of matching of the two solutions results in a set of conditions for determination of the optimal coordinate system, the order of which depends on the number of terms considered in the expansion in terms of $1/\sqrt{Re}$ as the perturbation parameter. In order to further simplify the condition for the optimal

coordinates and to obtain a more useful form, Davis[10] uses the Legner[7] form of the outer inviscid streamfunction expansion and we will adopt the same procedure here. Finally invoking the fact that the inviscid solution is separable to arbitrary order in the present set of (ξ,η) optimal coordinates, the proper form of the outer flow including the displacement effect is obtained. Using this form of the inviscid streamfunction in Laplace's equation governing the streamfunction, i.e., $\nabla^2 \psi_{in} = 0$, together with a suitable coordinate transformation relation to relate the conformal coordinates p and q with the optimal coordinate system ξ and η, the coordinate equation is developed. Finally the governing differential equations in terms of streamfunction and vorticity are developed in optimal coordinates from the corresponding equations in a generalized coordinate system as given by Lagerstrom[20] p. 66, by applying the suitable coordinate transformation manipulations. The necessary coordinate transformation relation, the coordinate equations to determine the optimal coordinate system and the flow equations together with the boundary conditions to solve these equations in optimal coordinates will be presented in their final forms as given by Davis.[10] The details of the derivation will not be repeated here.

In the present analysis the flow field is mapped into a conformal plane and the corresponding flow is then investigated in the optimal plane. A typical example of such a mapping of the flow field is presented in Figure 1, in which the two dimensional flow past a circular cylinder is shown in the physical, conformal and optimal plane in Figure 1a, 1b and 1c, respectively (see also Davis[10]).

The transformation of independent variables from the conformal (p,q) to the optimal (ξ,η) coordinate system is carried out using the following relations

$$\frac{\partial}{\partial p} = \frac{1}{J_r}\left(q_\eta \frac{\partial}{\partial \xi} - q_\xi \frac{\partial}{\partial \eta}\right)$$

and (2.2a,b)

$$\frac{\partial}{\partial q} = \frac{1}{J_r}\left(- p_\eta \frac{\partial}{\partial \xi} + p_\xi \frac{\partial}{\partial \eta}\right) \quad ,$$

where J_r is the Jacobian of the transformation matrix and is given by

$$J_r = p_\xi q_\eta - p_\eta q_\xi \quad . \tag{2.2c}$$

The rest of the coefficients of the metric tensor relating the optimal coordinate system (ξ,η) to the conformal coordinates (p,q) are given as

$$\alpha_r = g_{r_{22}} = p_\eta^2 + q_\eta^2 \quad ,$$

$$\beta_r = g_{r_{12}} = p_\xi p_\eta + q_\xi q_\eta \quad ,$$

$$\gamma_r = p_\xi^2 + q_\xi^2 \tag{2.3a,d}$$

and

$$J_r^2 = g_r = \alpha_r \gamma_r - \beta_r^2 = (p_\xi q_\eta - p_\eta q_\xi)^2 \quad .$$

Similar expressions can be obtained to relate a Cartesian coordinate system to the optimal coordinates. They are rewritten here as given by Davis[10]

$$\alpha = g_{22} = x_\eta^2 + y_\eta^2 = h^2\alpha_r \quad ,$$

$$\beta = g_{12} = x_\xi x_\eta + y_\xi y_\eta = h^2\beta_r \quad , \tag{2.4a,e}$$

$$\gamma = g_{11} = x_\xi^2 + y_\xi^2 = h^2\gamma_r$$

and

$$J^2 = g = \alpha\gamma - \beta^2 = (x_\xi y_\eta - x_\eta y_\xi)^2 = h^4 J_r^2 \quad ,$$

where

$$h = \left|\frac{d\zeta}{dz}\right| \quad .$$

We will now write down the governing differential equations in the (ξ,η) coordinate system.

1. The Navier-Stokes Equations

The non-dimensionalization used in the flow equations is as follows. All lengths are non-dimensionalized by the viscous length ν/U_r, where ν is the kinematic viscosity and U_r is the reference velocity in the flow. The streamfunction is non-dimensionalized by ν and the vorticity by U_r^2/ν. Finally the time is non-dimensionalized by ν/U_r^2.

With this non-dimensionalization the streamfunction equation is given in the (ξ,η) coordinate system as

$$f_{\eta\eta} - \frac{2\beta_r}{\gamma_r} f_{\xi\eta} + \frac{\alpha_r}{\gamma_r} f_{\xi\xi} + \frac{2}{\xi}\frac{\alpha_r}{\gamma_r} f_\xi = g \quad . \tag{2.5}$$

where the streamfunction ψ is defined in the spirit of similarity variables as

$$\psi = \xi f(\xi,\eta) \tag{2.6}$$

and the vorticity ω is likewise defined as

$$\omega = -\frac{\xi\gamma_r}{h^2 J_r^2} g(\xi,\eta) = -\xi H g(\xi,\eta) \tag{2.7}$$

where the inverse scale factor H is given as

$$H = \frac{\gamma_r}{h^2 J_r^2} = \frac{H_r}{h^2} \tag{2.8}$$

and H_r is the scale factor of transformation relating the optimal (ξ,η) coordinates to conformal (p,q) coordinates and is given by

$$H_r = \frac{\gamma_r}{J_r^2} \tag{2.9}$$

where γ_r and J_r are already defined in Equations (2.3c) and (2.3d).

Similarly h is the scale factor of transformation from the conformal to the physical plane and is given as

$$h = f'(\zeta) \quad , \tag{2.10}$$

where

$$\zeta = p+iq \quad . \tag{2.11}$$

The transformed vorticity transport equation is given by

$$g_{\eta\eta} + [\frac{2H_\eta}{H} - \frac{2\beta_r}{\gamma_r}\frac{H_\xi}{H} + \frac{J_r}{\gamma_r}(f+\xi f_\xi)]g_\eta$$

$$+ [\frac{H_\eta^2}{H^2} - \frac{2\beta_r}{\gamma_r}\frac{H_\xi H_\eta}{H^2} + \frac{\alpha_r}{\gamma_r}\frac{H_\xi^2}{H^2} - \frac{2}{\xi}\frac{\beta_r}{\gamma_r}\frac{H_\eta}{H} + \frac{2}{\xi}\frac{\alpha_r}{\gamma_r}\frac{H_\xi}{H}$$

$$+ \frac{4}{\xi}(\frac{\beta_r}{\gamma_r})_\eta - \frac{4}{\xi}\frac{\beta_r}{\gamma_r}(\frac{\beta_r}{\gamma_r})_\xi + \frac{12}{\xi^2}(\frac{\beta_r}{\gamma_r})^2 + \frac{J_r}{\gamma_r}\frac{H_\eta}{H}(f+\xi f_\xi) \qquad (2.12)$$

$$- \frac{J_r}{\gamma_r}(1 + \frac{\xi H_\xi}{H})f_\eta]g + [\frac{2\alpha_r}{\gamma_r}\frac{H_\xi}{H} - \frac{2\beta_r}{\gamma_r}\frac{H_\eta}{H} - \frac{\xi J_r}{\gamma_r}f_\eta]g_\xi$$

$$- \frac{2\beta_r}{\gamma_r}g_{\xi\eta} + \frac{\alpha_r}{\gamma_r}g_{\xi\xi} + \frac{2}{\xi}\frac{\alpha_r}{\gamma_r}g_\xi = \frac{1}{H}g_t \quad .$$

The boundary conditions are given as follows. The no-slip and zero injection conditions give at $\eta = 0$

$$f(\xi,0) = 0$$

and (2.13a,b)

$$f_\eta(\xi,0) = 0 \quad .$$

The asymptotic boundary condition far from the body gives

$$f(\xi,\eta) \to \eta - C$$

and as $\eta \to \infty$ (2.14a,b)

$$g(\xi,\eta) \to 0$$

where C is a constant and from the general definition of the displacement thickness Davis[10] has shown that C is a displacement constant in optimal coordinates.

We will be considering flows past semi-infinite bodies for which self-similar solutions exist to the boundary-layer equations at downstream infinity. Therefore the downstream boundary condition as $\xi \to \infty$, is given by the corresponding boundary-layer form and hence can be written as follows.

The coefficients α_r/γ_r and $J_r/\gamma_r \to 1$ as $\xi \to \infty$, since the present coordinates become conformal coordinates in this limit. Also β_r/γ_r, $f_{\xi\xi}$, f_ξ, $f_{\xi\eta}$, g_ξ, $g_{\xi\xi}$ and $g_{\xi\eta} \to 0$ at downstream infinity. The stream-function Equation (2.5) therefore reduces to boundary-layer form and is given by

$$f_{\eta\eta} = g \tag{2.15}$$

and the vorticity Equation (2.12) becomes

$$g_{\eta\eta} + fg_\eta + (1-2\beta)f_\eta g = 0 \tag{2.16}$$

where β is the Falkner-Skan pressure gradient parameter and is given as

$$\beta = \frac{2\delta}{\pi} \tag{2.17}$$

where δ is the slope of body surface asymptotically far downstream and therefore is a known quantity.

It is interesting to note that the Equations (2.15) and (2.16) are the similarity form of the boundary-layer equations. This shows that the variables chosen for the present analysis are self-similar in nature. Also substituting $f_{\eta\eta} = g$ into the vorticity equation (2.16) and integrating the resulting equation with respect to η once and making use of the boundary condition on f_η and the higher order derivatives of f as $\eta \to \infty$, the vorticity Equation (2.16) reduces to

$$f_{\eta\eta\eta} + ff_{\eta\eta} + \beta(1-f_{\eta}^2) = 0 \qquad (2.18)$$

which is the familiar Falkner-Skan equation (see Schlichting[21]).

Additional relations required to solve the flow equations are given in the following. From Equation (2.8), it can be shown that

$$\frac{H_\xi}{H} = -\frac{2h_\xi}{h} + \frac{H_{r_\xi}}{H_r} \qquad (2.19)$$

and

$$\frac{H_\eta}{H} = -\frac{2h_\eta}{h} + \frac{H_{r_\eta}}{H_r} \quad . \qquad (2.20)$$

This completes the description of the Navier-Stokes equations together with the necessary boundary conditions in the (ξ,η) coordinate system. The derivation of the coordinate equation will be briefly outlined in the subsequent section.

2. The Coordinate Equation

The coordinate equation is derived based on the inviscid flow information in the following way. It is noted from the viscous streamfunction f given by Equation (2.6) and the outer edge condition on f given by Equation (2.14a) that the outer inviscid streamfunction in ξ,η coordinates is represented as

$$\psi_{in} = \xi(\eta-C) \quad . \qquad (2.21)$$

If the flow is irrotational to arbitrary order, then the streamfunction should satisfy the Laplace equation $\nabla^2\psi_{in} = 0$, which can be written in our case as

$$\nabla^2(\xi(\eta-C)) = 0 \quad . \qquad (2.22)$$

Assuming $pq = \xi\eta$ and treating p in a similar manner as we have treated the transformed streamfunction ψ and vorticity ω it is possible to obtain coordinate relations of the form given in the following (see Davis[10]):

$$p = \xi t(\xi,\eta) \tag{2.23}$$

and

$$q = \frac{\eta}{t(\xi,\eta)} \quad . \tag{2.24}$$

Making use of these coordinate relations (2.23) and (2.24) and substituting into (2.22) and writing the Laplacian ∇^2 in the ξ and η coordinate system (with the help of the transformation of independent variable relations (2.2a,b) from the conformal (p,q) to the optimal (ξ,η) coordinate system) it is now possible to show that the coordinate Equation (2.22) reduces to

$$t_{\eta\eta} - \frac{2\beta_r}{\gamma_r} t_{\xi\eta} + \frac{\alpha_r}{\gamma_r} t_{\xi\xi} + \frac{2}{\xi}\frac{\alpha_r}{\gamma_r} t_{\xi} = 0 \tag{2.25}$$

where $t(\xi,\eta)$ is the coordinate relation function relating the two coordinate systems through the expressions given in (2.23) and (2.24).

Determination of the (ξ,η) coordinate system amounts to finding the solution of the partial differential Equation (2.25) with suitable boundary conditions.

The coefficients α_r, β_r, γ_r and the Jacobian J_r, appearing in the flow Equations (2.5, 2.12) and the coordinate Equation (2.25) can now easily be expressed as functions of ξ and η by substituting the coordinate relations (2.23) and (2.24) into Equations (2.3a-d). This results in

$$\alpha_r = (\xi^2 + \frac{2}{t^4})t_\eta^2 - \frac{2\eta t_\eta}{t^3} + \frac{1}{t^2} \quad ,$$

$$\beta_r = (\xi^2 + \frac{\eta^2}{t^4}) t_\xi t_\eta - \frac{\eta}{t^3} t_\xi + \xi t t_\eta \quad ,$$

$$\gamma_r = (\xi^2 + \frac{\eta^2}{t^4}) t_\xi^2 + 2\xi t t_\xi + t^2 \qquad (2,26a\text{-}d)$$

and

$$J_r = 1 + \frac{\xi t_\xi}{t} - \frac{\eta t_\eta}{t} \quad .$$

The boundary conditions for the coordinate Equation (2.25) are prescribed as follows. The coordinate Equation (2.25) is elliptic in nature and therefore needs boundary conditions around the boundaries in order to make the coordinate equation problem well posed. Since we will be considering symmetric bodies, the coordinate system is symmetric and therefore

$$t_\xi(0,\eta) = 0 \qquad (2.27)$$

The asymptotic boundary condition in the streamwise and transverse direction are given as

$$t(\xi,\eta) \sim 1 \qquad \text{as} \quad \xi \to \infty$$

and $\qquad (2.28a,b)$

$$t(\xi,\eta) \sim 1 \qquad \text{as} \quad \eta \to \infty$$

The two boundary conditions given by Equations (2.28a,b) imply that far from the body in either direction the optimal coordinates become conformal.

The remaining one condition is the boundary condition on $t(\xi,\eta)$ at the surface. It was shown by Davis[10] that this condition depends on the displacement surface over the body and hence it is treated as an unknown. In the following section it will be shown how an interacting type analysis is necessary in order to determine this missing boundary condition ($t(\xi,0)$) and therefore to solve the flow equations in optimal coordinates.

Referring back to the boundary condition (2.14a) on the streamfunction, i.e. $f \to \eta - C$ as $\eta \to \infty$, it is generally treated as $f_\eta \to 1$ as $\eta \to \infty$ and C is determined as $C(\xi)$ as $\eta \to \infty$ if ξ and η are not optimal coordinates. Therefore under normal conditions, one has no control over the function $C(\xi)$. However, it was already mentioned that there was one condition missing from the coordinate equation in order to describe the system in closed form. In fact the additional condition $C(\xi) \to C$ as $\eta \to \infty$, necessary for determining optimal coordinates, is used in determining the surface boundary condition $t(\xi,0)$. This clearly indicates that in order to solve the coordinate equation in closed form it is essential to solve at least the first-order boundary-layer flow such that the displacement surface function $C(\xi) \to C$ as $\eta \to \infty$. Since the coefficients α_r, β_r, γ_r and J_r etc. are functions of $t(\xi,\eta)$, they are therefore unknown and are determined as a part of the solution. This implies that the flow equations (2.5 and 2.12) through these coefficients are coupled to the coordinate equations and the coordinate Equation (2.25) is coupled to the flow equations through the boundary condition $t(\xi,0)$, the determination of which depends on the successful satisfaction of the condition $C(\xi) \to C$ on the flow equation solution as $\eta \to \infty$. Therefore the condition on the displacement surface $C(\xi) \to C$ serves as an additional condition on the flow and coordinate equations such that the coordinates are optimal.

It is now clear that the streamfunction equation boundary conditions are not over specified if we wish to prescribe $f_\eta \to 1$ and $f \to \eta - C$ as $\eta \to \infty$ to determine optimal coordinates. The extra boundary condition on the streamfunction $f(\xi,\eta)$ is replaced by the missing boundary condition on $t(\xi,\eta)$. Therefore the Equations (2.1) through (2.28) represent a

complete set of governing differential equations together with the necessary boundary conditions in order to determine the optimal coordinates for two-dimensional plane symmetric flow.

It is interesting to note that the coordinate equation is formulated based on the inviscid flow information whereas the viscous effects are confined to the flow equations only. Because of the inherent coupling between the coordinate equation in optimal coordinates and the flow equations, an interacting type phenomenon takes place while determining the viscous flow solution in optimal coordinates.

This brief description of the development of the optimal coordinates in the case of two dimensional laminar incompressible symmetric flow follows the more detailed analysis given by Davis[10].

The development of the parabolized vorticity and the streamfunction equations and also the boundary-layer equations are presented in the following.

3. The Parabolized Vorticity and Stream Function Equations

The parabolized vorticity and stream funcation equations are obtained from the full Navier-Stokes equation by neglecting all the terms in the governing differential Equations (2.5) and (2.12), which include second derivatives in the streamwise (ξ) direction. Also the cross derivative terms $f_{\xi\eta}$ and $g_{\xi\eta}$ and $\frac{\alpha_r}{\gamma_r} g_\xi$ are neglected. The relevant advantages of the use of the parabolized form of the Navier-Stokes equations are separately ellaborated in the numerical method of solution section. It is important to note that this approximation retains all of the terms which would arise in a second-order boundary-layer theory.

It can be shown that with the parabolic approximation, the streamfunction Equation (2.5) reduces to the boundary-layer form and is given by

$$f_{\eta\eta} = g \quad . \tag{2.29}$$

The parabolized vorticity equation reads as

$$\begin{aligned} & g_{\eta\eta} + [\frac{2H_\eta}{H} - \frac{2\beta_r}{\gamma_r}\frac{H_\xi}{H} + \frac{J_r}{\gamma_r}(f+\xi f_\xi)]g_\eta \\ & + [\frac{H_\eta^2}{H^2} - \frac{2\beta_r}{\gamma_r}\frac{H_\xi H_\eta}{H^2} + \frac{\alpha_r}{\gamma_r}\frac{H_\xi^2}{H^2} - \frac{2}{\xi}\frac{\beta_r}{\gamma_r}\frac{H_\eta}{H} + \frac{2}{\xi}\frac{\alpha_r}{\gamma_r}\frac{H_\xi}{H} \\ & + \frac{4}{\xi}(\frac{\beta_r}{\gamma_r})_\eta - \frac{4}{\xi}\frac{\beta_r}{\gamma_r}(\frac{\beta_r}{\gamma_r})_\xi + \frac{12}{\xi^2}(\frac{\beta_r}{\gamma_r})^2 + \frac{J_r}{\gamma_r}\frac{H_\eta}{H}(f+\xi f_\xi) \\ & - \frac{J_r}{\gamma_r}(1 + \frac{\xi H_\xi}{H})f_\eta]g + [\frac{2\alpha_r}{\gamma_r}\frac{H_\xi}{H} - \frac{2\beta_r}{\gamma_r}\frac{H_\eta}{H} - \frac{\xi J_r}{\gamma_r}f_\eta]g_\xi = 0 \end{aligned} \tag{2.30}$$

The necessary boundary conditions to close the parabolized streamfunction and vorticity equation set are as prescribed previously in Equations (2.13) through (2.18).

4. The Boundary-Layer Equations in Optimal Coordinates

The steady-state boundary-layer equations in optimal coordinates are obtained from the full Navier-Stokes Equations (2.5) and (2.12) by taking the limit of the equations as Reynolds number $Re \to \infty$, in inner boundary-layer variables. By making the boundary-layer approximation in Equations (2.5) and (2.12) it can be shown that many terms drop out and in addition the remaining coefficients h, H_r, γ_r, and J_r can be evaluated at the body surface, i.e. at $\eta = 0$. These coefficients can therefore be written as

$$h = h(\xi) \quad ,$$

$$\frac{J_r}{\gamma_r} = \frac{J_r(\xi)}{\gamma_r(\xi)}$$

and (2.31a-c)

$$H_r = t^2(\xi,0)$$

With these approximations the streamfunction Equation (2.5) remains the same, i.e.

$$f_{\eta\eta} = g \tag{2.32}$$

and the vorticity Equation (2.12) reduces to

$$g_{\eta\eta} + \frac{J_r}{\gamma_r}(f+\xi f_\xi)g_\eta - [\frac{J_r}{\gamma_r}(1 + \xi \frac{H_\xi}{H})f_\eta]g - \xi \frac{J_r}{\gamma_r} f_\eta g_\xi = 0 \tag{2.33}$$

The inverse scale factor H in the case of boundary-layer can be written as

$$H(\xi,0) = \frac{H_r}{h^2} = \frac{t^2(\xi,0)}{h^2(\xi,0)} \quad . \tag{2.34}$$

The expression for the scale factor h is given once the geometry is prescribed and will be given later in the respective example problem.

Now substituting $f_{\eta\eta} = g$ into the vorticity Equation (2.33) and integrating the resulting equation with respect to η and evaluating the constant of integration by making use of the boundary condition on f and its derivatives as $\eta \to \infty$, the vorticity equation can be written as

$$f_{\eta\eta\eta} + \frac{J_r}{\gamma_r}(f+\xi f_\xi)f_{\eta\eta} - \frac{J_r}{\gamma_r} f_\eta^2 - \frac{J_r}{\gamma_r}\frac{\xi}{2}\frac{H_\xi}{H} f_\eta^2$$

$$- \xi \frac{J_r}{\gamma_r} f_{\xi\eta} f = - \frac{J_r}{\gamma_r}(1 + \frac{\xi}{2}\frac{H_\xi}{H}) \qquad (2.35)$$

We could work with these variables, however it is convenient to instead develop variables similar to those of Görtler. In order to do this we define V, a normal velocity like variable, as

$$V = - f - \xi f_\xi \quad . \qquad (2.36)$$

Making suitable rearrangements in the Equation (2.35) and replacing f_η by F we get the final form of the boundary-layer equations as

$$F_{\eta\eta} - \frac{J_r}{\gamma_r} VF_\eta + \frac{J_r}{\gamma_r}\beta_i (1 - F^2) - \xi \frac{J_r}{\gamma_r} FF_\xi = 0 \qquad (2.37)$$

and

$$V_\eta = - F - \xi F_\xi \qquad (2.38)$$

where the pressure gradient parameter β_i is given by

$$\beta_i = (1 + \frac{\xi H_\xi}{2H}) \quad . \qquad (2.39)$$

In transformed variables, a displacement thickness like variable δ can be defined as

$$\delta_e = \int_0^\infty (1 - F)d\eta \qquad (2.40)$$

The necessary boundary conditions to solve the governing differential Equations ((2.38) and (2.39)) are as follows. The no-slip and zero-injection conditions at $\eta = 0$ give

$$F(\xi,0) = 0$$

and (2.41a,b)

$$V(\xi,0) = 0 \quad .$$

The asymptotic boundary condition in the transverse direction gives

$$F(\xi,\eta) \sim 1 \quad \text{as} \quad \eta \to \infty \tag{2.42}$$

The flow is symmetric about the line $\xi = 0$, therefore the symmetry condition can be written as

$$F_{\xi} = 0 \quad \text{at} \quad \xi = 0 \quad . \tag{2.43}$$

For the bodies we will be considering, at downstream infinity $J_r/\gamma_r \to 1$ and the pressure gradient parameter β_1 approaches the value of the Falkner-Skan pressure gradient parameter β and the equation reduces to the Falkner-Skan equation which can be rewritten as

$$F_{\eta\eta} - VF_{\eta} + \beta(1 - F^2) = 0 \tag{2.44}$$

and

$$V_{\eta} = - F \tag{2.45}$$

It is interesting to observe that the boundary-layer equations in the present coordinates show self-similar behavior and similarity solutions are automatically recovered whenever similarity exists. It is also important to remark that the present form of the boundary-layer equations is similar to those when written in Görtler variables.

This completes the general analysis for determination of the boundary-layer equations in optimal coordinates except for the missing boundary conditions $t(\xi,0)$. In the following we will develop a scheme to determine the surface boundary condition on $t(\xi,\eta)$.

5. The Surface Boundary Condition for the Boundary-Layer Equations

In the course of our previous discussion it was mentioned in Section II that the coordinate equation is coupled to the flow equation through the surface boundary condition on $t(\xi,\eta)$. The optimal coordinate condition states that the transformed displacement thickness C should be constant. We will make use of this condition to determine the missing boundary condition on $t(\xi,\eta)$. Since there is no explicit analytical relation relating the surface boundary condition on $t(\xi,0)$ and the displacement thickness, C in optimal coordinates, we must determine the value of $t(\xi,\eta)$ on the surface iteratively. The iterative relation which yields the value of $t(\xi,0)$ in optimal coordinates is determined in the following manner along with some other interesting properties of the equations.

Let us assume $\bar{\xi}$ and $\bar{\eta}$ are the coordinates that are optimal and hence are to be determined. The coordinates ξ and η are assumed not to be optimal but some suitable coordinate system which is used as an initial guess for the optimal coordinate system. Let us also assume that

$$f = A(\xi)\bar{f}(\bar{\xi},\bar{\eta}) \quad , \tag{2.46}$$

$$\eta = A(\xi)\bar{\eta} \tag{2.47}$$

and

$$\bar{\xi} = B(\xi) \quad , \tag{2.48}$$

where A and B are arbitrary functions of ξ.

Then it follows that

$$\frac{\partial}{\partial \xi} = B' \frac{\partial}{\partial \bar{\xi}} - \frac{A'}{A} \bar{\eta} \frac{\partial}{\partial \bar{\eta}} \tag{2.49}$$

and

$$\frac{\partial}{\partial \eta} = \frac{1}{A} \frac{\partial}{\partial \bar{\eta}} \tag{2.50}$$

where the prime denotes the differetiation of the dependent variable with respect to ξ. Using these coordinate transformation relations (2.49) and (2.50) in the boundary-layer Equation (2.35) along with the relation for $\bar{f}$ given by (2.46) gives

$$\bar{f}_{\eta\eta\eta} + \frac{J_r}{\gamma_r} A^2 (1 + \frac{\xi A'}{A}) [\bar{f} + \frac{\xi B'}{(1 + \xi \frac{A'}{A})} \bar{f}_{\bar{\xi}}] \bar{f}_{\eta\eta}$$

$$+ A^2 \frac{J_r}{\gamma_r} \beta_i (1 - f_{\eta}^2) - \xi \frac{J_r}{\gamma_r} A^2 B' \bar{f}_{\eta} \bar{f}_{\bar{\xi}\eta} = 0 \tag{2.51}$$

Since the Equation (2.35) is true in general, the Equation (2.51) should be identical except that the unbarred quantities should be replaced by barred quantities. Comparison of the two Equations (2.35) and (2.51) then requires that

$$A^2 \frac{J_r}{\gamma_r} (1 + \xi \frac{A'}{A}) = \frac{\bar{J}_r}{\bar{\gamma}_r} \quad , \tag{2.52}$$

$$\frac{\xi B'}{(1 + \frac{\xi A'}{A})} = \bar{\xi} = B(\xi) \quad , \tag{2.53}$$

$$A^2 \frac{J_r}{\gamma_r} \beta_i = \frac{\bar{J}_r}{\bar{\gamma}_r} \bar{\beta}_i \tag{2.54}$$

and

$$\xi \frac{J_r}{\gamma_r} A^2 B' = \bar{\xi} \frac{\bar{J}_r}{\bar{\gamma}_r} \quad . \tag{2.55}$$

Combining the relations given by Equations (2.52) and (2.55) we get

$$A^2 \frac{J_r}{\gamma_r} \left(1 + \frac{\xi A'}{A}\right) = \frac{\xi}{\bar{\xi}} \frac{J_r}{\gamma_r} A^2 B' \tag{2.56a}$$

which can be simplified to yield

$$\frac{\xi B'}{\left(1 + \frac{\xi A'}{A}\right)} = \bar{\xi} = B(\xi) \quad . \tag{2.56b}$$

The above relation is already satisfied by Equation (2.53). Therefore we can ignore one of the two relations given by Equations (2.52) and (2.55). Hereafter we will neglect the relation (2.55).

Equation (2.56b) gives

$$\frac{\xi B'}{\left(1 + \frac{\xi A'}{A}\right)} = B(\xi)$$

or rearranging we obtain

$$\frac{B'}{B} = \left(\frac{1}{\xi} + \frac{A'}{A}\right) \quad . \tag{2.57a}$$

Integrating both sides the Equation (2.57a) we get

$$B = K\xi A \tag{2.57b}$$

where K is a constant of integration which will be determined later.

Using the relation (2.57b) and (2.53) we can write

$$(1 + \frac{\xi A'}{A}) = \frac{B'}{KA} \quad . \tag{2.58}$$

Substituting the relation (2.58) into the Equation (2.52) we get

$$\frac{\bar{J}_r}{\bar{\gamma}_r} = \frac{AB'}{K} \frac{J_r}{\gamma_r} \tag{2.59}$$

and from the relation (2.57b) and (2.52) we can write

$$\bar{\xi} = K\xi A \quad . \tag{2.60}$$

Now substitution of $\bar{J}_r/\bar{\gamma}_r$ from Equation (2.59) into Equation (2.54) yields

$$A^2 \frac{J_r}{\gamma_r} \beta_i = \frac{AB'}{K} \frac{J_r}{\gamma_r} \bar{\beta}_i \quad . \tag{2.61}$$

Simplifying the relation (2.61) we obtain

$$\bar{\beta}_i = \frac{AK}{B'} \beta_i \tag{2.62}$$

where βi is given as

$$\beta_i = (1 + \frac{\xi H_\xi}{2H}) \tag{2.63}$$

which can be rewritten as

$$\beta_i = \frac{(\xi^2 H)_\xi}{(H\xi^2)} \frac{\xi}{2} \tag{2.64}$$

Using the relations (2.58) and (2.64) in the Equation (2.62) we can write $\bar{\beta}_i$ as

$$\bar{\beta}_i = \frac{(\xi^2 H)_\xi}{(\xi^2 H)} (\frac{\xi}{2}) \frac{1}{(1 + \frac{\xi A'}{A})} = \frac{(\xi^2 H)_\xi}{(\xi^2 H)} \frac{\xi}{2} \frac{A}{(\xi A)'} \quad . \tag{2.65}$$

Also we have from Equation (2.60)

$$\frac{d\bar{\xi}}{d\xi} = K \frac{d(\xi A)}{d\xi} = K(\xi A)' \tag{2.66a}$$

and

$$A = \frac{\bar{\xi}}{(\xi K)} \quad . \tag{2.66b}$$

Substituting the relations (2.66a) and (2.66b) into (2.65) we get

$$\bar{\beta}_i = \frac{(\xi^2 H)_{\bar{\xi}}}{(\xi^2 H)} \frac{\bar{\xi}}{2} \quad . \tag{2.67}$$

Comparing the expression for $\bar{\beta}_i$ in (2.67) with β_i in (2.64) we see that the quantity $(\xi^2 H)$ on the right hand side of Equations (2.67) and (2.64) determines the pressure gradient parameter regardless of the coordinate system.

With these relations, we proceed to determine the relations for the iterative scheme for determining the $(\bar{\xi},\bar{\eta})$ coordinate system given a (ξ,η) system.

If $\bar{\xi}$ and $\bar{\eta}$ coordinates are optimal then we know from Davis [10] analysis that

$$\bar{f}(\bar{\xi},\bar{\eta}) \sim \bar{\eta} - C \quad \text{as} \quad \eta \to \infty \tag{2.68}$$

where C is a constant which was already mentioned in the earlier discussion. C is related to the displacement function in optimal coordinates.

In general in the (ξ,η) coordinate system (which may not be optimal) the streamfunction $f(\xi,\eta)$ far from the body is given as

$$f \sim \eta - \ell(\xi) \tag{2.69}$$

with the help of relations (2.45) and (2.46) the Equation (2.69) can be written as

$$\bar{f}(\bar{\xi},\bar{\eta}) \sim \bar{\eta} - \frac{\ell(\xi)}{A(\xi)} \quad \text{as} \quad \bar{\eta} \to \infty \tag{2.70}$$

Comparing the two expressions for $\bar{f}(\bar{\xi},\bar{\eta})$ given by Equations (2.68) and (2.70) we get

$$C = \frac{\ell(\xi)}{A(\xi)} = \bar{\ell} \tag{2.71}$$

Also we can write from Equation (2.71)

$$A(\xi) = \frac{\ell(\xi)}{\ell} \quad . \tag{2.72}$$

Substituting the expression of $A(\xi)$ from Equation (2.71) and its derivative in the relations (2.59) through (2.61) we get

$$\frac{\bar{J}_r}{\bar{\gamma}_r} = \frac{\ell(\xi)(\xi\ell(\xi))'}{\bar{\ell}^2} \frac{J_r}{\gamma_r} \tag{2.73}$$

$$\bar{\xi} = \frac{K\xi\ell(\xi)}{\bar{\ell}} \tag{2.74}$$

and

$$\bar{\beta}_i = \frac{\ell(\xi)}{(\xi\ell(\xi))'} \beta_i \tag{2.75}$$

Also we can write J_r/γ_r in the present coordinate system for the boundary-layer flow from Equation (2.25d) as

$$\frac{J_r}{\gamma_r} = \frac{1}{t(t+\xi t_\xi)} \tag{2.76}$$

Similarly we can write an analogous expression for barred quantities as

$$\frac{\bar{J}_r}{\bar{\gamma}_r} = \frac{1}{\bar{t}(\bar{t}+\bar{\xi}\bar{t}_\xi)} \quad . \tag{2.77}$$

From the coordinate relation (2.23) we can write

$$p = \xi t = \bar{\xi}\bar{t} \tag{2.78}$$

Substituting $\bar{\xi}$ and ξ from the Equation (2.78) into the Equation (2.74) we get

$$\frac{t}{\bar{t}} = K\,\frac{\ell(\xi)}{\bar{\ell}} \tag{2.79}$$

Using the relations (2.76) and (2.77) in Equation (2.73) we can show that

$$\frac{1}{\bar{t}(\bar{t}+\bar{\xi}\bar{t}_{\xi})} = \frac{\ell(\xi)(\xi\ell(\xi))'}{\bar{\ell}^2}\,\frac{1}{t(t+\xi t_{\xi})} \tag{2.80a}$$

or

$$K\left(\frac{\ell}{\bar{\ell}}\right)\frac{1}{(\bar{\xi}\bar{t})_{\bar{\xi}}} = \left(\frac{\ell}{\bar{\ell}}\right)\left(\frac{\xi\ell}{\bar{\ell}}\right)\frac{1}{(\xi t)_{\xi}} \quad . \tag{2.80b}$$

Now using the relation (2.78) we can easily write, after rearranging the equation (2.80b) as

$$K\,\frac{dp}{d\xi} = \frac{d(\xi p)}{d\xi}\,\frac{1}{\bar{\ell}}\,\frac{dp}{d\bar{\xi}}$$

or (2.80c,d)

$$\frac{d\bar{\xi}}{d\xi} = \frac{d(\xi p)}{d\xi}\,\frac{1}{\bar{\ell}}\,\frac{dp}{d\bar{\xi}}$$

which can be simplified to give

$$\frac{d\bar{\xi}}{d\xi} = \frac{1}{K}\,\frac{1}{\bar{\ell}}\,\frac{d(\xi\ell)}{d\xi} \quad . \tag{2.80e}$$

In light of the relation for $\bar{\xi}$ given in Equation (2.74), the relation (2.80e) is true if and only if $K = 1$.

Therefore the appropriate relation and the one which can be used is

$$\frac{\bar{t}}{t} = \frac{\bar{\ell}}{\ell(\xi)} \tag{2.81}$$

where $\bar{t}$ is now the needed boundary condition on the surface for the coordinate function $t(\xi,\eta)$ and $\bar{\ell}$ is the displacement thickness function in optimal coordinates. The quantities t and $\ell(\xi)$ are the corresponding variables in the guessed (ξ,η) coordinate system.

This completes the brief outline of the development of the governing differential equations together with the required boundary conditions for the two dimensional symmetric incompressible flow in optimal coordinates. The details of the numerical analysis necessary to solve the given set of equations developed in this section are elaborated on in the the following section.

III. NUMERICAL METHODS OF SOLUTION

1. Boundary-Layer Solution Method

A marching procedure is made use of in determining the solution of the boundary-layer equations in optimal coordinates. The only difference between the present method and the boundary-layer forward marching approach used by numerous authors (see Blottner and Flügge Lotz[22] for example) is that an additional iterative loop has been introduced here in order to satisfy the condition of optimal coordinates. The coefficients α_r, β_r, γ_r and J_r which are functions of t, are evaluated at the surface if they are present in the boundary-layer equation. This fact represents an advantage of setting the iterative scheme for the optimal coordinate condition without solving the coordinate equation in each iteration. This implies that the surface boundary condition $t(\xi,0)$ on the coordinate Equation (2.25) can be computed once and for all by iterating the solution vectors of the boundary-layer equations such that the transformed displacement thickness function C is constant within a prespecified limit of accuracy. To compute $t(\xi,0)$ in each iteration the relation (2.81) is used to update the surface boundary condition $t(\xi,0)$.

In order to solve the boundary-layer equations, a coordinate transfromation similar to that used by Van de Vooren and Dijkstra[23], Davis[15] and Davis, U. Ghia and K. Ghia[16] is used in the ξ(streamwise) direction to achieve proper resolution of the flow field in the streamwise direction. The transformation which gives the appropriate flow field resolution is given by

$$S = 1 - A/\xi \log(1 + \xi/A) \tag{3.1}$$

where A is a constant, the value of which is chosen such that the vorticity, g, at the wall drops to one half the stagnation point value at about S = 0.5, where S is the transformed coordinate. The value of A which gives such a variation of vorticity $g(\xi,\eta)$ at the wall is found to be equal to 1 for the boundary-layer analysis. Apart from the advantages mentioned above, the transformation relation (3.1) transforms the semi-infinite domain of integration in the streamwise (ξ) direction into a finite domain in the new independent variable, such that S varies between 0 to 1 as ξ varies from 0 to ∞.

It is mentioned by Davis[15] that the vorticity g dies out exponentially to zero beyond a value of $\eta = 5.0$ for all Reynolds numbers in the case of laminar unseparated flow. The boundary-layer equation is therefore integrated up to $\eta = 6.0$ with an uniform step size of $\Delta\eta$.

In order to solve the boundary-layer equations, the momentum equation which is coupled to the normal velocity equation is linearized with respect to the previous step value and rewritten in new independent variables as

$$F_{\eta\eta} - \left(\frac{J_r}{\gamma_r} V\right)_G F_\eta + \left(\frac{J_r}{\gamma_r} \beta_i\right)_G (1 - F_G F) - \xi\left(\frac{J_r}{\gamma_r} F\right)_G F_S \frac{dS}{d\xi} \quad . \tag{3.2}$$

Then the normal velocity equation reads

$$V_\eta + F + \xi F_S \frac{dS}{d\xi} = 0 \tag{3.3}$$

where the subscript G stands for the guessed value of the dependent variables from the previous station or iteration.

An implicit finite difference scheme similar to that given by Blottner and Flügge-Lotz[22] is used to solve the parabolic momentum Equation (3.2). Once the momentum equation is solved the continuity equation is integrated with respect to η once to obtain the updated value of V to be used in the subsequent iteration of the momentum equation. In the numerical scheme, the F_η and $F_{\eta\eta}$ derivative terms are written in second order accurate central difference form and the S derivative is written as a two point backward difference. Application of such a scheme to the momentum Equation (3.2) results in a tria-diagonal system of equations in the η direction at each grid line given by S = constant. The Thomas algorithm[24] is employed to invert the set of simultaneous algebraic equations. The momentum and the continuity equations are solved simultaneously. The solution vector is iterated on due to the nonlinearities until the values of the solution obtained in two successive iterations do not differ by a prespecified accuracy limit. Repeating these steps at each grid line at S = constant, the solution procedure is marched from S = 0 to S = 1 to cover the entire semi-infinite domain in the streamwise direction. In order to initiate the marching process we need the initial profile of the solution vectors F and V at $\xi = 0$ and also the value of the displacement function $\bar{\ell}$ in optimal coordinates in order to calculate $t(\xi,0)$ along the surface of the body. The displacement thickness in optimal coordinates and the starting values of the solution vectors F and V at the stagnation point are determined in the following manner.

It was already mentioned in the Section II on the asymptotic boundary conditions for the coordinate Equation (2.25) that the optimal coordinates become conformal at downstream infinity. This implies that the displacement thickness function $\ell(\xi)$ at downstream infinity is the displacement thickness function $\bar{\ell}$ in optimal coordinates. Therefore in order to determine the displacement thickness function $\bar{\ell}$ the boundary layer Equations (3.2) and (3.3) are solved at downstream infinity. As $\xi \to \infty$, the boundary-layer equations yield the similarity form as given below.

$$F_{\eta\eta} - VF_{\eta} + \beta(1 - F^2) = 0 \tag{3.4}$$

and

$$V_{\eta} + F = 0 \tag{3.5}$$

where β assumes a value equal to zero for the bluned plate case and $\beta = 2\delta/\pi$ for the blunted wedge problem.

The above set of Equations ((3.4)-(3.5)) can easily be solved with the boundary condition prescribed by Equations (2.41a,b) and (2.42). Now writing the derivatives $F_{\eta\eta}$ and F_{η} in central difference form a set of triadiagonal system of equations are obtained and these can easily be inverted by applying Thomas algorithm. Once the solution is obtained, the displacement thickness $\bar{\ell}$ is calculated using the Equation (2.40). Finally, the initial profiles of F and V are obtained by solving the boundary-layer equations at $\xi = 0$. Again we note from Equations (3.2) and (3.3) at $\xi = 0$, that the boundary-layer equations assume a similarity form because of the symmetric condition $F_{\xi} = 0$ along the the stagnation line. The equations at the stagnation line, i.e. at $\xi = 0$, reduce to

$$F_{\eta\eta} - \frac{J_r}{\gamma_r} VF_\eta + \frac{J_r}{\gamma_r}(1 - F^2) = 0 \qquad (3.6)$$

and

$$V_\eta + F = 0 \qquad (3.7)$$

with the boundary conditions

$$F = 0$$

$$\text{at } \eta = 0 \qquad (3.8a,b)$$

$$V = 0$$

and

$$F \sim 1 \qquad \text{as } \eta \to \infty \quad . \qquad (3.8c)$$

The Equations (3.6) and (3.7) can easily be solved in exactly the same manner as in the case of downstream infinity. But in this case the solution of the boundary-layer Equations (3.6) and (3.7) has to be iterated on to satisfy the condition of optimal coordinates, in addition to the iteration required for the nonlinearity of Equation (3.6). Once the initial profile is obtained it is now possible to compute the solution of the Equations (3.2) and (3.3) in the entire flow field by using a forward marching process. After the determination of $t(\xi,0)$ at all of the grid points on the surface, the coordinate Equation (2.25) can be solved. The details of the numerical analysis for the coordinate Equation (2.25) is discussed in the following.

2. Optimal Coordinate Solution Method

The coordinate equation as given by (2.25) is elliptic in nature and requires four boundary conditions of which three are already specified by the Equations (2.27) through (2.28a,b). The fourth boundary condition is determined from the flow equations as mentioned in the preceding section.

Because of the elliptic nature of the equation an alternating direction implicit (ADI) method, first developed by Douglas[25], is made use of to obtain the coordinate equation solution. In order to apply the ADI scheme a fictitious unsteady term $\partial t/\partial v$ is added to the right hand side of the Equation (2.25). The resulting equation is marched in time and alternated with respect to the independent variables ξ and η at each half time step. The steady state solution is recovered in a two step process to obtain the asymptotic converged solution of the unsteady differential equation. Recognizing the fact that the transient solution is of no importance for the present analysis, certain measures are taken in order to achieve faster convergence. For example, the coefficient of the term $\partial t/\partial v$ is set equal to different constants for different problem parameters to improve the convergence rate of the ADI scheme.

A transformation of the independent variables is made in order to confine the domain of integration to a finite region besides providing the proper resolution in the η and ξ directions and preserving the uniform step size accuracy in the computational domain.[26] The transformation relations which serve these purposes are given in the following for the η variable and in (3.1) for the ξ variable. The variable η is replaced by

$$N = \frac{\eta}{\eta+5} \quad . \tag{3.9}$$

In Equation (3.1) the constant A as mentioned previously is chosen equal to 1. The transformation (3.1) together with (3.9) transform the quarter infinite domain in (ξ,η) coordinates to a unit square in the computational

domain of (S,N) coordinates. Using these transformation relations the coordinate Equation (2.25) is rewritten in new independent variables (S,N) as

$$t_{NN}\left(\frac{dN}{d\eta}\right)^2 + t_N \frac{d^2N}{d\eta^2} - \frac{2\beta_r}{\gamma_r} t_{SN}\left(\frac{dN}{d\eta}\right)\left(\frac{dS}{d\xi}\right) + \frac{\alpha_r}{\gamma_r}$$

$$\left(\frac{2}{\xi}\frac{dS}{d\xi} + \frac{d^2S}{d\xi^2}\right) t_S + \frac{\alpha_r}{\gamma_r} t_{SS}\left(\frac{dS}{d\xi}\right)^2 = \frac{\partial t}{\partial v} \quad . \tag{3.10}$$

The subscripts S,N in the Equation (3.10) represent the partial differentiation of the dependent variable with respect to the independent variables appearing.

The cross derivative term t_{SN} in the coordinate equations needs a special treatment because it plays an important role in the numerical solution of the coordinate equation. The cross derivative term appears in the equation because of the non-orthogonality of the (ξ,η) coordinate system. The coordinate system depends on the displacement effect. The magnitude of this cross derivative term is also an indication of the degree to which the optimal coordinates are non-orthogonal, i.e. vary from conformal coordinates in this case. One must also be careful in formulating the numerical scheme for the cross derivative since it is well known that the cross derivative if improperly handled can cause numerical instability.[27] In many situations this term is small and can be treated explicitly[28] in an otherwise implicit scheme. In the present analysis, in order to be consistent with the numerical scheme, an implicit treatment of the cross derivative has been developed using a three level finite difference scheme similar to that followed by Mitchell.[29] This type of

the treatment of the cross-derivative term allows one to break the single term $t_{\xi\eta}$ into combinations of unidirectional derivatives with respect to the independent variables ξ and η. The cross derivative $t_{\xi\eta}$ is written using the three level grid points as shown in Figure 2. Then the cross-derivative at the grid point m,n can be expressed in second order accurate difference form as

$$t_{\xi\eta} = [-DF \frac{\Delta N}{\Delta S} t_{NN}|_{m,n} + DF \frac{\Delta N}{\Delta S} t_{NN}|_{m-1,n}$$

$$+ \frac{1}{2\Delta S} t_N|_{m,n} - \frac{1}{2\Delta S} t_N|_{m-1,n} - DF \frac{\Delta S}{\Delta N} t_{SS}|_{m,n}$$

$$- \frac{2DF}{\Delta N} t_S|_{m,n} + \frac{(DF - \frac{1}{4})}{2} \frac{\Delta S}{\Delta N} t_{SS}|_{m,n-1}$$

$$+ \frac{(DF - \frac{1}{4})}{\Delta N} t_S|_{m,n-1} + \frac{(DF + \frac{1}{4})}{2} \frac{\Delta S}{\Delta N} t_{SS}|_{m,n+1}$$

$$+ \frac{(DF + \frac{1}{4})}{\Delta N} t_S|_{m,n+1}](N_\eta S_\xi) \quad . \qquad (3.11)$$

The other terms in Equation (3.11) are written as three point central differences. It can be shown that in order to maintain diagonal dominance in the inversion scheme, DF should be taken equal to 0, 1/4 or - 1/4 according to whether the coefficient of the $t_{\xi\eta}$ term in Equation (3.10) is zero, positive or negative. Keeping track of this property provides stability to the system. The ADI numerical method of solution using this difference scheme is described in the following.

During the first half time step, denoted by the star (*) step, the ADI algorithm for the coordinate Equation (3.10) is advanced from time v^n to $v^* = v^n + \frac{\Delta v}{2}$ by the following relation:

$$
\begin{aligned}
&(N_\eta^2 + 2\frac{\beta_r}{\gamma_r} DF \frac{\Delta N}{\Delta S} N_\eta S_\xi) t^*_{NN} + (N_{\eta\eta} - 2\frac{\beta_r}{\gamma_r} N_\eta S_\xi \frac{1}{2\Delta S}) t^*_N \\
&+ (4\frac{\beta_r}{\gamma_r}\frac{DF}{\Delta N} N_\eta S_\xi + \frac{2}{\xi}\frac{\alpha_r}{\gamma_r} S_\xi + \frac{\alpha_r}{\gamma_r} S_{\xi\xi}) t^n_S \\
&+ (\frac{\alpha_r}{\gamma_r} S_\xi^2 + 2\frac{\beta_r}{\gamma_r} DF \frac{\Delta S}{\Delta N} N_\eta S_\xi) t^n_{SS} \\
&- 2\frac{\beta_r}{\gamma_r} N_\eta S_\xi DF \frac{\Delta N}{\Delta S} t_{NN}|_{m-1,n} + 2\frac{\beta_r}{\gamma_r} N_\eta S_\xi \frac{1}{2\Delta S} t_N|_{m-1,n} \\
&- \frac{(DF - \frac{1}{4})}{2}\frac{\Delta S}{\Delta N} 2\frac{\beta_r}{\gamma_r} N_\eta S_\xi t_{SS}|_{m,n-1} \\
&- \frac{(DF - \frac{1}{4})}{\Delta N} 2\frac{\beta_r}{\gamma_r} N_\eta S_\xi t_S|_{m,n-1} \\
&- \frac{(DF + \frac{1}{4})}{2} 2\frac{\beta_r}{\gamma_r} N_\eta S_\xi \frac{\Delta S}{\Delta N} t_{SS}|_{m,n+1} \\
&- 2\frac{\beta_r}{\gamma_r} N_\eta S_\xi \frac{(DF + \frac{1}{4})}{\Delta N} t_S|_{m,n+1} = \frac{t^* - t^n}{\Delta v}
\end{aligned}
\tag{3.12}
$$

where Δv is the time step.

The starred (*) quantities in Equation (3.12) are considered to be unknown whereas the dependent variables with superscript n are assumed to be known from the preceding half time step (n). The Equation (3.12) is solved along lines of constant S or ξ. Writing the t_N and t_{NN} terms in central difference form, the Equation (3.12) can be shown to reduce to a set of simultaneous equations in triadiagonal form. These algebraic equations can be inverted by applying the Thomas algorithm.

During the second half time step, Equation (3.12) is marched forward to a new time level $v^{n+1} = v^* + \frac{\Delta v}{2}$ using the relation given below:

$$\left(\frac{\alpha_r}{\gamma_r} S_\xi^2 + 2\frac{\beta_r}{\gamma_r} DF \frac{\Delta S}{\Delta N} N_\eta S_\xi\right) t_{SS}^{n+1} + \left(4\frac{\beta_r}{\gamma_r}\frac{DF}{(\Delta N)} N_\eta S_\xi + \frac{2}{\xi}\frac{\alpha_r}{\gamma_r} S_\xi\right.$$

$$\left. + \frac{\alpha_r}{\gamma_r} S_{\xi\xi}\right) t_S^{n+1} + \left(N_{\eta\eta} - 2\frac{\beta_r}{\gamma_r} N_\eta S_\xi \frac{1}{2(\Delta S)}\right) t_N^*$$

$$+ \left(N_{\eta\eta} - 2\frac{\beta_r}{\gamma_r} N_\eta S_\xi DF \frac{\Delta N}{\Delta S}\right) t_{NN}^* - \left(2\frac{\beta_r}{\gamma_r} N_\eta S_\xi DF \left(\frac{\Delta N}{\Delta S}\right)\right) t_{NN}\Big|_{m-1,n}$$

$$+ 2\frac{\beta_r}{\gamma_r} N_\eta S_\xi \frac{1}{2(\Delta S)} t_N\Big|_{m-1,n} - \frac{(DF - \frac{1}{4})}{2}\left(\frac{\Delta S}{\Delta N}\right) 2\frac{\beta_r}{\gamma_r} N_\eta S_\xi t_{SS}\Big|_{m,n-1}$$

$$- \frac{(DF - \frac{1}{4})}{\Delta N} 2\frac{\beta_r}{\gamma_r} N_\eta S_\xi t_S\Big|_{m,n-1}$$

$$- 2\frac{\beta_r}{\gamma_r} N_\eta S_\xi \frac{(DF + \frac{1}{4})}{\Delta N} t_S\Big|_{m,n+1} = \frac{t^{n+1} - t^*}{\Delta v} \qquad (3.13)$$

where the starred (*) quantities are known from the previous half time step calculation and the dependent variables with superscript (n+1) are considered to be unknown in the Equation (3.13). Writing the derivatives t_{SS} and t_S in second order accurate central difference form, the differential Equation (3.13) can be solved in an identical manner to the star (*) step. The solution procedure for the coordinate equation alternates between the constant ξ and constant η directions in one complete time step. The steady state solution is achieved as an asymptotic converged solution to the unsteady Equation (3.10). Since the initial guessed coordinates assumed for the iteration procedure are assumed to be conformal, the initial conditions for $t(\xi,\eta)$ at each grid point is taken to be 1.

Next we discuss the numerical solution of the Navier-Stokes equations in optimal coordinates. However, rather than solving the complete equations we solve a parabolized version. The solution of the complete equations should follow in a similar manner.

3. Solution of Parabolized Navier-Stokes Equations

The parabolized vorticity and streamfunction equations unlike the boundary-layer equations, are coupled with the coordinate equation because the coefficients α_r, β_r, γ_r and H_r are no longer functions of ξ only but are functions of η as well. This fact calls for the simultaneous treatment of the flow Equations ((2.29)and (2.30)) and the coordinate Equation (3.10). Therefore, the iterative scheme described in the case of boundary-layer analysis is modified slightly to accommodate the simultaneous treatment of the flow equations and the coordinate equation. Details of the scheme are presented in the following.

In order to solve the vorticity and streamfunction equations more efficiently transformations of the independent variables are made. The transformation relations are the same as given in case of the coordinate equation and are given by the Equations (3.1) and (3.9). The only difference in the use of the relation (3.1) for the case of parabolized Navier-Stokes analysis is in the value of the constant A, which, in this case is chosen to be $4.0 + 0.4\ q_w$, where $q_w = \bar{q}_w \sqrt{Re}$. Re is the Reynolds number based on the nose radius of curvature, a and $\bar{q}_w$ is the value of q at the wall. The dependence of the constant A on Re, in the streamwise stretching is introduced in order to achieve the desired flow field resolution in the streamwise direction for different Reynolds numbers. The transformation relation (3.9) in the η direction has a viscous type stretching built into it, such that it always places the viscous layer in approximately the lower half of the unit square region of integration while the inviscid flow is contained in the upper half. This type of flow field resolution in the η direction is appropriate in light of the fact that for all unseparated flow cases, as was mentioned in the case of boundary-layer analysis, the viscous effects are confined within the region $\eta < 5$ or in the transformed variable $N < 0.5$. The transformation relation (3.9) therefore allows one to obtain proper grid spacing in the physical flow field near the wall, where the gradients of the flow variables are large as compared to their asymptotic values far away from the wall. Various other advantages of the transformation relations (3.1) and (3.9) are elaborated on in the case of boundary-layer analysis and will not be repeated here.

Because of the boundary condition $f \to \eta - C$ as $\eta \to \infty$, a new streamfunction $\bar{h}$ is defined such that

$$f = \bar{h} + \eta \tag{3.15}$$

The steady state streamfunction-vorticity equations in the transformed variables can now be written as

$$(N_\eta)^2 \bar{h}_{NN} + N_{\eta\eta}(1 + \bar{h}_N) = g \tag{3.16}$$

and

$$\begin{aligned} N_\eta^2 g_{NN} + [&2 \frac{H_N}{H} N_\eta - 2 \frac{\beta_r}{\gamma_r} S_\xi \frac{H_S}{H} + \frac{J_r}{\gamma_r} (\eta + \bar{h} + \xi \bar{h}_S S_\xi) \\ &+ N_{\eta\eta}] g_N N_\eta + [(\frac{N_\eta H_N}{H})^2 - 2 \frac{\beta_r}{\gamma_r} S_\xi N_\eta \frac{H_S H_N}{H^2} + \frac{\alpha_r}{\gamma_r} (\frac{S_\xi H_S}{H})^2 \\ &- \frac{2}{\xi} \frac{\beta_r}{\gamma_r} N_\eta \frac{H_N}{H} + \frac{2}{\xi} \frac{\alpha_r}{\gamma_r} S_\xi \frac{H_S}{H} + \frac{4}{\xi} N_\eta (\frac{\beta_r}{\gamma_r})_N - \frac{4}{\xi} \frac{\beta_r}{\gamma_r} S_\xi (\frac{\beta_r}{\gamma_r})_S \\ &+ \frac{12}{\xi^2} (\frac{\beta_r}{\gamma_r})^2 + \frac{J_r}{\gamma_r} \frac{N_\eta H_N}{H} (\eta + \bar{h} + \xi S_\xi \bar{h}_\xi) - \frac{J_r}{\gamma_r} (1 + \frac{\xi S_\xi H_S}{H}) \\ &(1 + \bar{h}_N N_\eta)] g + [2 \frac{\alpha_r}{\gamma_r} \frac{S_\xi H_S}{H} - 2 \frac{\beta_r}{\gamma_r} \frac{N_\eta H_N}{H}] S_\xi g_\xi = 0 \quad . \end{aligned} \tag{3.17}$$

The corresponding boundary conditions are given in the following. The no slip and zero injection conditions on the surface give

$$\bar{h} = 0$$

and $$\text{at} \quad \eta = 0 \tag{3.18a,b}$$

$$\bar{h}_\eta = -1$$

The infinity boundary conditions are given by

$$\bar{h}_\eta \sim 0$$

and as $\eta \to \infty$ (3.19a,b)

$$g(\xi,\eta) \quad 0$$

At $\xi = 0$, symmetry is made use of to compute the vorticity and streamfunction along the stagnation plane.

The asymptotic boundary condition as $\xi \to \infty$ is given by Equation (3.16) along with (3.17) evaluated as $\xi \to \infty$. Equation (3.16) remains the same whereas (3.17) reduces to

$$(N_\eta)^2 g_{NN} + (\eta + \bar{h} + 1)N_\eta g_N + (1 - 2\beta)(1 + \bar{h}_N N_\eta)g \tag{3.20}$$

where β is the Falkner-Skan pressure gradient parameter and is a known quantity for a given problem.

It is observed from Equations (3.16) and (3.17) that the streamfunction and the vorticity equations are second-order partial differential equations with respect to η. Therefore two boundary conditions for each of the dependent variables $\bar{h}$ and g are needed in order to integrate the equations. There are three boundary conditions on $\bar{h}$ and one boundary condition on g. These type of boundary conditions are not the most convenient ones for the Thomas algorithm. However, the solution to the flow equations can be obtained by a superposition method as described by Davis, U. Ghia and K. Ghia,[16] by determining a coe-ficient C_1 such that

$$g(\xi,\eta) = C_1 g_H(\xi,\eta) + g_p(\xi,\eta) \tag{3.21}$$

with C_1 given by

$$C_1 = - \frac{1 + \frac{\partial(\bar{h}_{p_2})}{\partial\eta}}{\frac{\partial(\bar{h}_{p_1})}{\partial\eta}} \tag{3.22}$$

where g_H and g_p are the homogeneous and particular solutions respectively of the vorticity Equation (3.17) and $\bar{h}_{p_1}$ and $\bar{h}_{p_2}$ are the particular solutions of the streamfunction Equation (3.16) corresponding to the forcing function $g_H(\xi,\eta)$ and $g_p(\xi,\eta)$.

The governing flow equations are therefore integrated along the curves of constant ξ for all η, using the implicit finite difference method of Blottner and Flügge-Lotz[22] as described in the case of boundary-layer analysis. Once the required convergence is achieved on the solution vectors, the $t(\xi,0)$ value is updated using the iterative relation (2.81). With this surface boundary condition distribution on t, the coordinate equation is integrated employing the two step time dependent ADI relaxation method, as described previously in boundary-layer analysis. The converged solution is then stored to calculate the new values of J_r, α_r, β_r, and H_r to be used subsequently in the flow equations. Before starting a new iteration in the flow equations after this step, the edge quantity $\bar{h}(\xi,\infty)$ is checked for satisfaction of the condition of optimal coordinates, i.e. $\ell(\xi) \to C$, a constant. If this condition is not satisfied within a prescribed accuracy limit, then the entire cycle is repeated to calculate a new set of values for the solution vectors g, f and t.

This completes the method of solving the flow equations in optimal coordinates including the generation of the optimal coordinates. The application of the analysis to specific problems is discussed in the following section.

IV. APPLICATION TO SYMMETRIC TWO-DIMENSIONAL FLOW PROBLEMS

In order to demonstrate the application of the principles described in the previous sections we will generate the solutions for two-dimensional incompressible laminar symmetric flow. Two geometries are considered as examples; the flow past a semi-infinite wedge, and the flow past a semi-infinite thick flat-plate, see Figures 3a,b and 4 and 5 respectively. Boundary-layer as well as the parabolized vorticity-streamfunction form of the flow equations are used for the present analysis. Details of the analysis are presented in the following.

1. The Blunted Wedge Example

The two dimensional incompressible flow past a semi-infinite wedge as shown in the Cartesian plane in Figure 3a is considered here. The axis of the wedge is oriented in the direction such that the flow is symmetric about the wedge axis. The body surface in the physical plane as shown in Figure 3a is mapped to the line $q = 0$ and the corresponding flow in the physical (x,y) plane is mapped into a stagnation point type flow which is the upper half of the ζ plane (see Figure 3b). This type of mapping is achieved by applying a Schwarz-Christoffel transformation which results in

$$z = \frac{\nu}{U_r} \frac{(n+1)}{2} \zeta^{\frac{2}{n+1}} \tag{4.1}$$

where $\zeta = q + ip$. The scale factor of the transformation is given by

$$h^2 = \left|\frac{dz}{d\zeta}\right|^2 = \left(\frac{\nu}{U_r}\right)^2 \left|q^2 + p^2\right|^{\frac{1-n}{1+n}} \quad . \tag{4.2}$$

The factor ν/U_r appearing on the right hand side of Equation (4.1), non-dimensionalizes the coordinates q and p. The n, appearing in the exponent of the transformation relation (4.1) is related to the semi-wedge angle δ as

$$n = \frac{\delta}{\pi - \delta} \quad . \tag{4.3}$$

Recognizing that the point $(y_o, 0)$ transforms to the point $(q_w, 0)$, (see Figures 3a and 3b), the nose radius of curvature a can be written, using Newton's formula, as

$$a = \left(\frac{1+n}{1-n}\right) q_w^{\frac{2}{1+n}} \frac{\nu}{U_r} \tag{4.4}$$

where q is equal to q_w at the wall. Defining the Reynolds number based on the nose radius of curvature such that $Re = U_r a/\nu$, it can be shown from the relation (4.4) that the location of the wedge surface in the transformed plane is given by

$$q_w = \left[Re \frac{1-n}{1+n}\right]^{\frac{1+n}{2}} \quad . \tag{4.5}$$

It is observed from the equation (4.5) that keeping the Reynolds number Re constant, the effects of body shape on the flow can be studied by changing n, whereas keeping n fixed, the effects of Reynolds number on the flow can be investigated by varying Re.

It will be shown later that the conformal transformation used here to transform the physical flow field into a stagnation point flow in the conformal plane, allows one to obtain similarity type variables and similarity solutions are recovered whenever similarity exists. In addition, the downstream boundary conditions at infinity are automatically satisfied. The mapping also allows one to obtain simpler boundary conditions in relating the optimal (ξ,η) coordinates to conformal (p,q) coordinates.

Since the numerical calculation is to be carried out in optimal coordinates, the transformation relation can be rewritten in optimal coordinates. Using the coordinate relation given in Equations (2.23) and (2.24), the transformation relation reads in optimal coordinates as

$$z = \frac{\nu}{U_r} \frac{1+n}{2} \left(\frac{\eta}{t} + i\xi t\right)^{\frac{2}{1+n}} \tag{4.6}$$

and the scale factor h is given by

$$h^2 = \left(\frac{\nu}{U_r}\right) \left|\left[\left(\frac{\eta}{t}\right)^2 + (\xi t)^2\right]\right|^{\frac{1-n}{1+n}} \quad . \tag{4.7}$$

It can be shown that the similarity solutions are recovered in the case of a blunted wedge in terms of the present variables ξ and η if the exponent n is related to the Falkner-Scan pressure gradient parameter β given by

$$\beta = \frac{2n}{1+n} \quad . \tag{4.8}$$

It is interesting to note that the mapping given by the Equation (4.6) yields the limiting cases of the thin flat plate and the vertical wall when $\beta = 0$, $Re = 0$ and $\beta = 1$ and $Re \neq 0$ respectively.

The scale factor of the transformation in optimal coordinates is rewritten in nondimensional form as

$$h = [(\xi^2 t^2 + (\frac{\eta}{t} + q_w)^2)]^{\frac{1-\beta}{2}} \quad . \tag{4.9}$$

It is important to note that the independent variable η is defined here (i.e. in Equation (4.9)), in such a way that $\eta = 0$ corresponds to the value of the conformal coordinate q at the wall and it is denoted by q_w. With this new definition of the independent variable η, the body is always placed at $\eta = 0$ in the optimal coordinate plane and $\eta = C$ represents the displacement surface in optimal coordinates.

The additional relations required for the solution of the governing differential Equations (2.29) and (2.30) are given as follows

$$\frac{h_\xi}{h} = \frac{(1-\beta)\ [\xi^2 t^2 + \xi^2 t_\xi t + (\frac{\eta}{t} + q_w)(-\frac{\eta}{t^2} t_\xi)]}{[\xi^2 t^2 + (\frac{\eta}{t} + q_w)^2]} \tag{4.10}$$

and

$$\frac{h_\eta}{h} = \frac{(1-\beta)\ [\xi^2 t_\eta t + (\frac{\eta}{t} + q_w)(\frac{1}{t} - \eta \frac{t_\eta}{t^2})]}{[(\xi^2 t^2) + (\frac{\eta}{t} + q_w)^2]} \quad . \tag{4.11}$$

Along the stagnation streamline, i.e. $\xi = 0$, the term $h_\xi/\xi h$ appearing in the $H_\xi/\xi H$ term in the vorticity Equation (2.30) becomes undefined and hence, must be evaluated with the proper limit process.

The limit process gives

$$\lim_{\xi \to 0} \left(\frac{h_\xi}{\xi h}\right) = \left.\frac{h_{\xi\xi}}{h}\right|_{\xi=0}$$

Hence,

$$\left.\frac{h_{\xi\xi}}{h}\right|_{\xi=0} = \frac{(1-\beta)\ [t^2 - (\frac{\eta^2}{t^4} + \frac{q_w \eta}{t^3})\ t\ t_{\xi\xi}]}{(q_w + \frac{\eta}{t})^2} \quad . \tag{4.12}$$

In order to performa the boundary-layer analysis for the blunted wedge problem, the coordinates are normalized with respect to the nose radius of curvature a, at the stagnation point, such that the wall location of the blunted wedge surface is given as

$$\bar{q}_w = \frac{q_w}{a^{\frac{n+1}{2}}} = (1-\beta)^{\frac{1}{2-\beta}} \tag{4.13}$$

This type of normalization is adopted in order to remove the explicit apperance of the Reynolds number Re from the analysis.

The scale factor of the transformation can then be written as

$$h = [\bar{q}_w^{-2} + \xi^2 t^2]^{\frac{1-\beta}{2}} \tag{4.14}$$

and the inverse scale factor H is given by

$$H(\xi,0) = \frac{H}{h^2} = \left.\frac{t^2}{(\bar{q}_w^{-2} + \xi^2 t^2)^{1-\beta}}\right|_{\eta=0} \quad . \tag{4.15}$$

Now the pressure gradient parameter β_i, appearing in the boundary layer equation is given as

$$\beta_i = [1 + \frac{(\beta-1)\ t\xi^2\ (t_\xi \xi + t)}{(\bar{q}_w^{-2} + \xi^2 t^2)} + \frac{\xi t_\xi}{t}]_{\eta=0} \qquad (4.16)$$

This completes the necessary details required to solve the flow equations.

The cooredinate equations required to generate optimal coordinates are given by Equation (2.25) and the three boundary conditions are given in Equations (2.27) through (2.28a,b). The fourth boundary condition $t(\xi,0)$ is to be determined iteratively and the iterative scheme required to compute the missing boundary condition is given in detail in Section II.

This completes the mathematical formulation of the blunted wedge problem in optimal coordinates. The details of the numerical method used to solve the governing differential equations are presented in Section III.

2. The Blunted Plate Example

In this example problem, two dimensional symmetric flow past a semi-infinite blunted plate is obtained in optimal coordinates. The body geometry is shown in the physical (x,y) plane in Figure 4. The body is mapped to the line $q = 0$ in the conformal plane ζ, as shown in Figure Figure 5, by applying the Schwarz-Christoffel transformation and results in a relation given by

$$\frac{dz}{d\zeta} = (\frac{2LU_r}{\pi\nu} - \zeta^2)^{1/2} \qquad (4.17a)$$

Integration of (4.17a) gives the transformation relation

$$z = \frac{1}{2}\left[\zeta\left(\frac{2}{\pi}\frac{U_r L}{\nu} - \zeta^2\right)^{1/2} + \frac{2U_r L}{\nu\pi}\sin^{-1}\left(\frac{\zeta}{\sqrt{\frac{2U_r L}{\nu\pi}}}\right)\right] \tag{4.17}$$

The x,y coordinates are nondimensionalized by the viscous length ν/U_r where ν is the kinematic viscosity and U_r is some reference speed.

Since the mapping is conformal, the scale factors in both directions are the same and are given by

$$h^2 = h_1^2 = h_2^2 = \left|\frac{dz}{d\zeta}\right|^2 \tag{4.18}$$

which gives for the present geometry

$$h^2 = \left[(p^2 + q^2 - Re_L)^2 + 4Re_L\, q^2\right]^{1/2} \tag{4.19}$$

where

$$Re_L = \frac{U_r L}{\nu}\,\frac{2}{\pi}$$

The Reynolds number is defined based on the nose radius of curvature as $Re = U_r a/\nu$. The nose radius of curvature at the stagnation point can be shown to be related to the thickness of the plate L, by the following relation

$$a = \frac{(Re_L + q_w^2)^{3/2}}{q_w} \tag{4.20}$$

where q_w is the coordinate q at the body surface. The flow past different body shapes can be studied by a suitable combination of the

parameters Re_L and q_w, whereas the effects of Reynolds number can be studied by varying Re, keeping Re_L and q_w fixed.

The conformal mapping used here transforms the flow in the physical (x,y) plane into a stagnation point flow in the conformal (p,q) plane. The advantages of this type of transformation are the same as mentioned in the blunted wedge example problem.

It is interesting to note that as a limiting case, as $Re_L \to 0$, the transformation (4.17b) represents the flow past a parabola which corresponds to the flow past the thin semi-infinite flat plate in the physical plane. Therefore the analysis includes the flow past the thin semi-infinite flat plate as a special case as $Re_L \to 0$.

The governing differential equations and the boundary conditions remain the same as given in the previous example problem by Equations (2.5) through (2.81), except that in order to recover the correct asymptotic form at downstream infinity, the value of β in Equations (2.18) and (2.44) is set equal to zero to give the Blasius equation, which is the appropriate downstream boundary condition for the blunted plate problem.

The scale factor h, in optimal coordinates can be written as

$$h(\xi,\eta) = \left[\left(\xi^2 t^2 + \left(q_w + \frac{\eta}{t}\right)^2 - Re_L\right)^2 + 4Re_L\left(q_w + \frac{\eta}{t}\right)^2\right]^{1/2} . \qquad (4.21)$$

The additional relations required for the parabolized vorticity-streamfunction Equations (2.29) and (2.30) are given as

$$H = \frac{H_r}{h^2} = \frac{\gamma_r}{J_r^2}\left(\frac{1}{h^2}\right) , \qquad (4.22)$$

which can be written in optimal coordinates as

$$H(\xi,\eta) = \frac{\gamma_r}{J_r^2} \frac{1}{[(\xi^2 t^2 + (q_w + \frac{\eta}{t})^2 - Re_L)^2 + 4Re_L(q_w + \frac{\eta}{t})^2]^{1/2}} . \tag{4.23}$$

Also,

$$\frac{h_\xi}{h} = \frac{[t^2\xi^2 + (q_w + \frac{\eta}{t})^2 - Re_L)(tt_\xi\xi^2 + t^2\xi - (q_w + \frac{\eta}{t})(\frac{\eta}{t^2} t_\xi)) - 2Re_L(q_w + \frac{\eta}{t})\frac{\eta}{t^2} t_\xi]}{[(\xi^2 t^2 + (q_w + \frac{\eta}{t})^2 - Re_L)^2 + 4Re_L(q_w + \frac{\eta}{t})^2]} \tag{4.24}$$

and

$$\frac{h_\eta}{h} = \frac{[(t^2\xi^2 + (q_w + \frac{\eta}{t})^2 - Re_L)(t_\eta t\xi^2 + (q_w + \frac{\eta}{t})(\frac{1}{t} - \frac{\eta t_\eta}{t^2})) + 2Re_L(q_w + \frac{\eta}{t})(\frac{1}{t} - \frac{\eta t_\eta}{t^2})]}{[(\xi^2 t^2 + (q_w + \frac{\eta}{t})^2 - Re_L)^2 + 4Re_L(q_w + \frac{\eta}{t})^2]} . \tag{4.25}$$

As previously, we need the following limit expression. Lim $\xi \to 0$ $h_\xi/\xi h$ can be shown to be equal to

$$\lim_{\xi \to 0} (\frac{h_\xi}{\xi h}) = \frac{h_{\xi\xi}}{h}\bigg|_{\xi=0} = \frac{[((q_w + \frac{\eta}{t})^2 - Re_L)t^2 - (q_w + \frac{\eta}{t})(\frac{\eta}{t^2} t_{\xi\xi})) - 2Re_L(q_w + \frac{\eta}{t})\frac{\eta}{t^2} t_{\xi\xi}]}{[(q_w + \frac{\eta}{t})^2 + Re_L]^2} \tag{4.26}$$

For the boundary-layer analysis the coordinates (x,y) are normalized with respect to the radius of curvature a. Then the transformation relation (4.17b) in nondimensional form becomes

$$z = \frac{1}{2} [\zeta(b + \zeta^2)^{1/2} + b \sin^{-1} (\frac{\zeta}{b^{1/2}}) \tag{4.27}$$

where

$$b = \frac{2L}{\pi a} . \tag{4.28}$$

Now defining $\alpha = q_w/a^{1/2}$ and substituting into the radius of curvature expression, we can show that the body shape parameter α, in the conformal plane, is related to the thickness of the plate in the physical plane by the relation

$$\alpha^{2/3} = b + \alpha^2 \quad . \tag{4.29}$$

The shape of the body for various values of the parameter α, is shown in Figure 6. As a special case of the parameter $\alpha = 1$, the transformation relation (4.27) gives flow past a parabola.

The scale factor for the boundary-layer in optimal coordinates is written as

$$h^2 = [\xi^4 t^4 + 2\xi^2 t^2 (2\alpha^2 - \alpha^{2/3}) + \alpha^{4/3}]^{1/2} \quad . \tag{4.30}$$

The governing differential equations for the boundary-layer analysis are the same as given in the previous example problem by Equations (2.37) through (2.45) except that in the downstream infinity condition (2.44), β is set equal to zero to give the appropriate downstream boundary condition for the blunted plate problem.

The remaining relations required for the boundary-layer solution are

$$H = \frac{H_r}{h^2} = [(\xi^4 t^4 + 2\xi^2 t^2 (2\alpha^2 - \alpha^{2/3}) + \alpha^{4/3})^{-1/2} \; t^2]_{\eta=0} \quad , \tag{4.31}$$

$$\beta_i = \left[1 - \frac{\xi(\xi^3 t^4 + \xi^4 t^3 t_\xi + (\xi t^2 + \xi^2 t t_\xi)(2\alpha^2 - \alpha^{2/3}))}{(\xi^4 t^4 + 2\xi^2 t^2 (2\alpha^2 - \alpha^{2/3}) + \alpha^{4/3})} + \frac{\xi t_\xi}{t}\right]_{\eta=0} \tag{4.32}$$

and

$$H_r = \frac{\gamma_r}{J_r^2} = t^2(\xi,0) \quad . \tag{4.33}$$

As was mentioned in our first example problem, the coordinate equations in this case remain the same as were given by Equations (2.25) through (2.28), except for the surface boundary condition $t(\xi,0)$. Details of the determination of the surface boundary condition $t(\xi,0)$ are presented in Section II of this analysis.

This completes the mathematical modelling of the blunted plate problem. Details of the solution procedure are discussed in the section on numerical method of solution. The results of the present analysis are discussed in the following section.

V. RESULTS AND DISCUSSION

In the present study an effort has been made to demonstrate that a set of optimal coordinates dependent on the displacement effect can be generated numerically for two-dimensional symmetric incompressible laminar flow past blunt and sharp nosed bodies. Various critical aspects of the viscous flow analysis in optimal coordinates for high as well as low Reynolds number were discussed in the previous sections. The present investigation is therefore viewed as an initial step for generating flow dependent coordinate systems numerically. The present analysis has provided us with useful information in order to understand and investigate the inviscid and viscous interaction problem in a different manner.

Present calculations were confined to flow past semi-infinite bodies under conditions such that separation does not occur. The reasons for choosing such body shapes are firstly, because they are the easiest ones to analyze, flows involving separation, for example, being much more difficult. Secondly, for comparison purposes the simple body shapes such as a parabola, vertical wall and thin flat plate, possess previously obtained accurate analytical or numerical solutions which can be used as a basis for comparison.

The solutions were obtained using the governing differential equations developed for the example problems in Section II and numerical technique described in Section III. The solution steps for the coupled set of flow equations and the coordinate equations are presented in

Figures (7-9). The results for specific example cases are discussed in the following.

1. Boundary Layer Results in Optimal Coordinates

1a. Blunted Wedges:

In the mathematical formulation of the wedge problem for the boundary-layer analysis in Section IV, it was shown that the flow past different blunted wedge shapes can be characterized by a single parameter β, related to the slope of the wedge at downstream infinity, where β is the Falkner-Skan pressure gradient parameter. In the present analysis, boundary-layer solutions are obtained for β between 0 and 1, where $\beta = 1$ represents flow against a vertical wall, commonly known as Hiemenz flow and $\beta = 0$ represents the flow past a parabolic cylinder.

Plots of the pressure gradient parameter β_i, for various values of the downstream Falkner-Skan pressure gradient parameter β are presented in Figure 10. Figure 10 shows that the pressure gradient for the case of the parabola approaches zero at downstream infinity and therefore the Blasius solution for flow past a flat plate is the correct solution asymptotically at downstream infinity. Figure 10 also shows the β_i distribution for other values of the downstream Falkner-Skan parameter β which corresponds to increasing the downstream asymptotic wedge angle. If the downstream wedge angle is increased to 90°, the Hiemenz flow or the flow past a vertical wall is obtained and the pressure gradient parameter becomes constant over the wall surface for this flow.

The streamwise distributions of the skin-friction coefficient $g(p,\bar{q}_w)$ are shown in Figure 11 including flow past the parabola given by $\beta = 0$. For all values of β, the skin friction coefficient attains at the stagnation point a value of 1.233 which is the exact value of skin friction coefficient for the stagnation flow against a vertical wall. For the case of a parabola, the skin friction approaches the flat plate solution at downstream infinity. This is as it should be, since the appropriate downstream flow in the case of parabola is governed by the Blasius flat plate solution. With increasing β, the skin friction coefficient approaches the corresponding Falkner-Skan solution at downstream infinity. Observe that for $\beta = 0.7$, the skin friction profile is very close to that of the flow against a vertical wall, giving an indication that the flow is approaching the stagnation flow.

The displacement thickness functions for β between 0 and 1 are obtained in optimal coordinates and their values in conformal coordinates are shown in Figure 12. Displacement thickness results obtained at the stagnation point show very good agreement with those of Davis[15] as well as those of Van Dyke.[9] The displacement thickness for the case of a parabola also approaches asymptotically the appropriate value obtained for the Blasius flat plate solution at downstream infinity. As expected, the displacement thickness approaches a constant value as the downstream wedge angle is increased by increasing the value of Falkner-Skan parameter β to 1. Since the displacement thickness in conformal coordinates is constant, according to optimal

coordinate theory, the conformal coordinates for stagnation flow (i.e. for $\beta = 1$), are optimal coordinates.

1b. Blunted Plates:

It was previously shown in Section IV (see Figure 6) that for boundary-layer analysis, the flow past the blunted plate is characterized by a parameter α. Various body shapes for the blunted plate problem are shown in Figure 6 with their corresponding values of the parameter α. In the blunted plate case, $\alpha = 1$ represents a flow past a parabola and $\alpha = 0$ represents the flow past a semi-infinite thick plate with sharp corners. This type of blunt body is considered in order to study the displacement flow past bodies with smooth as well as blunted shoulders and to investigate the effects of such convex corner flows on the optimal coordinate configuration.

The surface skin friction distributions shown in Figure 13 are presented for the bluntness parameter α between 0.2 and 1. The skin friction variation for flow past the parabola has already been discussed in the case of the blunted wedge problem and the results of the same are presented here for the sake of comparison with the skin friction variation for different values of the parameter α. Figure 6 shows that decreasing the value of the parameter α, results in a body shape having larger curvature around the corner. The viscous flow past such bodies would experience larger and larger turning angles around the corner. This fact is displayed in the skin friction plots, which show that with decreasing values of α, the skin friction shows an earlier drop, larger gradients, and a smaller region of adjustment to the

downstream infinity value as compared to the skin friction variation for flow past a parabolic surface. Similar features are also displayed by other flow quantities such as pressure gradient and displacement thickness for decreasing values of α, in Figures 14 and 15 respectively. These characterstic features of the flow quantities such as are shown in the skin friction and the displacement thickness are consistent with the pressure gradient plots obtained for the viscous flow past the corresponding body shapes, represented by the parameter α. One of the flow cases which we will study further is the flow past a blunt body represented by $\alpha = 0.2$ which will turn out to be a case near separation. A classical boundary-layer analysis of flow past a body which is represented by α less than approximately 0.2 would indicate the occurance of flow separation aft of the corner. This fact has previously been observed by Davis[14] in his interacting flow analysis for high Reynolds number flow past a body represented by $\alpha = 0.1$. Considerable numerical difficulties were encountered in order to obtain converged solution for the flow past a blunt body given by α less than 0.2. The pressure gradient parameter in such cases reaches limiting values below -0.199 and the shear stress drops to zero with an infinite slope aft of the corner indicating the onset of separation at that point and no solution could be achieved beyond the separation point indicating that the present solution technique must be modified if one wishes to compute separated flows correctly. We will see in the later part of our discussion that the optimal coordinates for the case of $\alpha = 0.2$ exhibit critical behavior for this near separated flow case.

1c. Optimal Coordinates for Blunted Wedges and Blunted Plates:

It was mentioned in the preceeding section that the displacement thickness is constant for flow past a vertical wall (Hiemenz flow). The condition for optimal coordinates requires that the displacement thickness should be constant in optimal coordinates. This implies that the conformal coordinate system should be optimal for the stagnation flow. The validity of the statement is justified from the fact that the coordinate equation for optimal coordinates yields a constant solution equal to 1 for the coordinate function $t(\xi,\eta)$ in the entire flow field.

The optimal coordinate (ξ,η) system and the conformal (p,q) coordinate system for values of the wedge parameter β between 0.7 and 0.0 are presented in Figures 16 through 18. The optimal coordinates for the wedge parameter $\beta = 0.7$ show little difference from the conformal coordinate system as shown in Figure 16a because the flow represented by $\beta = 0.7$ has characteristics very close to stagnation flow. The differences between the two coordinate systems disappear as we go far from the body which is obvious from the coordinate plots of Figure 16b for flow past the same body shape. With a decrease of the wedge angle at downstream infinity, thereby decreasing the parameter β, the initial differences between the optimal coordinates and the conformal coordinates near the surface of the body increase and this difference dies out as we go far from the body. This can be seen in the optimal coordinate plots shown in Figures 17a and 17b for the flow given by the parameter $\beta = 0.5$. Another interesting feature

displayed in the optimal coordinate plots for $\beta = 0.5$ in Figure 17a is that the variations in the η direction are larger than the variations in the ξ direction. Similar features are also exhibited in the optimal coordinate plots for $\beta = 0.3$ as shown in Figures 18a and 18b except that the optimal coordinates show larger initial differences with respect to the conformal coordinates near the body surface. This difference subsequently disappears as the downstream conditions are reached. The optimal coordinates for the flow past the parabola are presented in Figures 19a and 19b. The optimal coordinates approach the corresponding conformal coordinate system asymptotically at downstream infinity. This characteristic of the coordinate function is in complete agreement with the asymptotic approach of the downstream condition of the displacement flow past a parabola.

Next, the optimal coordinates are obtained for blunted plates for various values of the parameter α. Typical optimal coordinates are presented for α in the range between 0.2 and 0.7 in Figures 20 through 23. The plots of the coordinates near the surface of the body are shown in Figures 20a, 21a, 22a, and 23a. There are larger differences between the optimal coordinates and the corresponding conformal coordinates near the surface. The differences between the two coordinates, as anticipated, disappear near downstream infinity. This is clear from the plots of the coordinates shown in Figures 20b, 21b, 22b, and 23b. Also the gradients of the curve represented by

ξ = C (where C is a constant), near the surface and around the shoulder region decrease with an increase of shoulder bluntness of the blunt body.

2a. Parabolized Navier-Stokes Results in Optimal Coordinates:

The parabolized vorticity-stream function results are obtained for the blunted plate and the blunted wedge problems for low as well as high Reynolds number cases. The numerical solutions are obtained with a step sizes of $\Delta S = 1/40$ and $\Delta N = 1/100$. For a few cases of the problem parameters, the solutions are obtained with larger step sizes of $\Delta S = 1/20$ and $\Delta N = 1/60$. In order to solve the coupled set of coordinate and flow equations two different approaches of treating the partial differential equations were explored. In one case the solution of the parabolic vorticity-stream function equations, and the * (star) level step of the ADI scheme to solve the coordinate equations are carried out simultaneously. At each station represented by ξ = constant, the condition of the optimal coordinates is enforced before advancing to the next station in the streamwise direction. During this operation the (n+1) level coordinate distribution is kept unaltered. Once the condition of optimal coordinates is satisfied by the edge quantities of the flow equation in the entire flow field, the (n+1) level step of the ADI scheme is performed. The above steps are repeated to obtain the converged solution of the coordinate equation.

In the second approach the flow equations are uncoupled from the coordinate equation iteration by linearizing the coefficients dependent

on the coordinate function $t(\xi,\eta)$ by using the preceding iteration value of the coordinate function. The condition of optimal coordinates is not checked until the coordinate solutions are iterated to give a converged solution. The flow charts of both the numerical approaches are presented in Figures 8 and 9.

The first scheme described here was very successful in obtaining accurate converged solution for the blunted wedge cases. Considerable difficulty was encountered with this scheme in obtaining solutions for the blunted plate problem. However, the second scheme was successful in achieving converged solutions for the blunted plate cases. In general, both schemes displayed poor convergence on the coordinate equations for high Reynolds number flow cases, especially in the case of the blunted plate problem.

The fictitious time step Δv used in the ADI scheme was found to vary with the body shape parameter β or α and the Reynolds number Re. A time step of 10 was found to be optimum for obtaining a converged solution of the problems for low and moderately high Reynolds numbers of up to 100. Beyond this value of Reynolds number a larger time step was necessary. For example, for Reynolds number equal to 10^4, a time step of 100 was used to obtain the converged solutions. It was also observed that the convergence process was very much improved by taking initially a larger time step and subsequently reducing it as the iteration proceeded. A further improvement in convergence was achieved by suitable averaging of the two levels of solutions and using the averaged values of the solution vectors at the beginning of the next iteration.

2b. Blunted Wedges

The streamwise distributions of the vorticity function $g(p,q_w)$ at the wall for the case of the parabola are presented in Figure 24 for Reynolds numbers between 0 and 10^4. As the Reynolds number increases, the value of the vorticity function $g(p,q_w)$ at the stagnation point approaches the stagnation flow value given by the Hiemenz solution. At $Re = 10^4$ the skin friction value approaches the stagnation flow value of 1.233 and the Navier-Stokes solution matches with the present boundary-layer solution at the stagnation point for the flow past a parabola. The variations of the vorticity function for the thin flat plate case, which is obtained from the flow past a parabola with $Re = 0$ is also shown in Figure 24. A comparison between the present results and those of Davis[15] for leading edge skin friction on a parabola is given in Figure 25 for Reynolds numbers between 0.1 and 10^4. The agreement for all Reynolds numbers is good. There are small differences between the two results at moderately high Reynolds number between 300 and 1000 as shown in Table 1. Figures 26 and 27 show the vorticity function distribution along the surface of the blunted wedges for $\beta = 0.7$ and 0.5 respectively. Results of the present calculations at the stagnation point for $\beta = 0.7$ and 0.5 agree well with the corresponding results of Davis, U. Ghia and K. Ghia[16] obtained by solving the full Navier-Stokes equations. At downstream infinity the results of the present calculations approach the boundary-layer limit exactly.

2c. Blunted Plates:

The blunted plate analysis using parabolized Navier-Stokes equations is characterized by two parameters, the bluntness parameter α and the Reynolds number Re based on the nose radius of curvature at the stagnation point. Figure 28 shows typical results for skin friction for the blunt plate given by $\alpha = 0.7$. Retaining the value of α and increasing the Reynolds number Re, the shoulder influence is further removed from the point $(0,q_w)$. The leading edge will appear more like a vertical surface for the oncoming stream for high Reynolds number flow cases and the flow in the vicinity of the point $(0,q_w)$ will approach the stagnation flow. Therefore, it is found that with an increase of the value of Re, the vorticity value at the point $(0,q_w)$ approaches the stagnation flow value. The vorticity function $g(p,\bar{q}_w)$ drops along the surface from the stagnation point value to the Blasius value for a flat plate at downstream infinity. Decreasing the value of the parameter α decreases the bluntness of the shoulder. The skin friction distribution for $\alpha = 0.5$ as shown in Figure 29 displays larger gradients and an earlier drop from the stagnation point value as compared to the skin friction distribution for the parameter $\alpha = 0.7$ for the same Reynolds number.

2d. Optimal Coordinates for Blunted Wedges and Blunted Plates:

In the case of boundary-layer analysis we have analyzed the effects of the body shape parameter on the optimal coordinates. In this case the effects of varying the Reynolds number Re have been investigated. The optimal coordinates for flow past blunted wedges and blunted plates

have been obtained for laminar unseparated flow cases. The coordinate calculations were specialized to the limiting cases of flow past a parabolic cylinder, the thin flat plate and the flow against the vertical wall.

The streamwise distributions of the coordinate function for the case of a parabola are shown in Figure 30a for various Reynolds numbers Re, which vary from 0 to 10^4. The coordinate function $t(\xi,0)$ monotonically approaches the correct downstream condition at infinity. With increasing Re, the variations approach the boundary-layer distribution and results of $t(\xi,0)$ match exactly with the boundary-layer solution at Re = 10^4 as shown in Figure 30b, except near the leading edge. For the case of a thin flat plate, the optimal coordinates are obtained by setting Re = 0 in the parabola problem. Results of the surface distribution of $t(\xi,\eta)$ for the thin flat plate are also shown along with the results for the parabola in Figure 30a. Effects of Re on the optimal coordinates for increasing value of the downstream wedge angle are presented in Figures 31 and 32 for wedge parameters of β = 0.3 and 0.5, respectively. Similar features as described in the case of the parabola are observed in these cases. The coordinate distribution for β = 0.7, which represents a flow closer to a stagnation flow, is shown in Figure 33. As anticipated, the parabolized Navier-Stokes solutions agree with the boundary-layer solutions at lower Reynolds number than the cases discussed earlier.

The optimal coordinates were obtained for the blunted plate cases for Reynolds number between 0.1 and 100. Reynolds numbers larger than

a value of 100 were not obtained because of poor convergence of the present numerical scheme. Typical plots of the surface value of the coordinate function are shown in Figures 34 and 35 for $\alpha = 0.7$ and 0.5 and for Reynolds numbers between 0.1 and 100. In all these cases with increasing values of Re, the coordinate function at the surface tends to assume a boundary-layer variation. Since $\alpha = 1$ represents the case of a parabola, the optimal coordinate results for this case have already been discussed along with the blunted wedge cases and will not be repeated here.

The conformal and the optimal coordinate plots for the thin flat plate and the parabola are shown in Figures 36(a,b) and 37(a,b) respectively. The initial differences between the two coordinate systems, such as are observed in Figure 36a for the flat plate case and in Figure 37a for the case of a parabola, tend to reduce as we go further downstream from the body surface. This is clear from the plots shown in Figures-36b and 37b.

Figure 38a shows the conformal and the optimal coordinates near the surface of a blunted wedge represented by $\beta = 0.5$ and for Reynolds number Re = 100. Further downstream of the blunted wedge surface, the optimal coordinates, as shown in Figure 38b, tend to merge with the corresponding conformal coordinates.

VI. CONCLUSIONS

In the present analysis of viscous flow, it has been successfully demonstrated that it is possible to numerically generate a particular set of flow dependent coordinates called optimal coordinates. Results of the integration of these coordinate equations reveal that the optimal coordinates used here may be viewed as a generalized form of conformal coordinates. The optimal coordinates considered here automatically degenerate into convenient sets of coordinates for specific flow fields; for example, in the case of first-order boundary-layer flow past a thin flat plate, the optimal coordinates degenerate into parabolic coordinates, which are the most natural form of the coordinates for the thin flat plate. Similarly for the case of flow against a vertical wall, the optimal coordinates become simple Cartesian coordinates, for both, the boundary-layer flow and the Navier-Stokes flow.

The advantages of viscous flow analysis in optimal coordinates are as follows. Firstly, the boundary-layer solution obtained in optimal coordinates is uniformly valid throughout the entire flowfield. Secondly, similarity conditions are automatically satisfied when similarity exists, with the present form of the coordinates.

The results of the optimal coordinate calculations using parabolized Navier-Stokes equations for the case of the parabola and blunted wedges have shown excellent agreement with the existing results using full Navier-Stokes equations for all Reynolds numbers. This indicates

that the parabolic approximation to the Navier-Stokes equations is a more accurate representation of the full Navier-Stokes equations if the equations are generated in optimal coordinates. The works of Davis[15] and U. Ghia and Davis[31] which used the parabolized Navier-Stokes equations in conformal coordinates (which are semi-optimal in nature) have shown reasonable agreement with full Navier-Stokes results even for low Reynolds numbers, and therefore it was to be expected that the use of optimal coordinates in the parabolic form of the Navier-Stokes equations would further improve the results. The results of the present calculations verify this assumption.

The governing differential equations and the numerical scheme developed in the present study for boundary-layer analysis was found to be successful in predicting first order optimal coordinates.

Present numerical calculations showed that the cross-derivative term β_r, in the coordinate equation can be treated explicity or implicitly in the numerical solution of the coordinate equations for boundary-layer analysis, whereas it was found to be essential to treat the same cross-derivative term β_r implicitly for the parabolized Navier-Stokes analysis for the low Reynolds number cases.

In the parabolized Navier-Stokes analysis, the coordinate equation solution scheme encountered certain difficulties which are worth mentioning. The first iterative scheme mentioned in the parabolic Navier-Stokes analysis displayed poor convergence of the solution of the coordinate equation for high Reynolds numbers. However the use of the second or the uncoupled iterative scheme was found to improve

the convergence of the problem for most blunt body cases. It was also observed in general that the relaxation process of the coordinate equation becomes very sensitive to the fictitious time step, Δv, and the initialization process of the coordinate function for high Reynolds number cases. While the second scheme enjoys a greater flexibility of choice of the time step Δv and the initialization process of the coordinate function as compared to the first, difficulties were still encountered for Reynolds numbers greater than 100 for blunted plate problems. Therefore a future effort should be made to resolve the problem of poor convergence for high Reynolds number.

REFERENCES

1. Kaplun, S., "The Role of Coordinate System in Boundary-Layer Theory," Journal of Applied Mathematics and Physics, (ZAMP), 5, Vol. V., 1954, pp. 111-135.

2. Latta, G.E., "Singular Perturbation Problem," Ph.D. Thesis, California Institute of Technology, 1951.

3. Von Misses, R. and Friedrichs, K.O., "Fluid Dynamics," Chapter IV, Brown University Notes, Summer 1941.

4. Weyl, H., "On the Differential Equations of the Simplest Boundary Layer Problems," Ann. Math. 43, No. 2, April 1942, pp. 381-407.

5. Segel, L.A., "A Uniformly-Valid Asymptotic Expansion of the Solution to an Unsteady Boundary-Layer Problem," J. Math. and Physics, 39, 1960, pp. 189-197.

6. Crespo da Silva, M.R.M. and Davis, R.T., "A Study of Optimal Coordinate Theory with Application to Several Physical Problems," International Journal of Engineering Science, 1977, Vol. 15, pp. 455-464.

7. Legner, H.H., "On Optimal Coordinates and Boundary Layer Theory," Doctoral Thesis, Department of Aeronautics and Astronautics, Stanford University, July 1971.

8. Zauderer, E., "Boundary Layer and Uniform Asymptotic Expansions for Diffraction Problems," SIAM J. Appl. Math., 19, pp. 575-600.

9. Van Dyke, M.D., "Higher Approximations in Boundary Layer Theory - Parabola in Uniform Stream," J. of Fluid Mechanics, Vol. 19, Part 1, 1964, pp. 145-159.

10. Davis, R.T., "A Study of the Use of Optimal Coordinates in the Solution of the Navier-Stokes Equations," AFL Report No. 74-12-14, Department of Aerospace Engineering, University of Cincinnati.

11. Thompson, J.F., Thames, F.C. and Mastin, C.W., "Automatic Numerical Generation of Body Fitted Curvilinear Coordinate System for Field Containing Any Number of Arbitrary Two Dimensional Bodies," Journal of Computational Physics, (15), 1974, pp. 229.

12. Thames, F.C., Thompson, J.F. and Mastin, C.W., "Numerical Solutions for Viscous and Potential Flow About Arbitrary Two Dimensional Bodies Using Body Fitted Coordinate System," Journal of Computational Physics, 24, 1977, pp. 245-273.

13. Thompson, J.F., Thames, F.C., Mastin, C.W. and Shanks, S.P., "Use of Numerically Generated Body Fitted Curvilinear Coordinate Systems for Solution of the Navier-Stokes Equation," Proceedings of the AIAA 2nd Computational Fluid Dynamics Conference, Hartford, Connecticut, 1975.

14. Davis, R.T., "Numerical Solution of the Incompressible Navier-Stokes Equations for Two-Dimensional Flows at High Reynolds Number," First International Conference on Numerical Ship Hydro-dynamics. Edited by Joanna W. Scot and Nils Salveson, Vol. 20-22, October 1975.

15. Davis, R.T., "Numerical Solutions of Navier-Stokes Equations for Symmetric Laminar Incompressible Flow Past a Parabola," Journal of Fluid Mechanics, Vol. 51, Part 3, 1972, pp. 417-433.

16. Davis, R.T., Ghia, U. and Ghia, K.N., "Laminar Incompressible Flow Past Blunted Wedges," Int. Journal of Computers and Fluids, Vol. 2, 1974, pp. 211-223.

17. Ghia, U. and Davis, R.T., "Solution of Navier-Stokes Equations for Flow Past a Class of Two-Dimensional Semi-Infinite Bodies," Preliminary Version published as AIAA Paper No. 74-12, also Final Version in AIAA Journal, Vol. 12, No. 12, December 1974.

18. Werle, M.J. and Bernstein, J.M., "A Comparative Numerical Study of Approximation to Navier-Stokes Equations for Incompressible Separated Flow," Report No. AFL 74-7-12, Department of Aerospace Engineering, University of Cincinnati, August 1974.

19. Van Dyke, M.D., "Perturbation Methods in Fluid Mechanics," Academic Press, New York and London, 1969.

20. Lagerstrom, P.A., "Laminar Flow Theory," in "Theory of Laminar Flows," edited by F.K. Moore, Princeton University Press, 1964.

21. Schlichting, H., "Boundary Layer Theory," McGraw-Hill Series in Mechanical Engineering, McGraw Hill Book Company, New York.

22. Blottner, F.G. and Flugge-Lotz, I., "Finite Difference Computation of the Boundary Layer With Displacement Thickness Interaction," J. Mechnique, 2, 1963, pp. 397-423.

23. Van de Vooren, A.I. and Dijkstra, D., "The Navier-Stokes Solution for Laminar Flow Past a Semi-Infinite Flat Plate," J. Engineering Math., 4, 1970, pp. 9-27.

24. Thomas, L.H., "Elliptic Problems in Linear Difference Equations Over a Network," Watsons Science Computing Lab. Report, Columbia University, 1949.

25. Douglas, J., "On the Numerical Integration of $[(\partial^2 u/\partial x^2)+(\partial^2 u/\partial y^2) = (\partial u/\partial t)]$ by Implicit Methods," J. SIAM, 3, 1955, pp. 42-65.

26. Roache, P.J., "Computational Fluid Dynamics," Hermosa Publishers, Albuquerque, NM, 1976.

27. Iynger, S.R.K. and Jain, M.K., "Comparative Study of Two and Three Level ADI Methods for Parabolic Equations with a Mixed Derivative," International Journal for Numerical Methods in Engineering," Vol. 10, 1976, pp. 1309-1315.

28. Ghia, U. and Ghia, K.N., "Numerically Generation of a System of Curvilinear Coordinates for Turbine Cascade Flow Analysis," Lecture Notes on Physics, Vol. 59, June 1976, pp. 197-204.

29. Mitchel, A.R., "Computational Methods in Partial Differential Equations," John Wiley and Sons, Ltd.

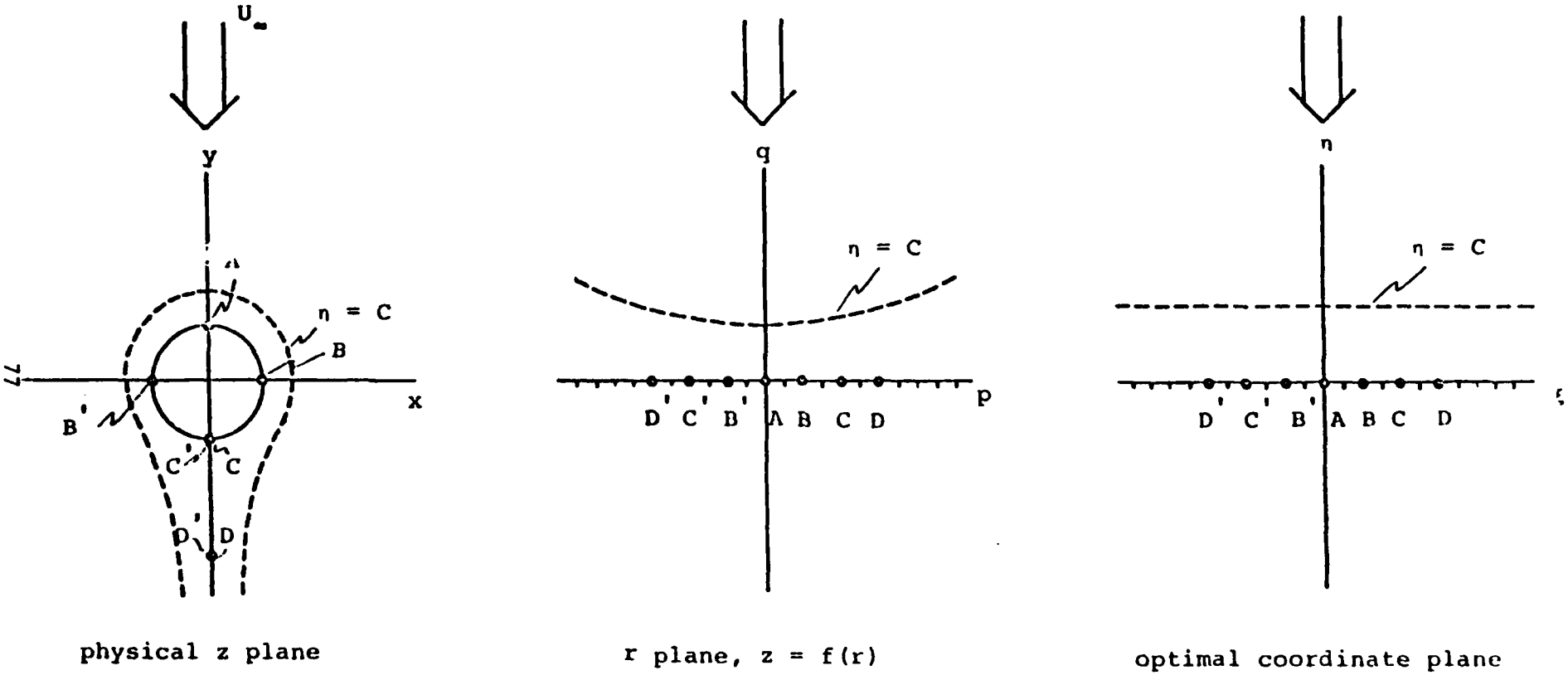

physical z plane

r plane, z = f(r)

optimal coordinate plane

Figure 1. RELATIONSHIP BETWEEN THE PHYSICAL, CONFORMAL, AND OPTIMAL COORDINATE PLANES (After Davis[10])

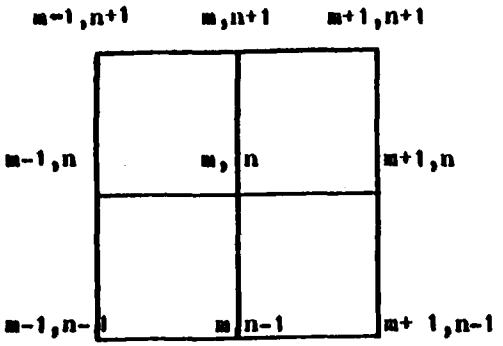

For $\beta_r = 0$

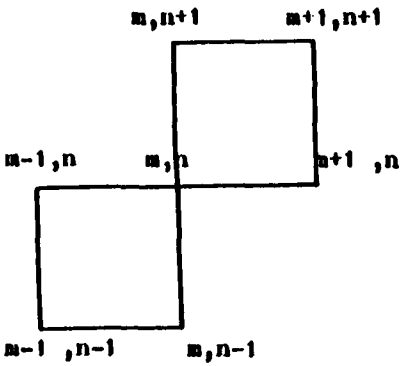

For $\beta_r < 0$

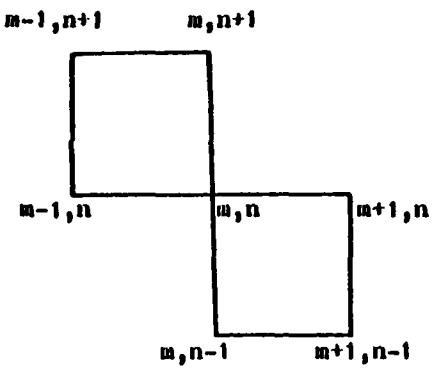

For $\beta_r > 0$

FIG. 2. VARIOUS SCHEMES FOR A MIXED DERIVATIVE

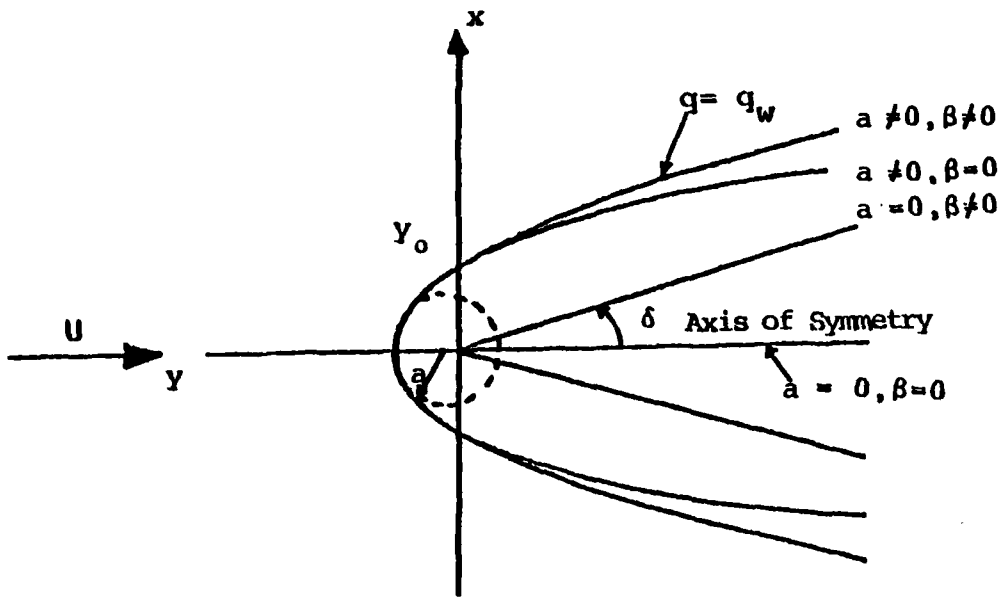

PHYSICAL PLANE

FIG. 3a. BLUNTED WEDGE IN CARTESIAN COORDINATES
(After Davis[16])

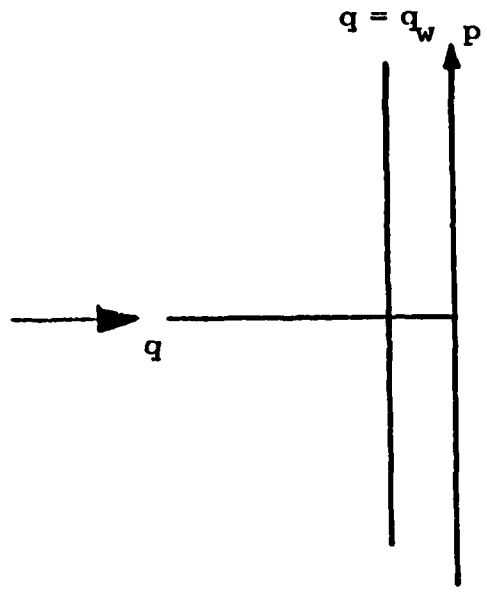

CONFORMAL PLANE

FIG. 3b. BLUNTED WEDGE IN CONFORMAL COORDINATES
(After Davis[16])

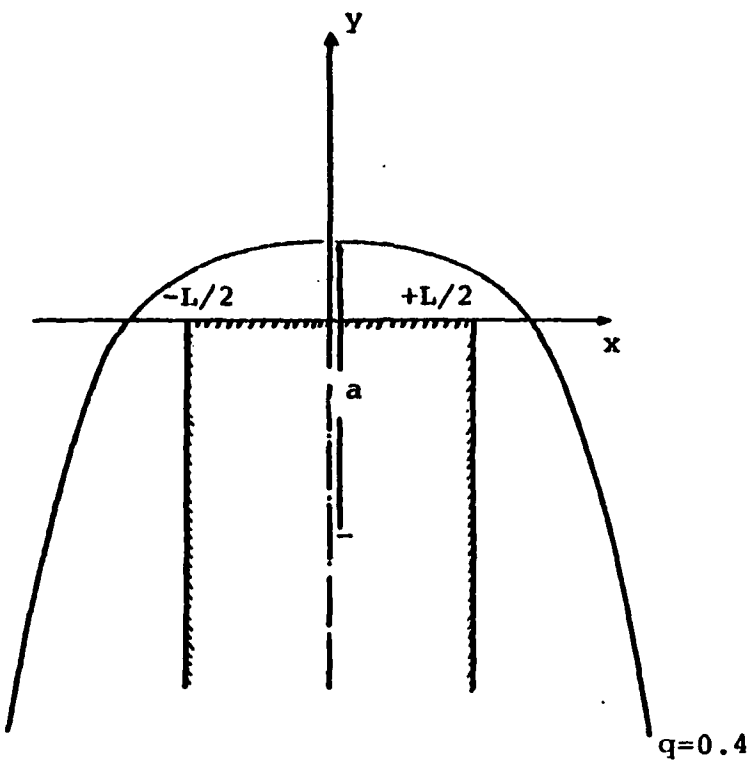

PHYSICAL PLANE

FIG. 4. SEMI-INFINITE THICK PLATE IN CARTESIAN COORDINATES

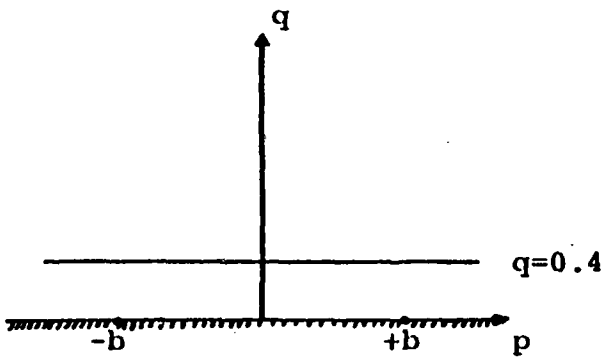

CONFORMAL PLANE

FIG. 5. SEMI-INFINITE THICK PLATE IN CONFORMAL COORDINATES

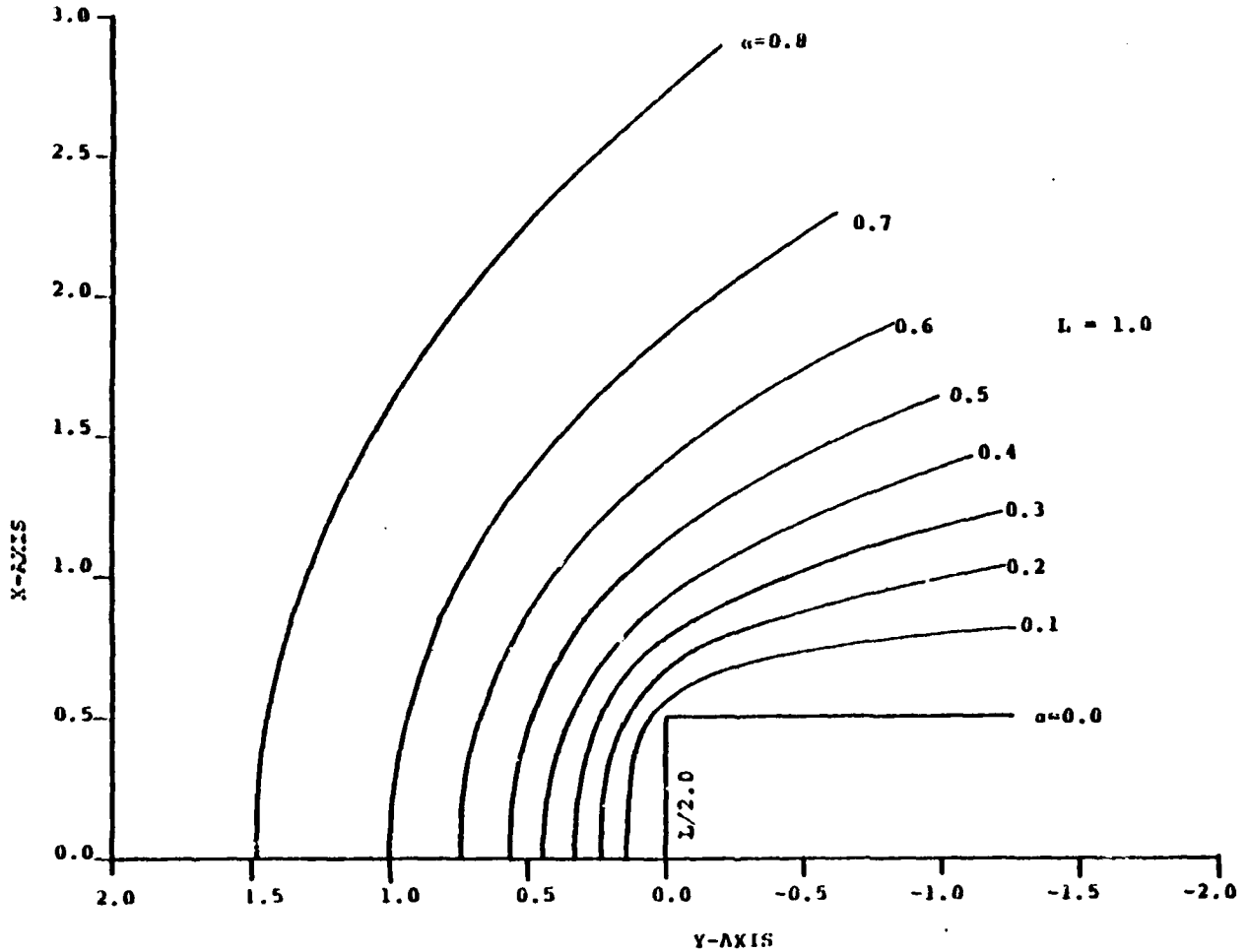

FIG. 6. BODY SHAPES IN THE PHYSICAL PLANE

AD-A080 443 CINCINNATI UNIV OH DEPT OF AEROSPACE ENGINEERING AND--ETC F/G 20/4
CALCULATION OF OPTIMAL COORDINATES FOR TWO-DIMENSIONAL INCOMPRE--ETC(U)
JUL 79 R T DAVIS, R K ROUT N00014-76-C-0359
UNCLASSIFIED AFL-79-7-47 NL

2 OF 2
AD A080443

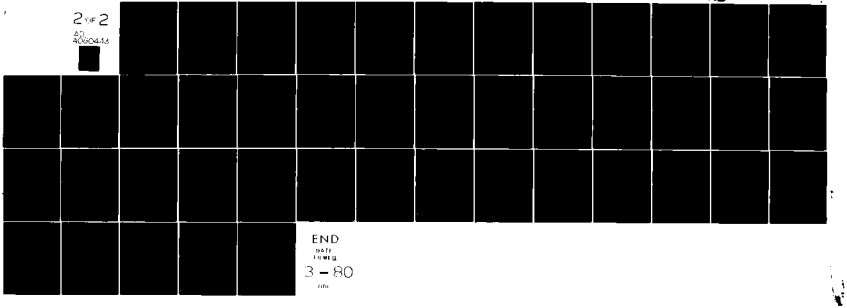

END
DATE FILMED
3-80
DTIC

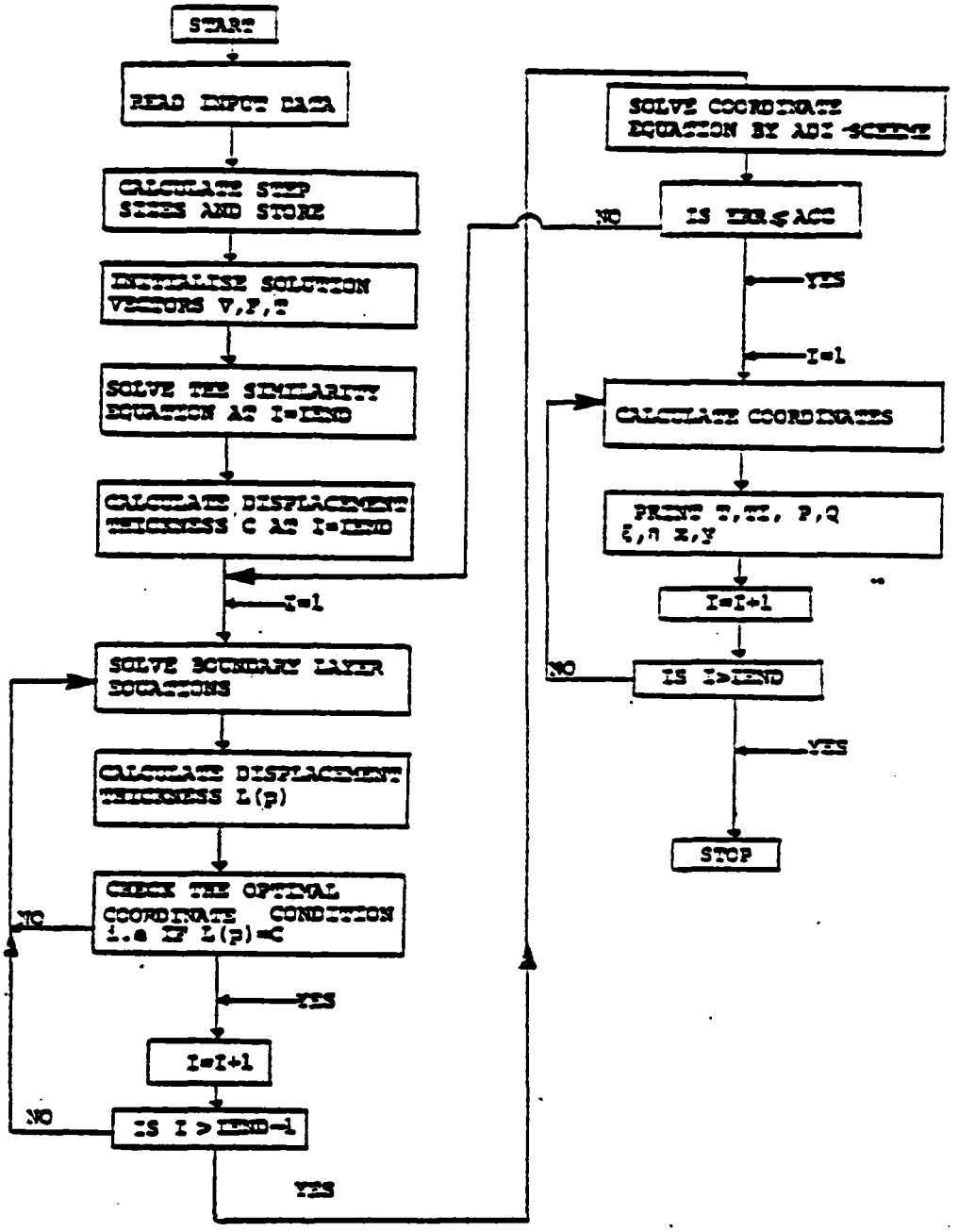

FIG. 7. FLOW CHART FOR SOLVING BOUNDARY-LAYER EQUATIONS IN OPTIMAL COORDINATES

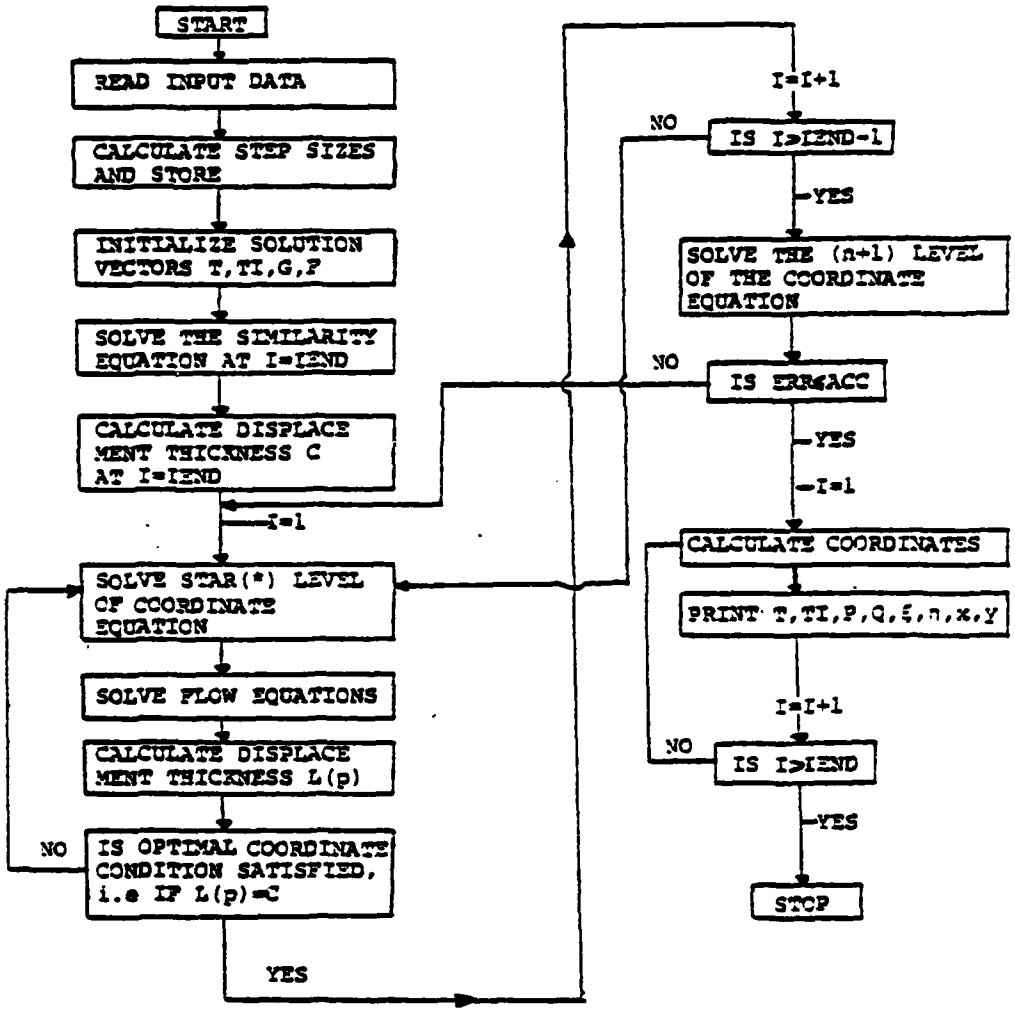

FIG. 8. FLOW CHART FOR SOLVING PARABOLIZED NAVIER-STOKES EQUATIONS IN OPTIMAL COORDINATES BY COUPLED SCHEME

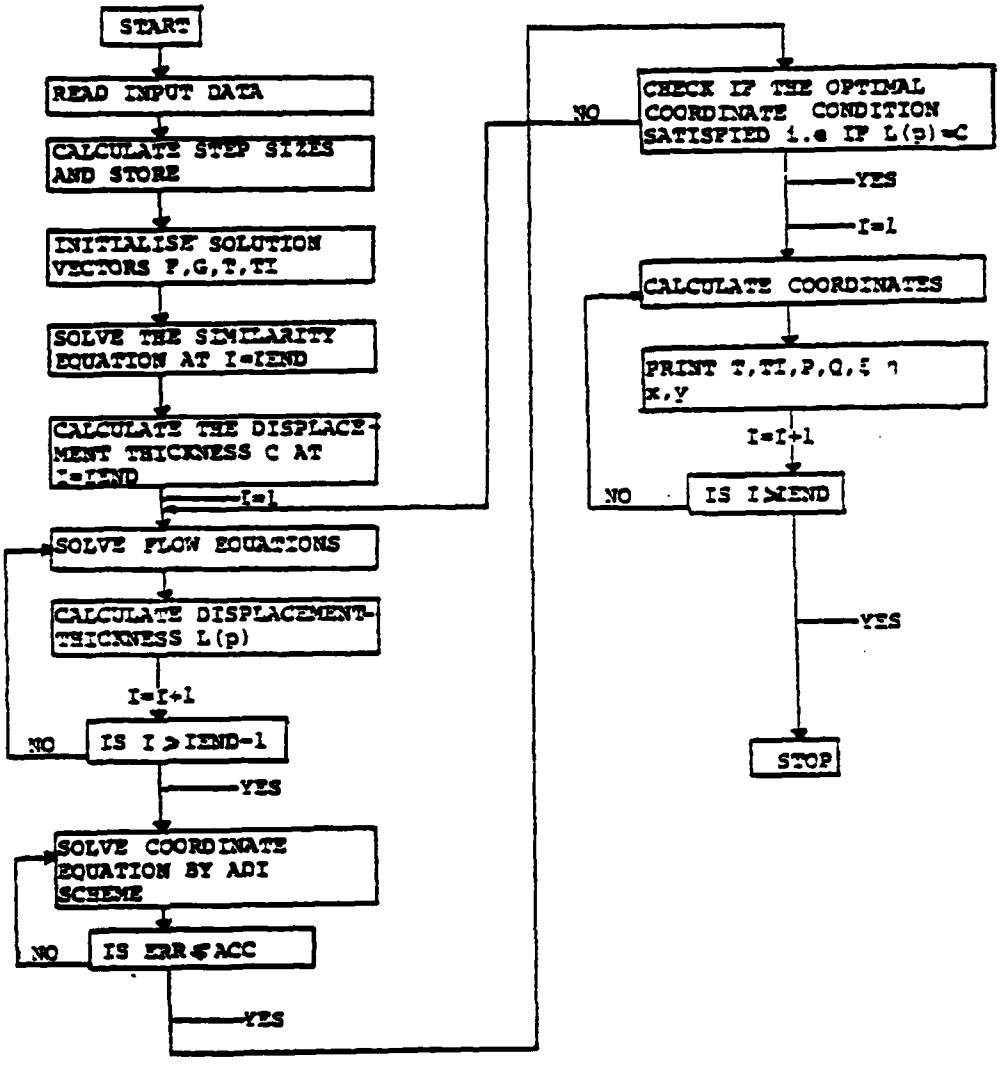

FIG. 9. FLOW CHART FOR SOLVING PARABOLIZED NAVIER-STOKES EQUATIONS IN OPTIMAL COORDINATES BY UNCOUPLED SCHEME

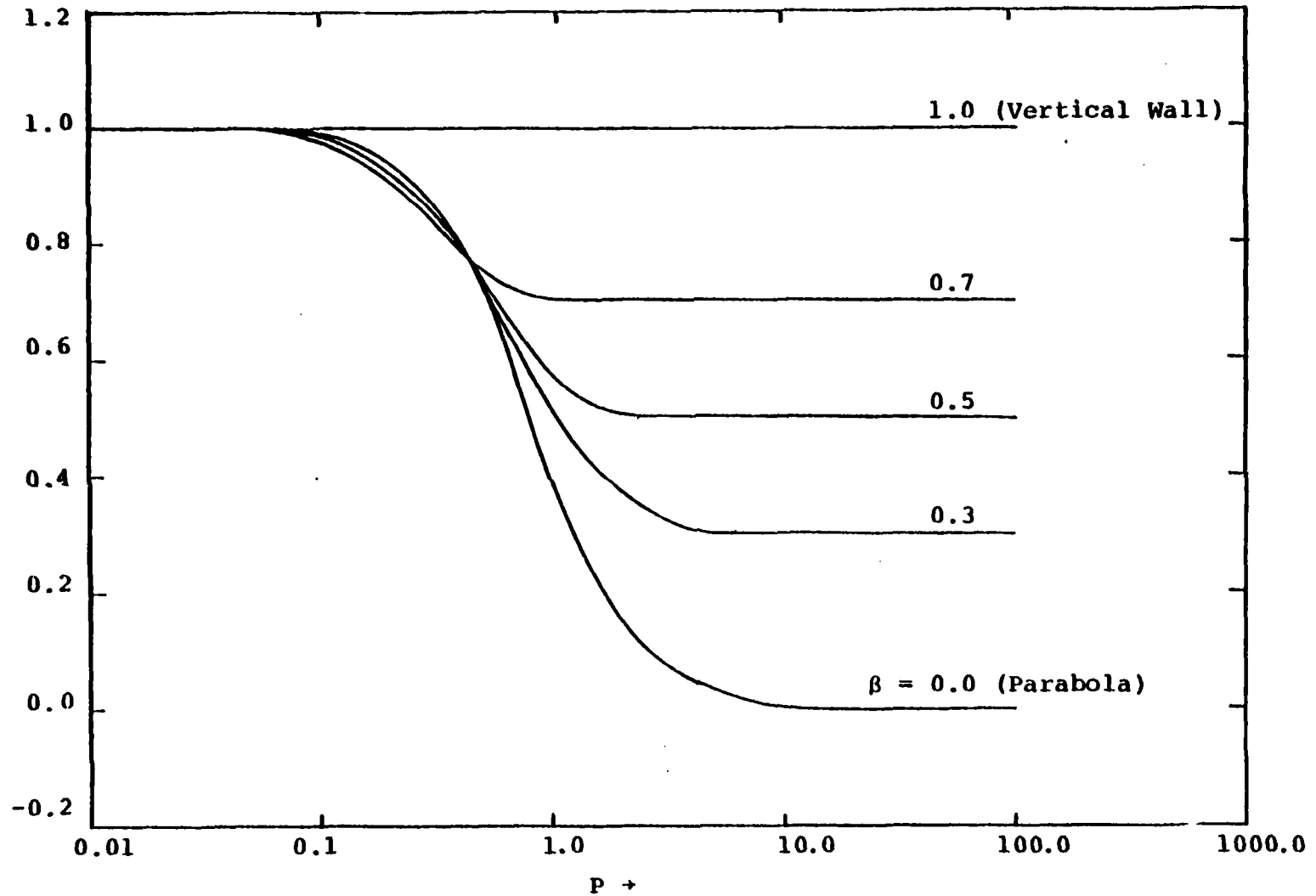

FIG. 10. PRESSURE GRADIENT DISTRIBUTIONS FOR BLUNTED WEDGES

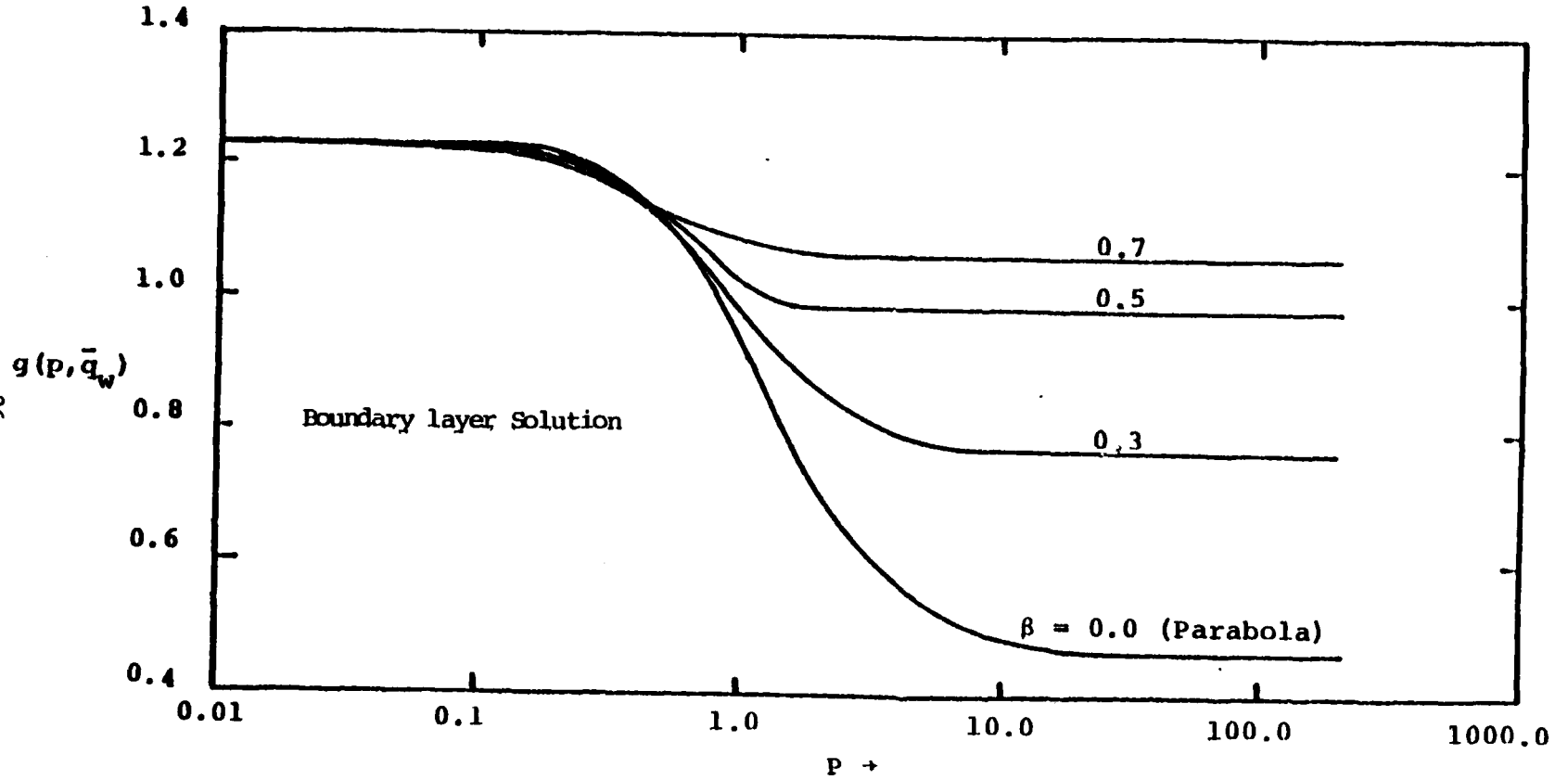

FIG. 11. SKIN FRICTION DISTRIBUTIONS FOR BLUNTED WEDGES

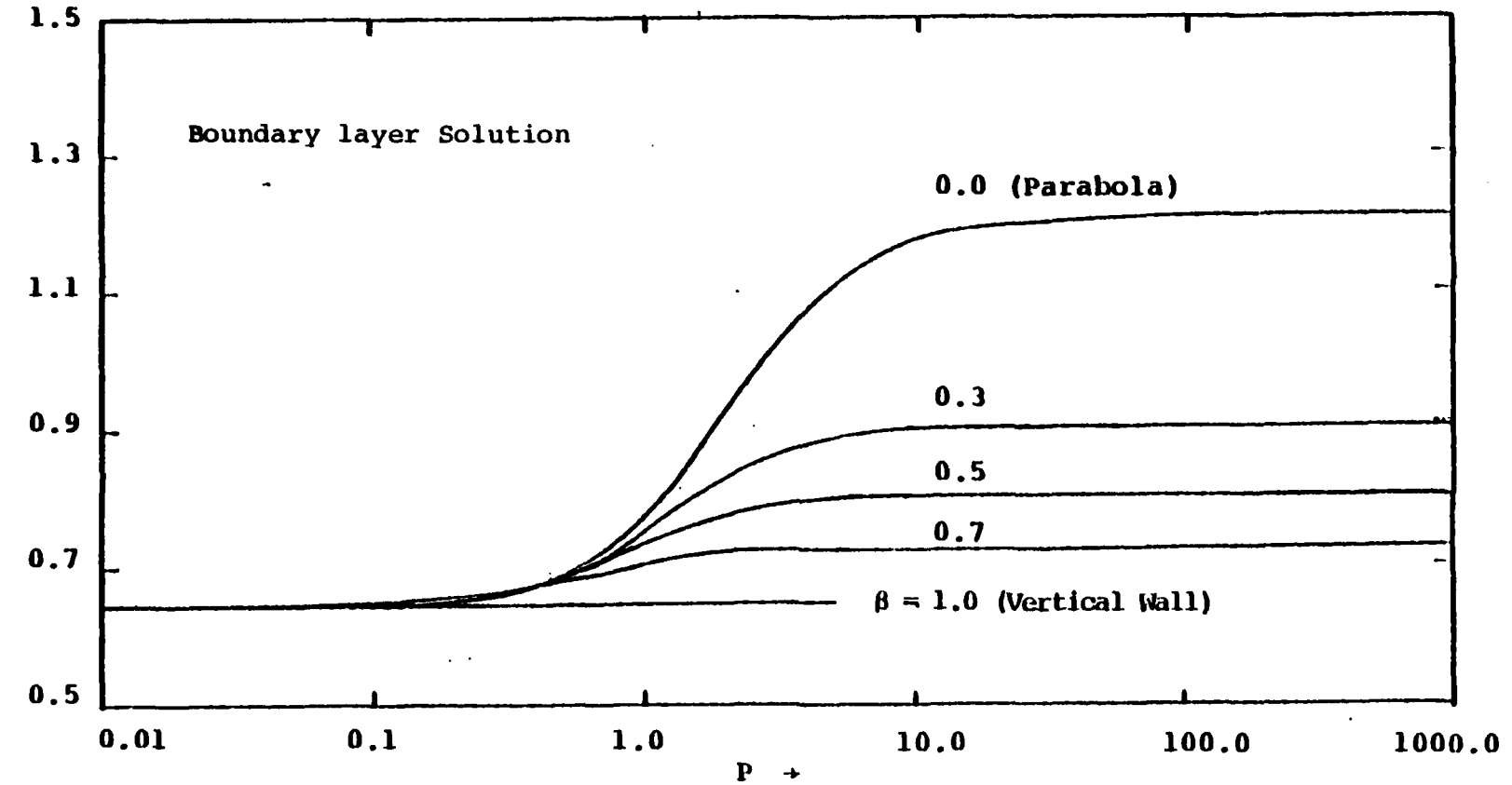

FIG. 12. DISPLACEMENT FUNCTION DISTRIBUTIONS FOR BLUNTED WEDGES

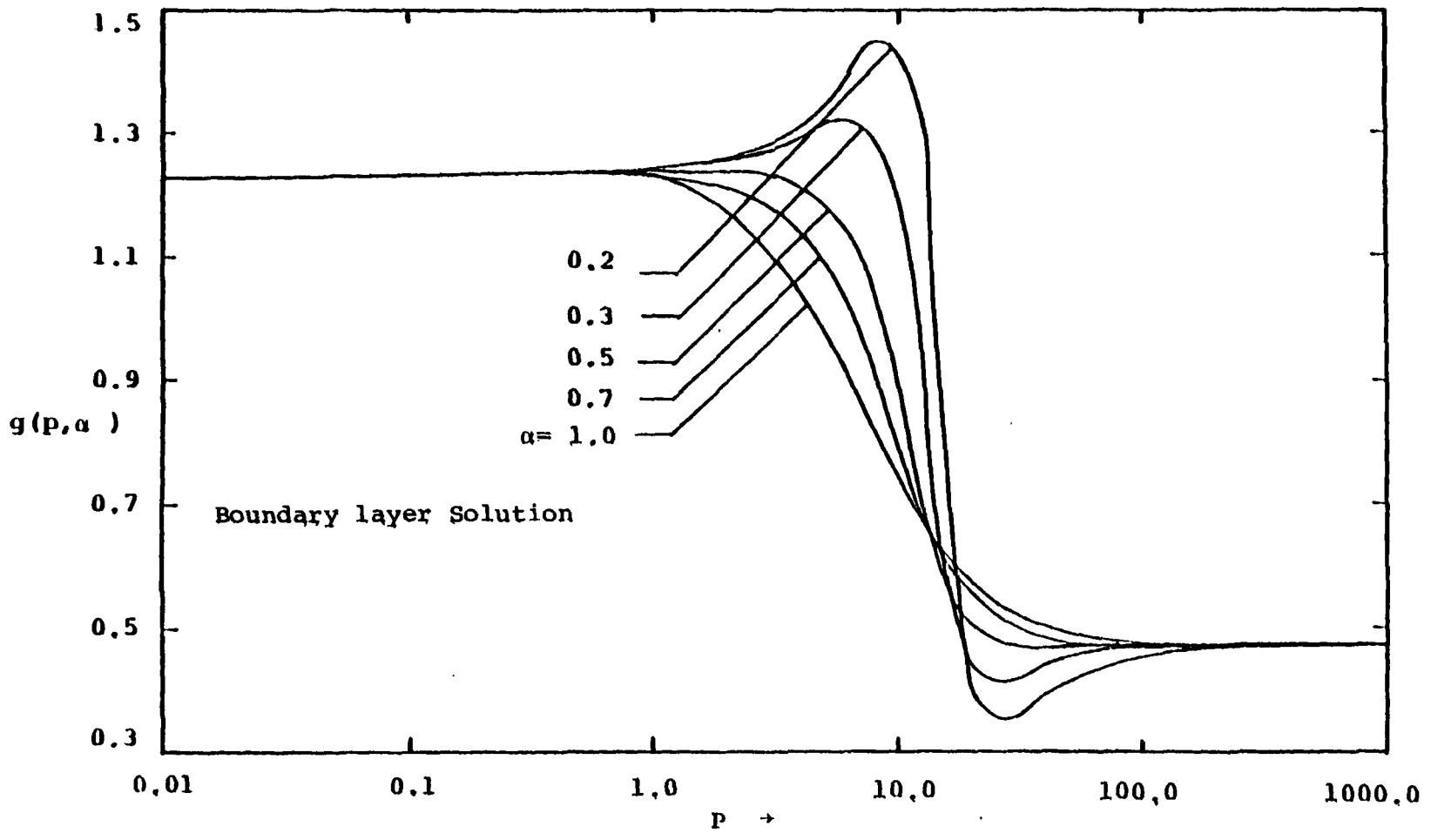

FIG. 13. SKIN FRICTION DISTRIBUTIONS FOR BLUNTED PLATES

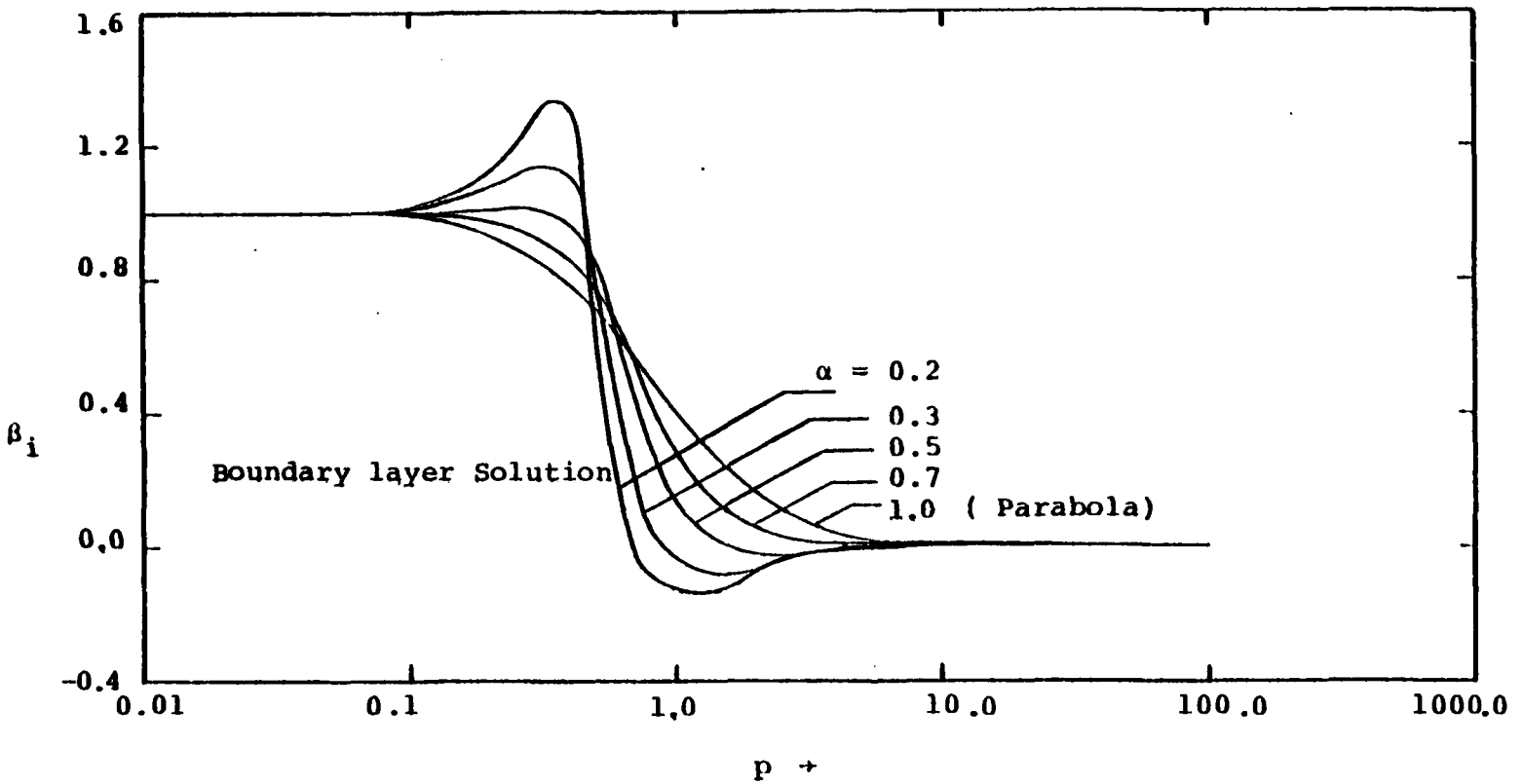

FIG. 14., PRESSURE GRADIENT DISTRIBUTIONS FOR BLUNTED PLATES

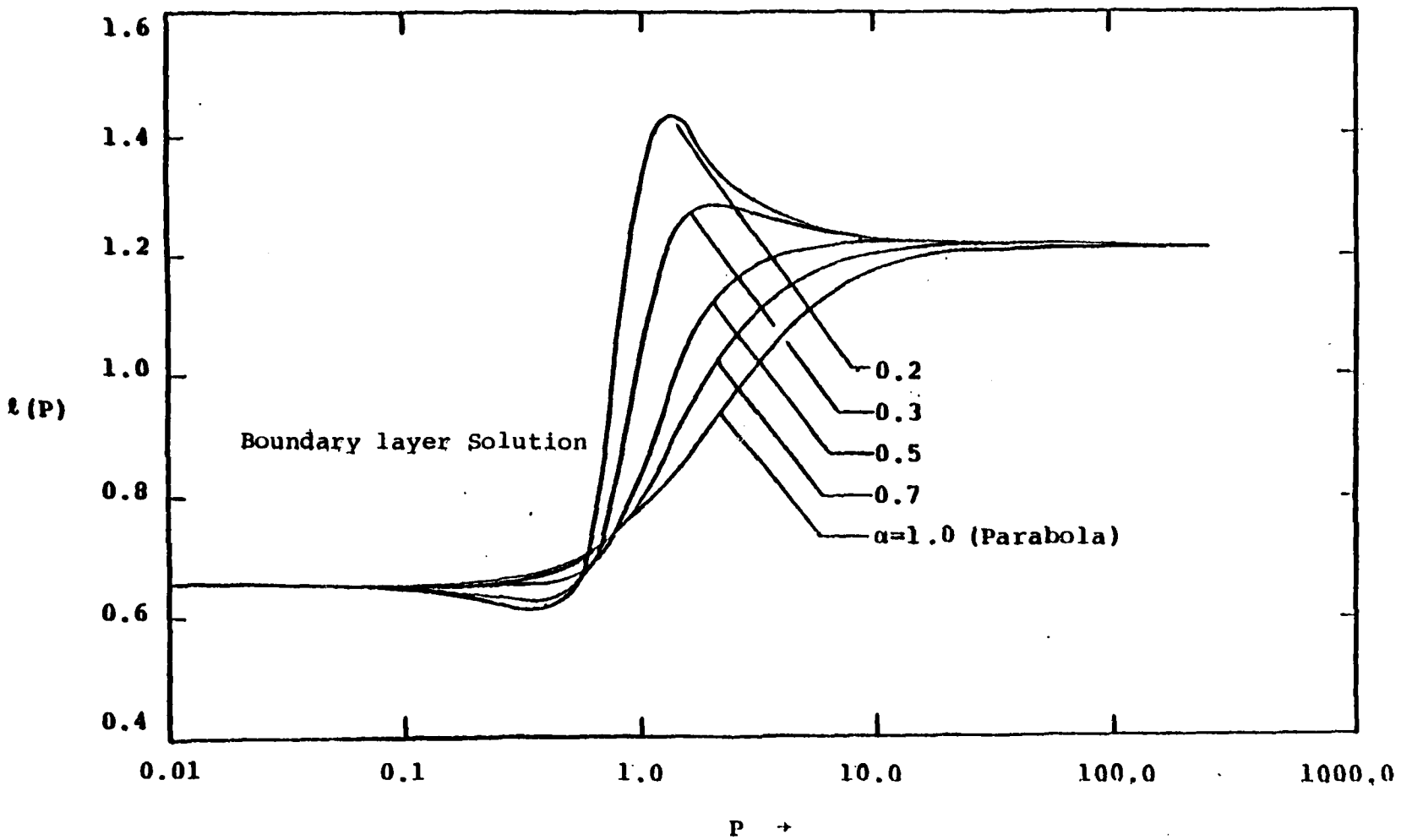

FIG. 15. DISPLACEMENT FUNCTION DISTRIBUTIONS FOR BLUNTED PLATES

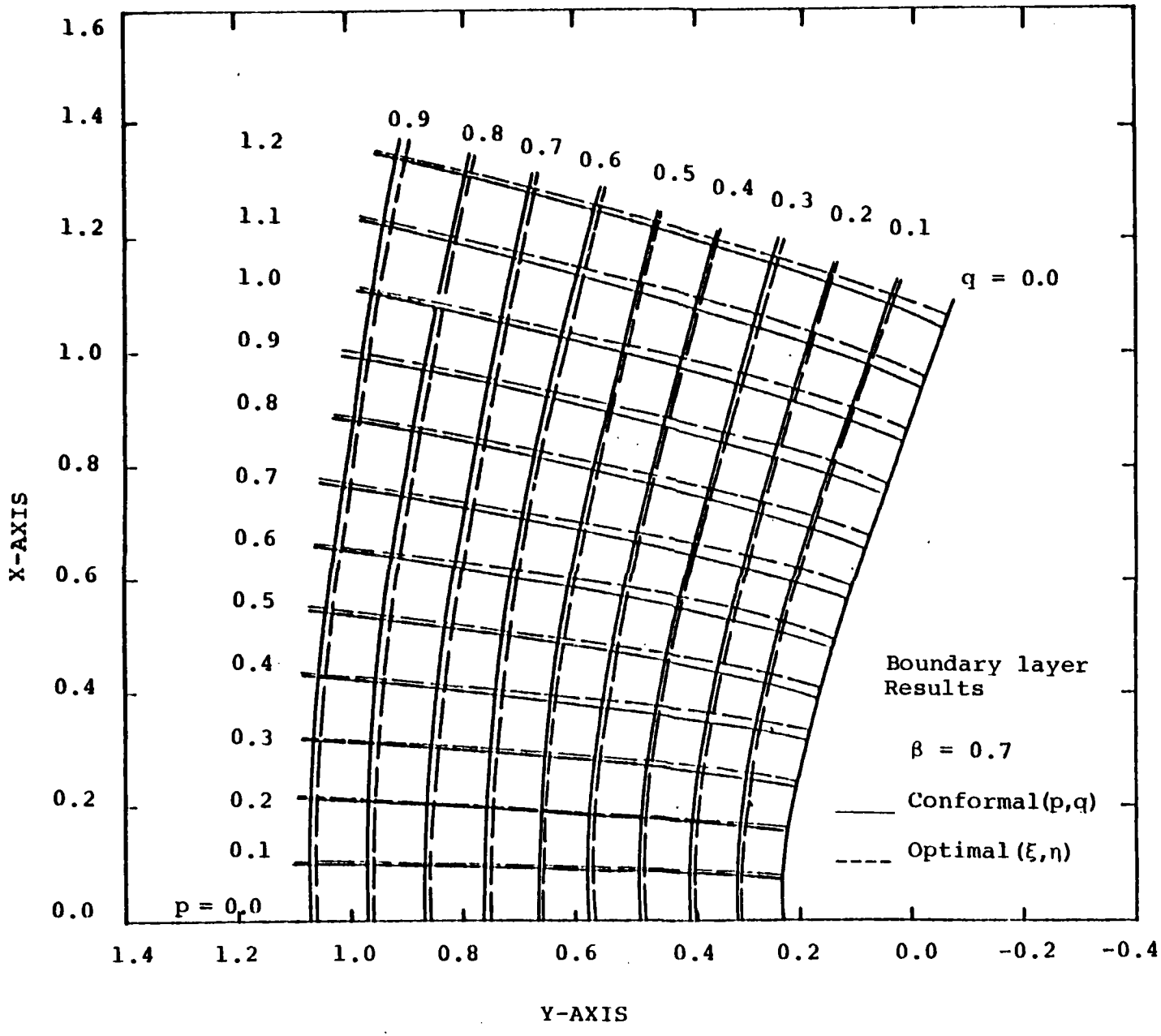

FIG. 16a. CONFORMAL AND OPTIMAL COORDINATES FOR BLUNTED WEDGE

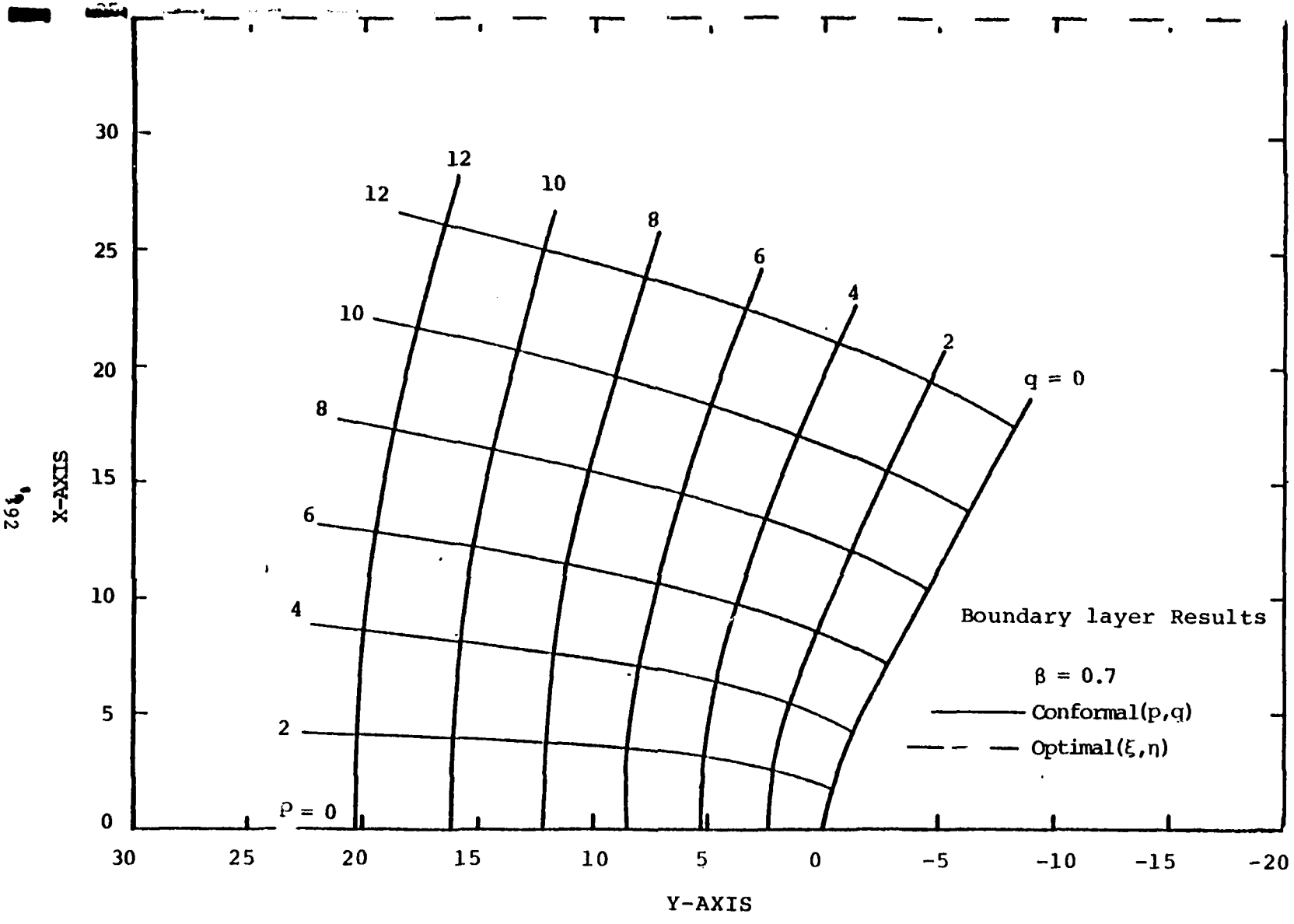

FIG. 16b. CONFORMAL AND OPTIMAL COORDINATES FOR BLUNTED WEDGE

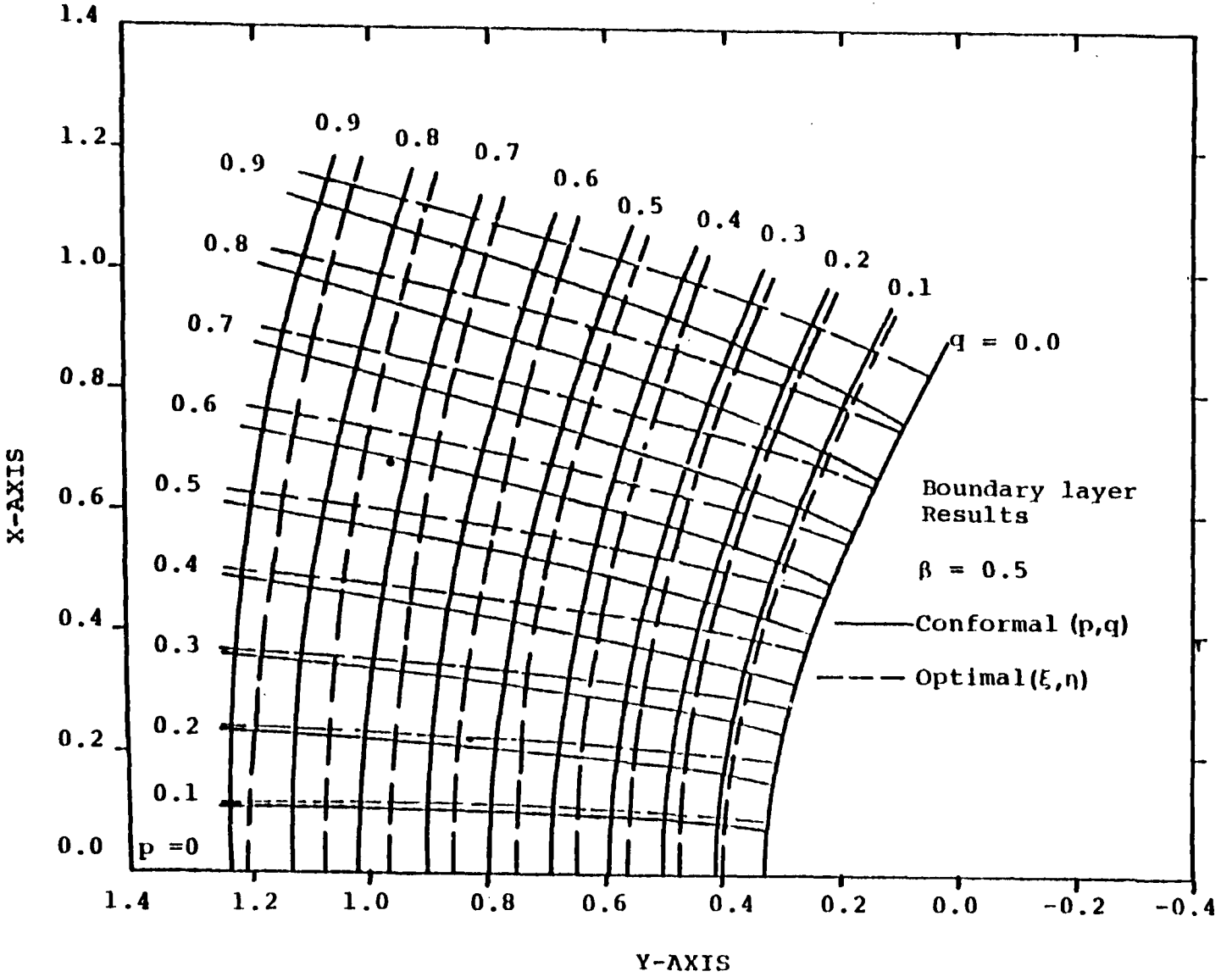

FIG. 17a. CONFORMAL AND OPTIMAL COORDINATES FOR BLUNTED WEDGE

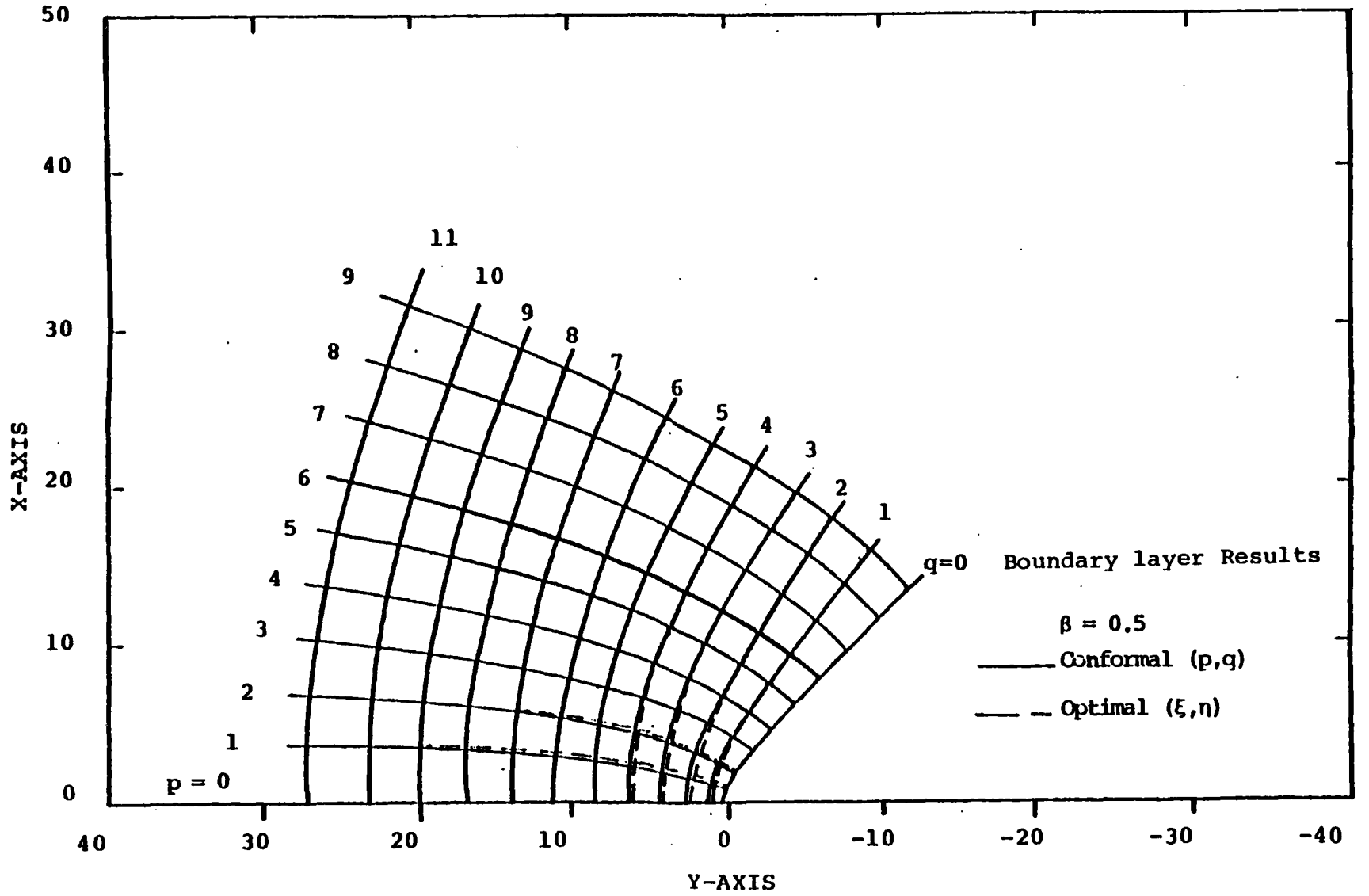

FIG. 17b. CONFORMAL AND OPTIMAL COORDINATES FOR BLUNTED WEDGE

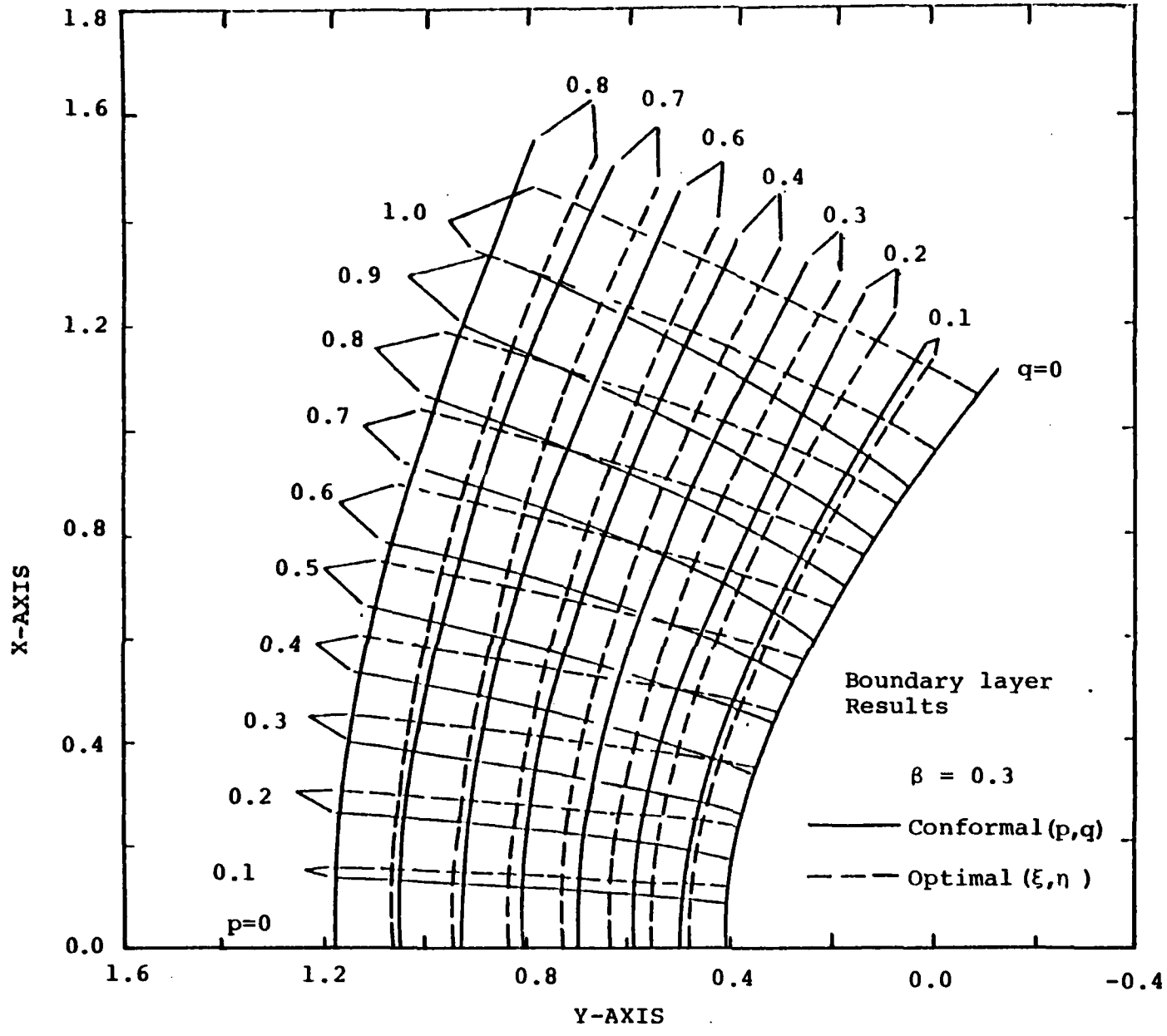

FIG. 18a. CONFORMAL AND OPTIMAL COORDINATES FOR BLUNTED WEDGE

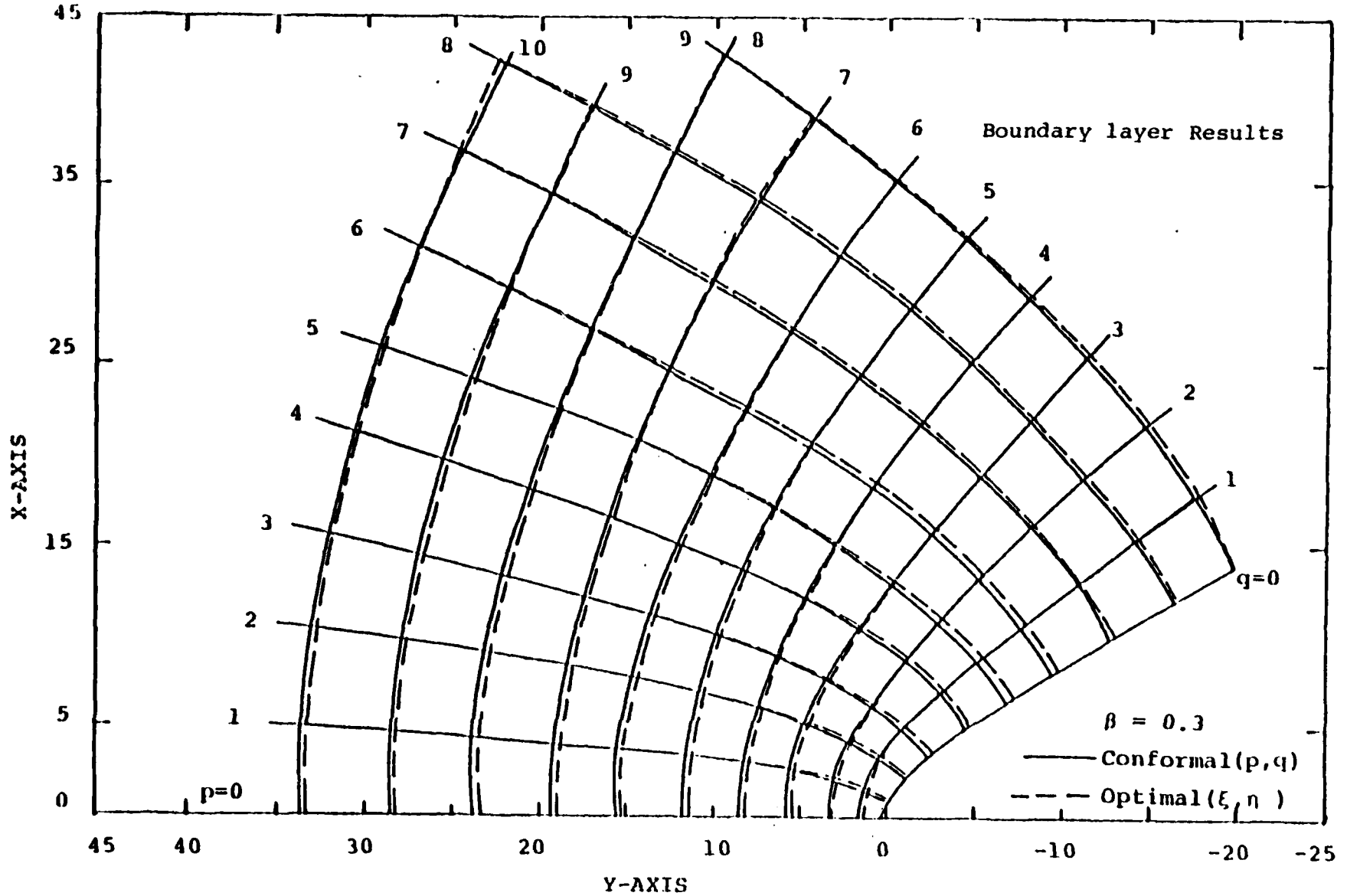

FIG. 18b. CONFORMAL AND OPTIMAL COORDINATES FOR BLUNTED WEDGE

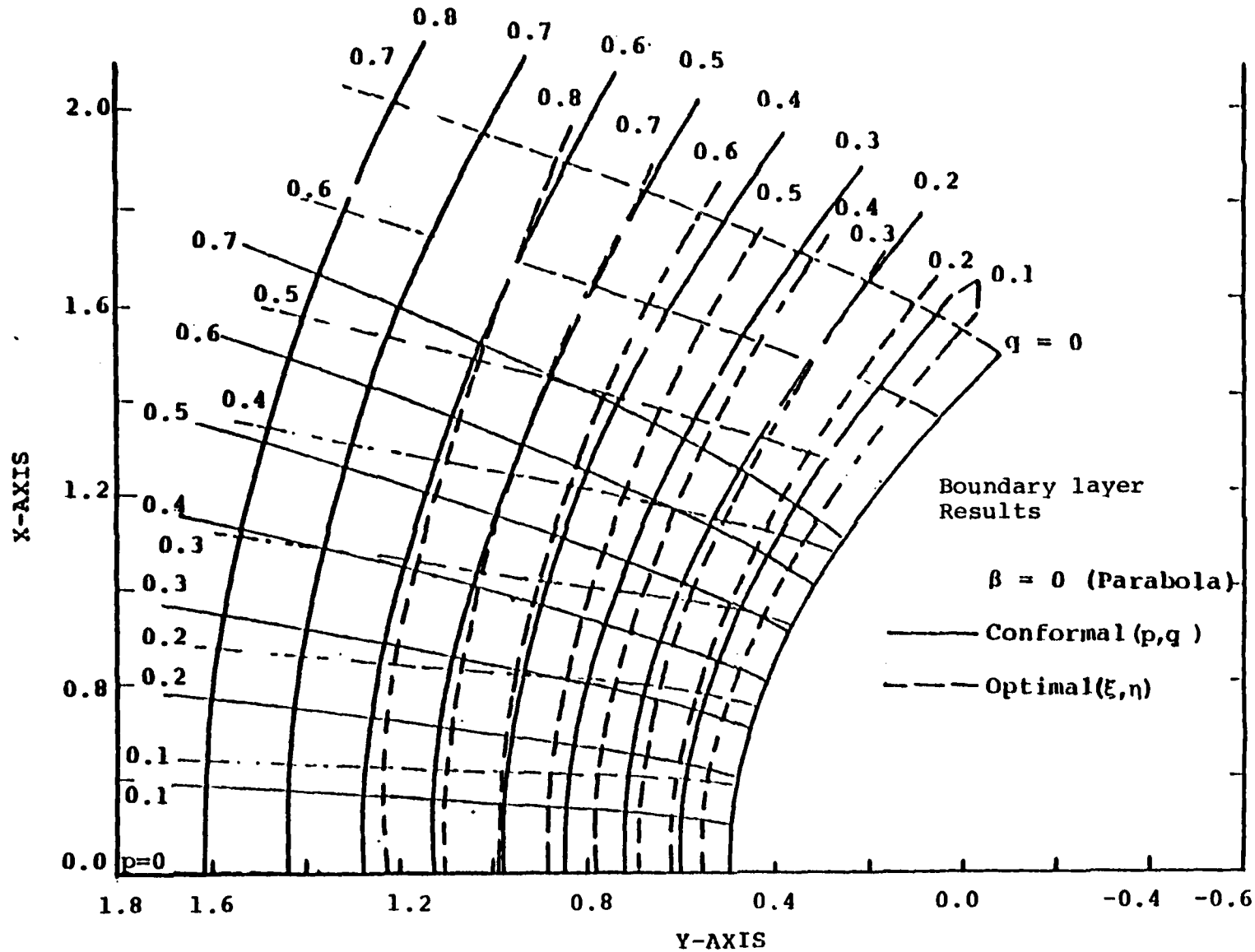

FIG. 19a. CONFORMAL AND OPTIMAL COORDINATES FOR PARABOLA

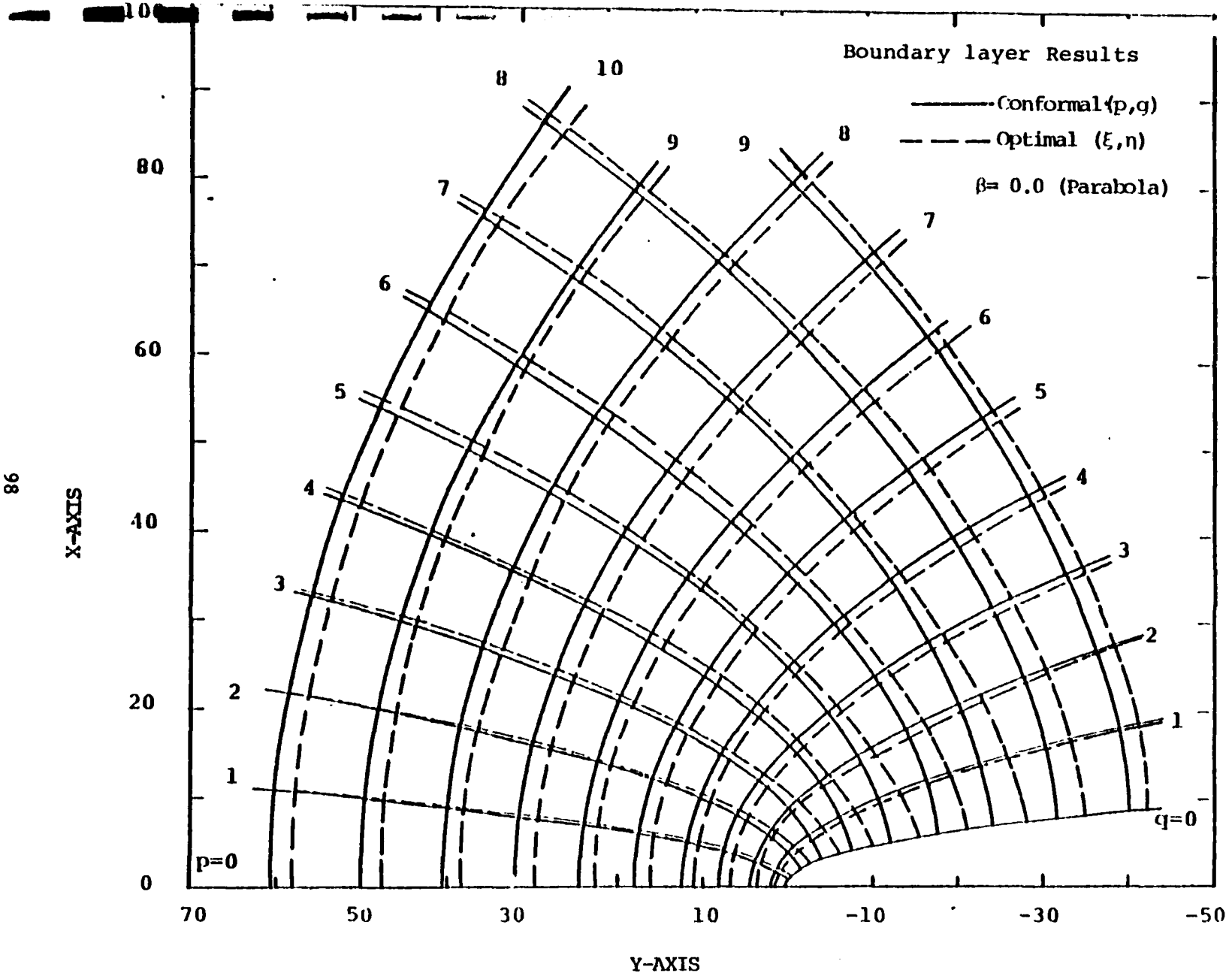

FIG. 19b. CONFORMAL AND OPTIMAL COORDINATES FOR PARABOLA

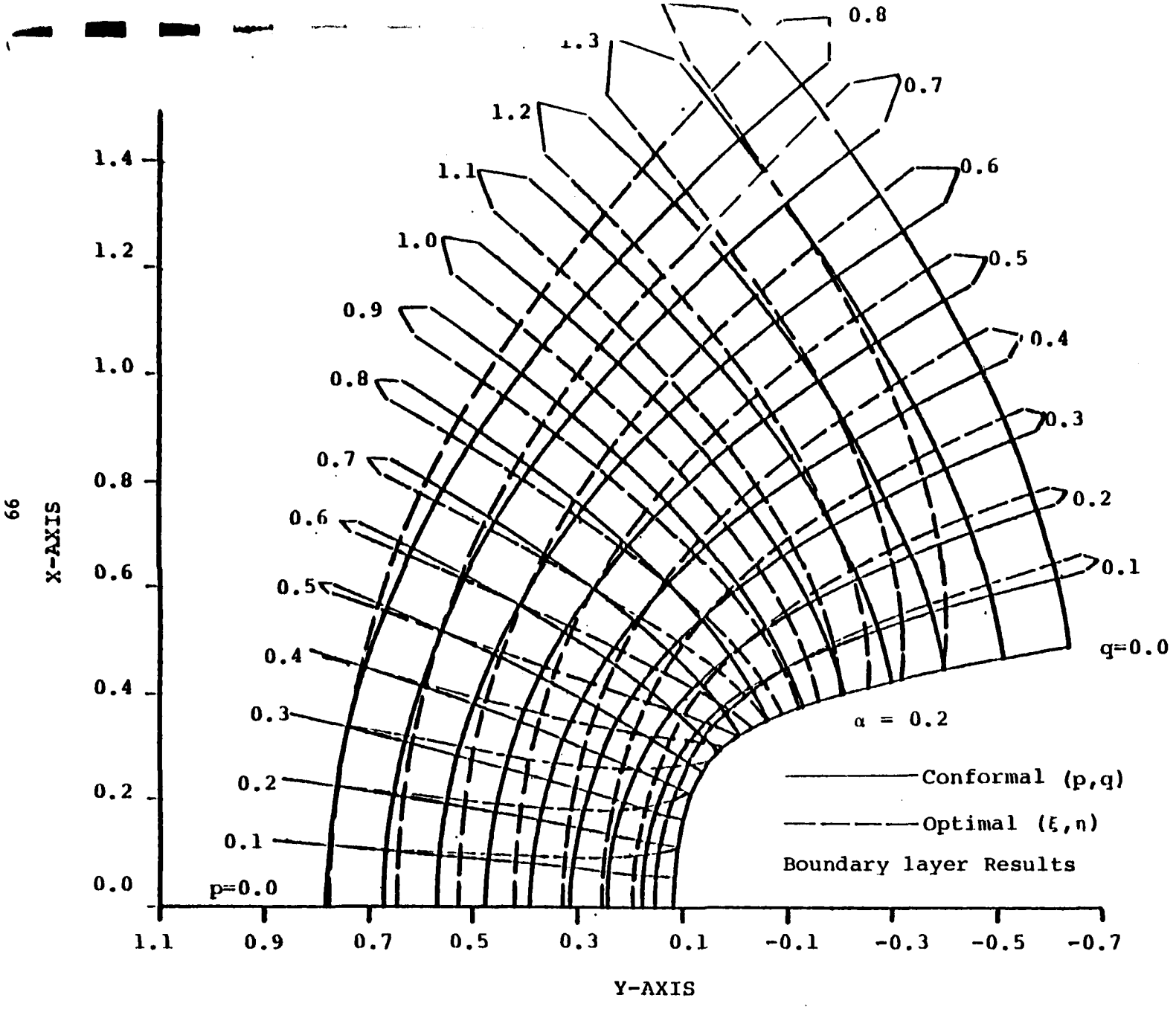

FIG. 20a. CONFORMAL AND OPTIMAL COORDINATES FOR BLUNTED PLATE

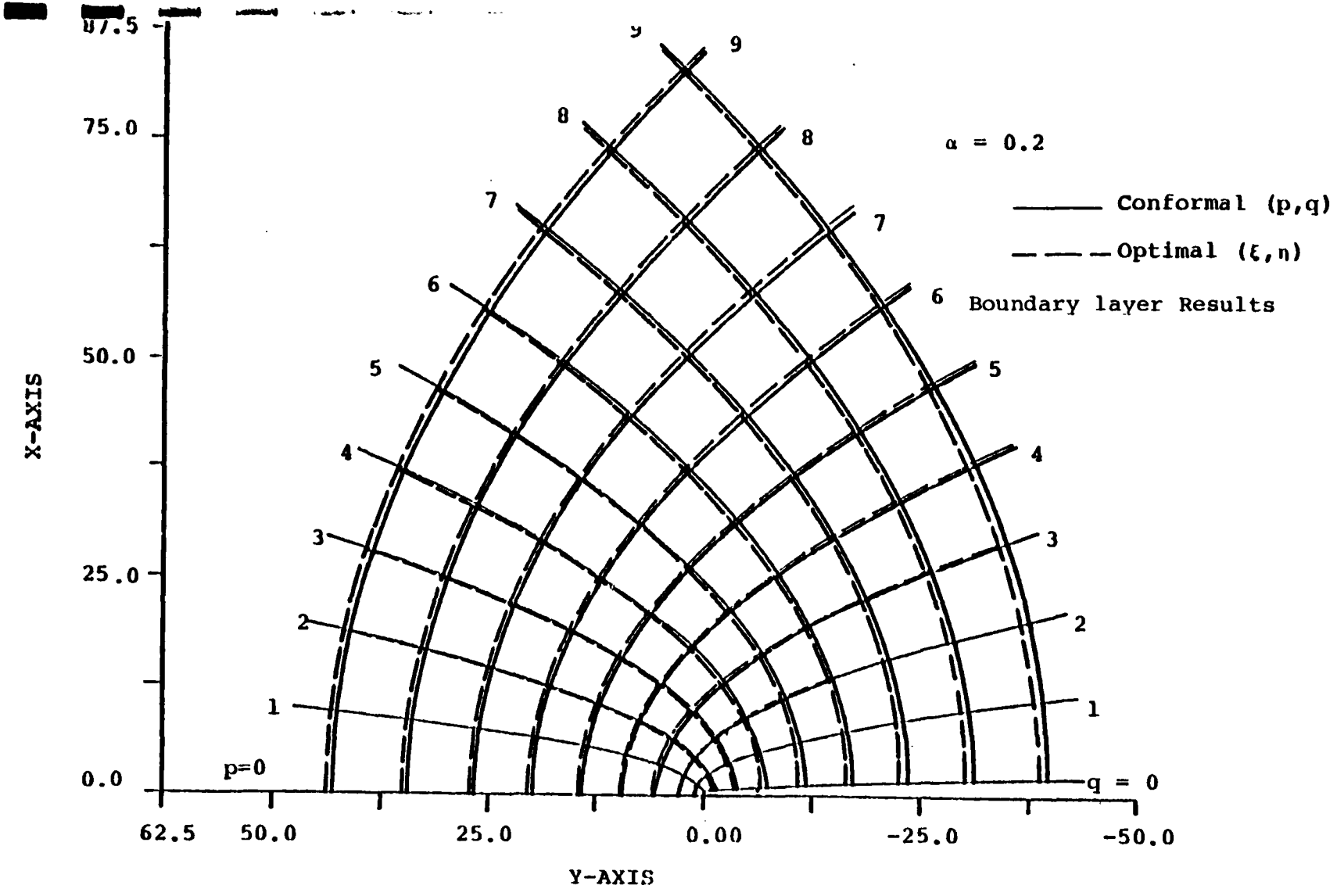

FIG. 20b. CONFORMAL AND OPTIMAL COORDINATES FOR BLUNTED PLATE

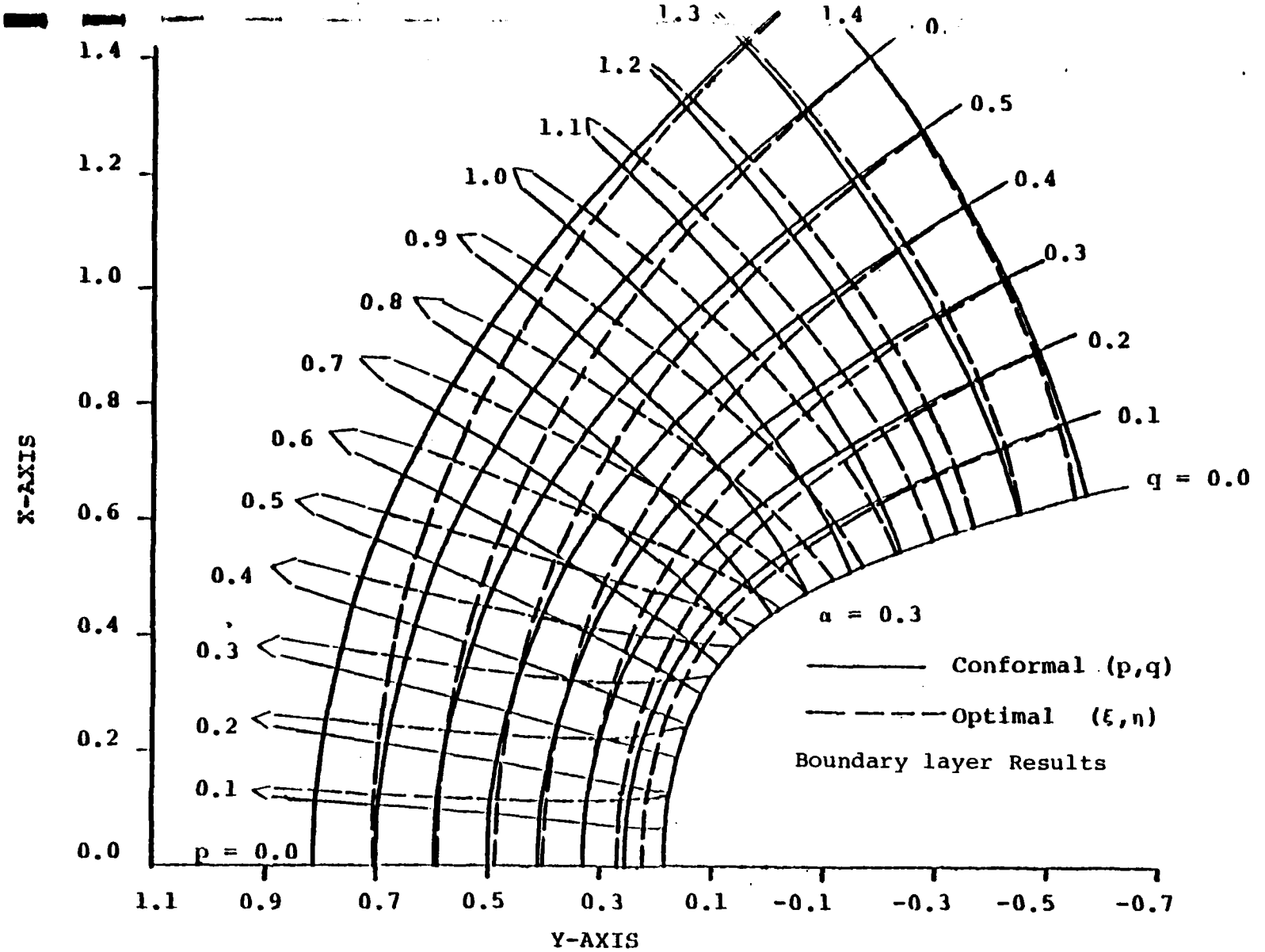

FIG. 21a. CONFORMAL AND OPTIMAL COORDINATES FOR BLUNTED PLATE

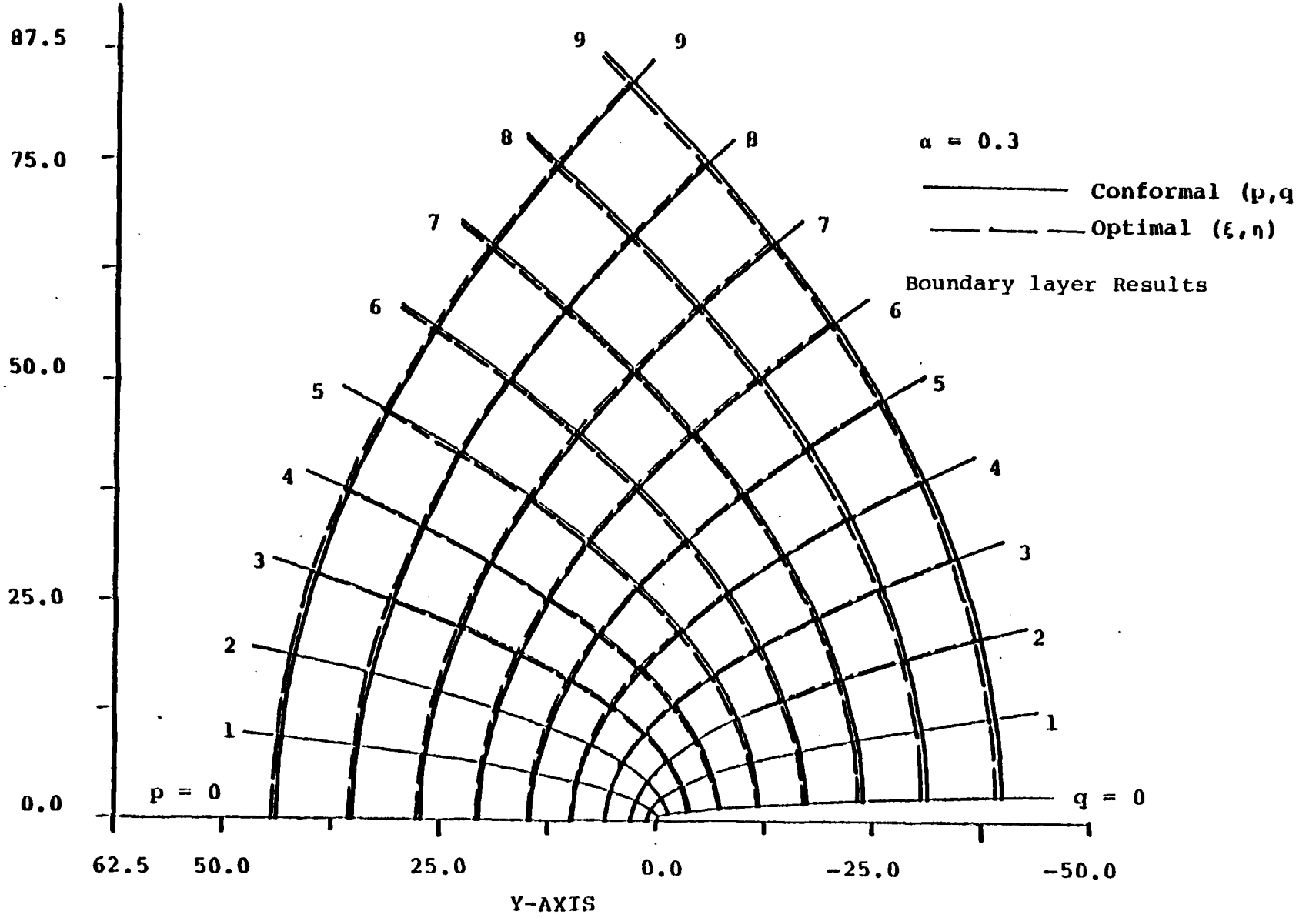

FIG. 21b. CONFORMAL AND OPTIMAL COORDINATES FOR BLUNTED PLATE

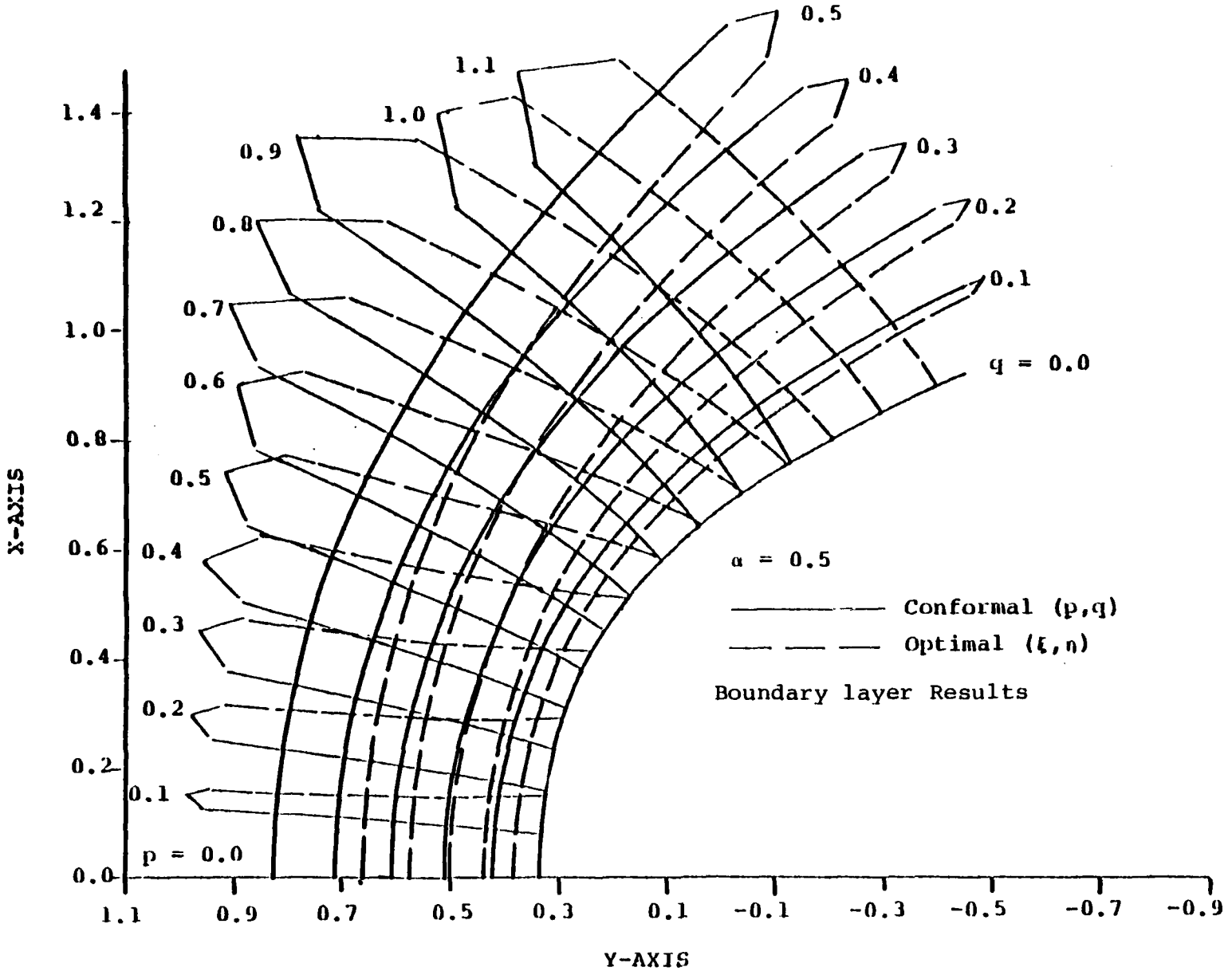

FIG. 22a. CONFORMAL AND OPTIMAL COORDINATES FOR BLUNTED PLATE

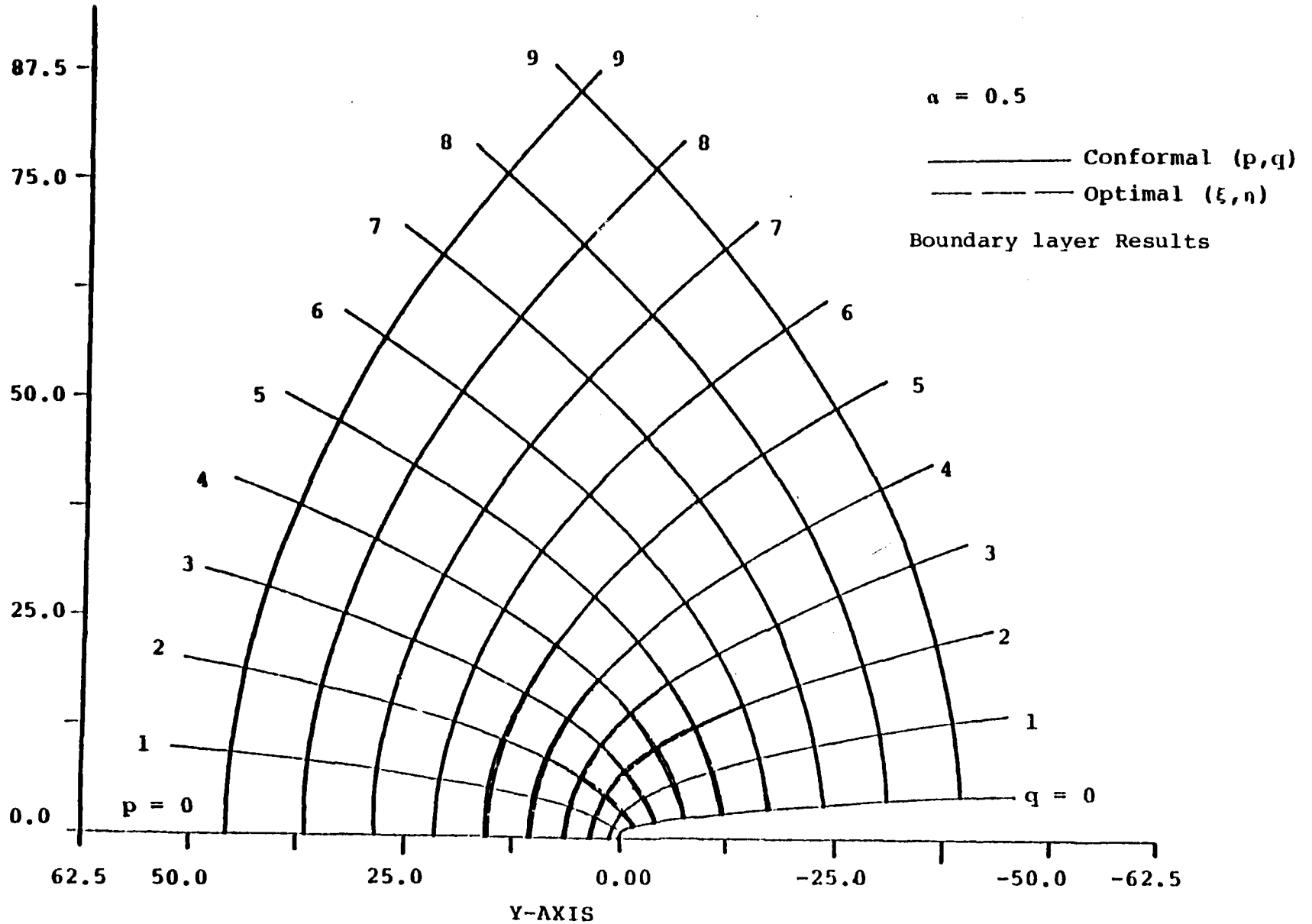

FIG. 22b. CONFORMAL AND OPTIMAL COORDINATES FOR BLUNTED PLATE

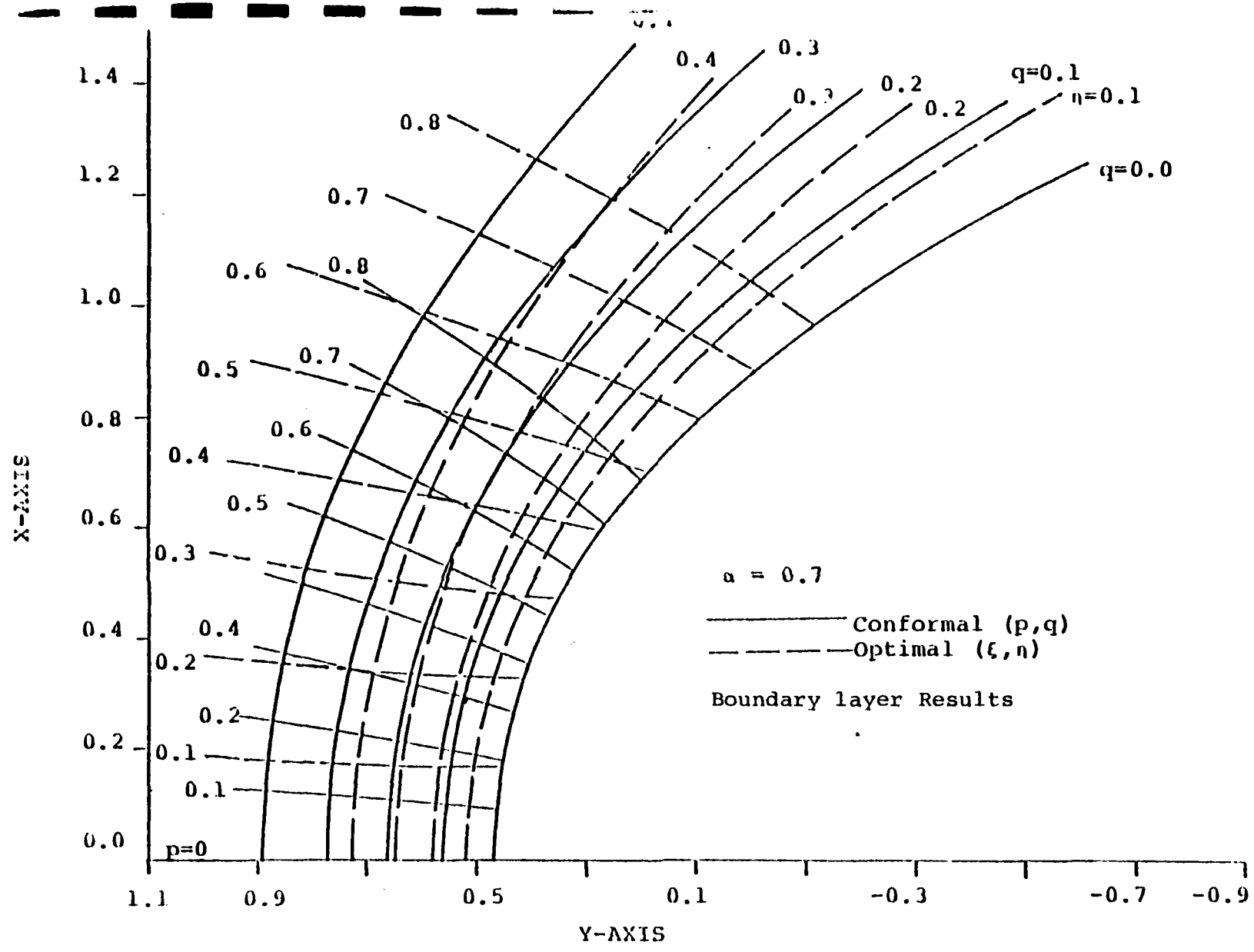

FIG. 23a. CONFORMAL AND OPTIMAL COORDINATES FOR BLUNTED PLATE

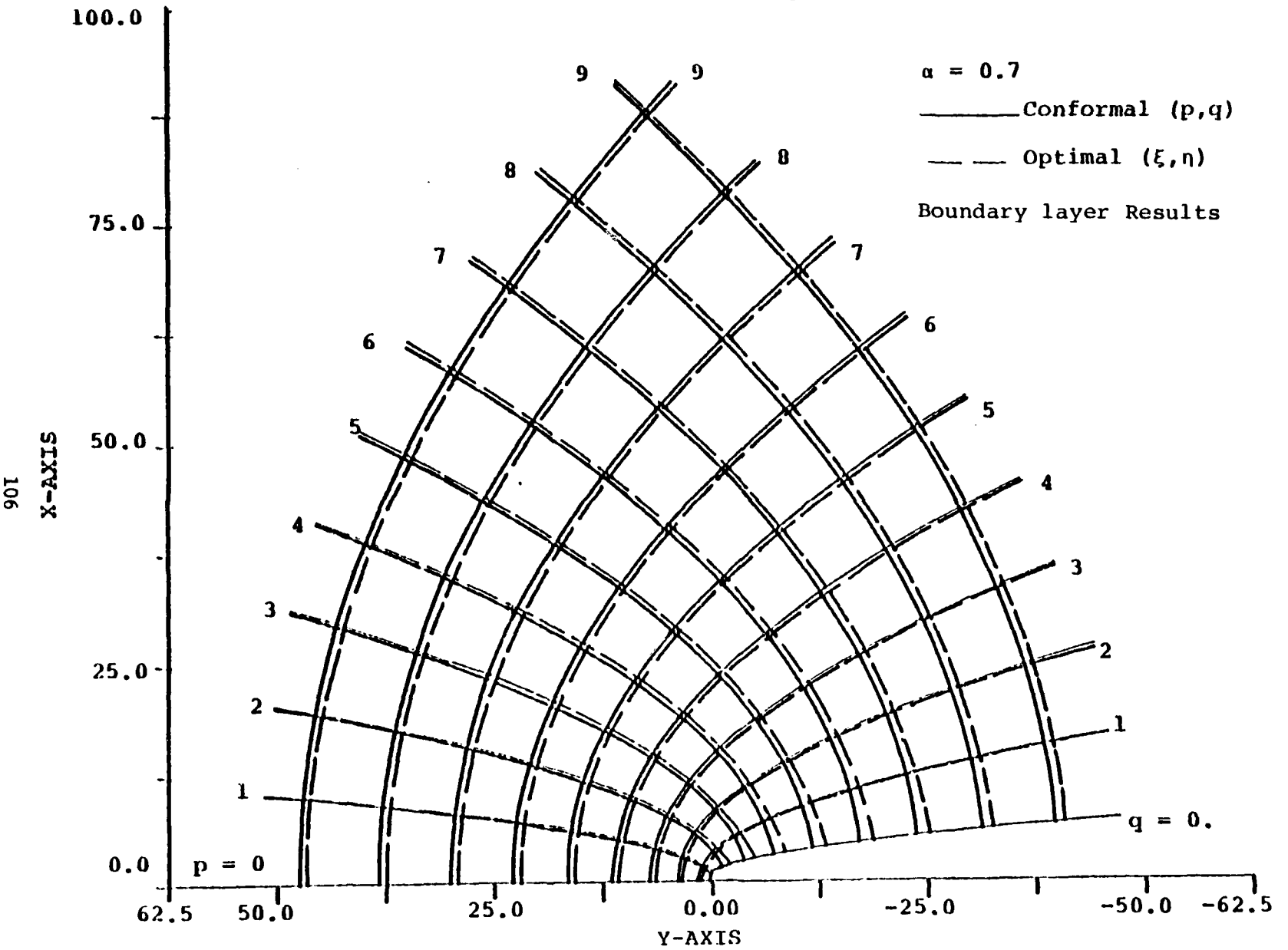

FIG. 23b. CONFORMAL AND OPTIMAL COORDINATES FOR BLUNTED PLATE

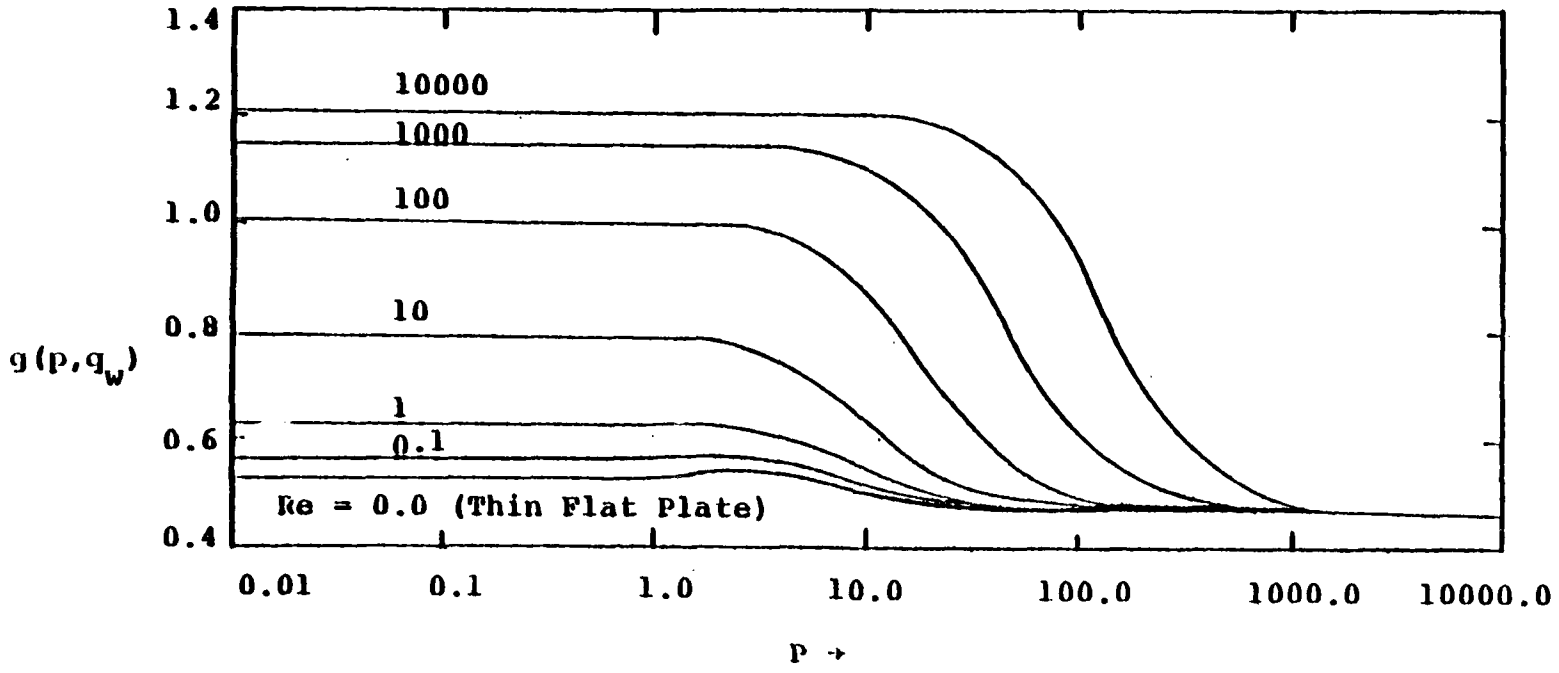

FIG. 24. SKIN FRICTION DISTRIBUTIONS FOR PARABOLIC CYLINDERS

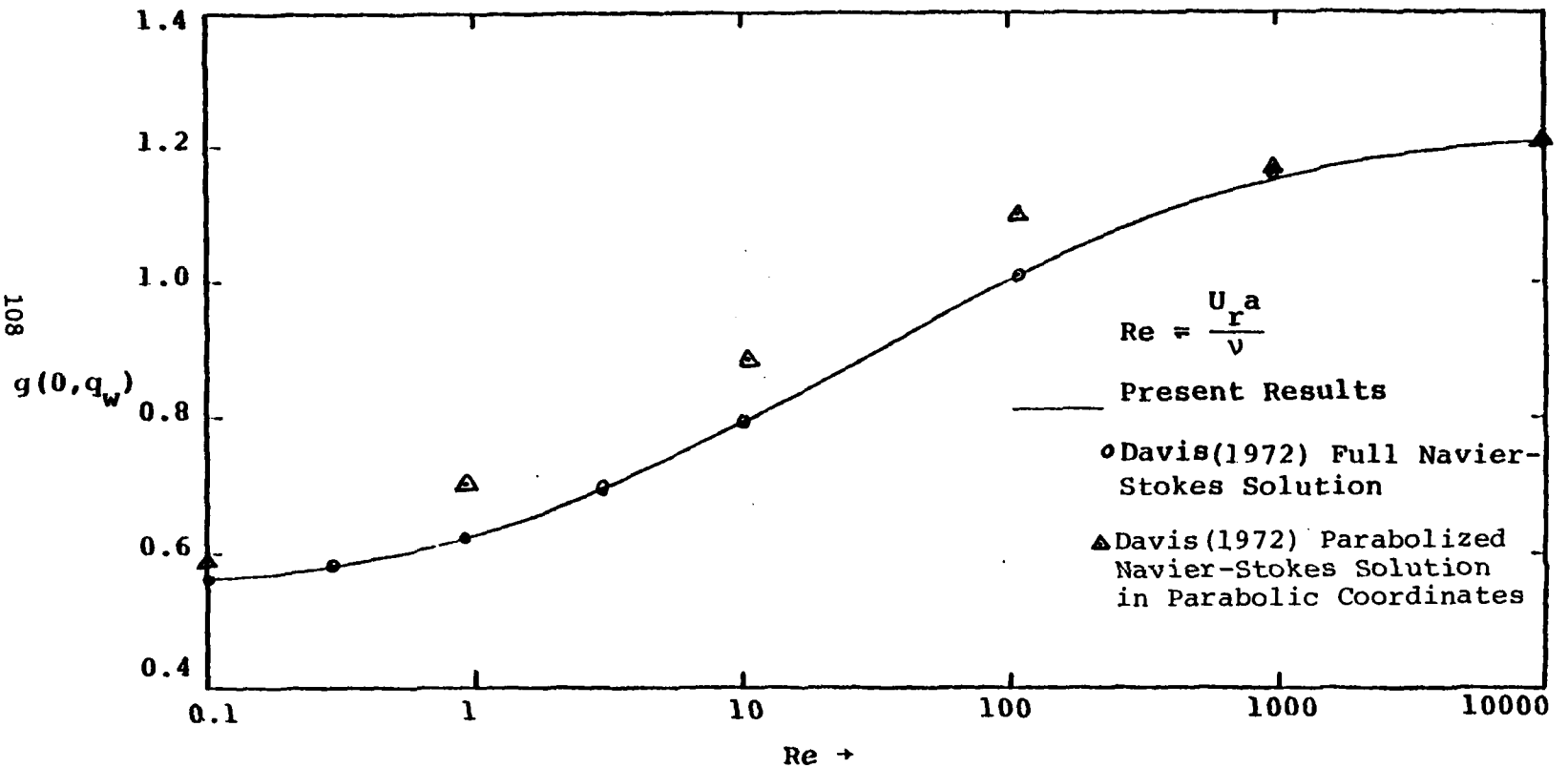

FIG. 25. SKIN FRICTION AT THE LEADING EDGE OF PARABOLIC CYLINDERS

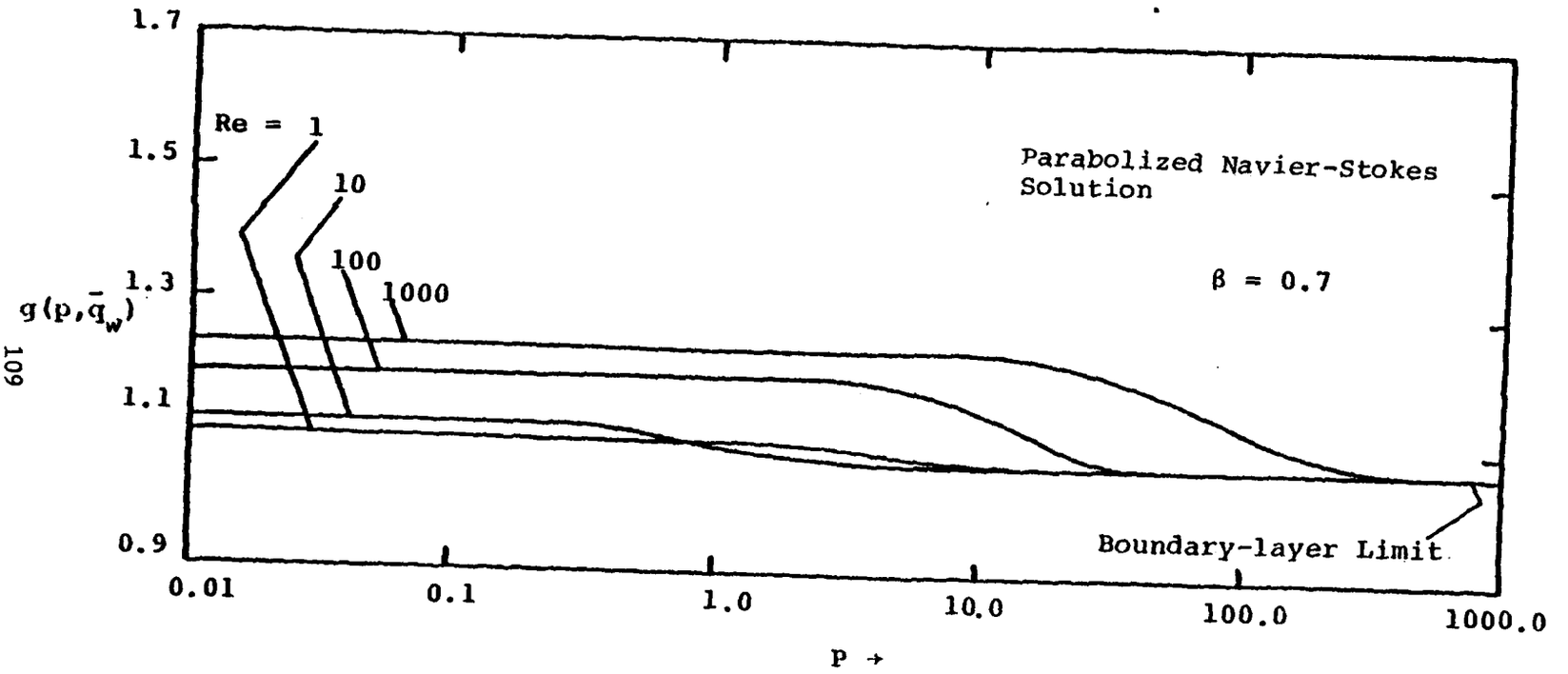

FIG. 26. SKIN FRICTION DISTRIBUTIONS FOR BLUNTED WEDGE

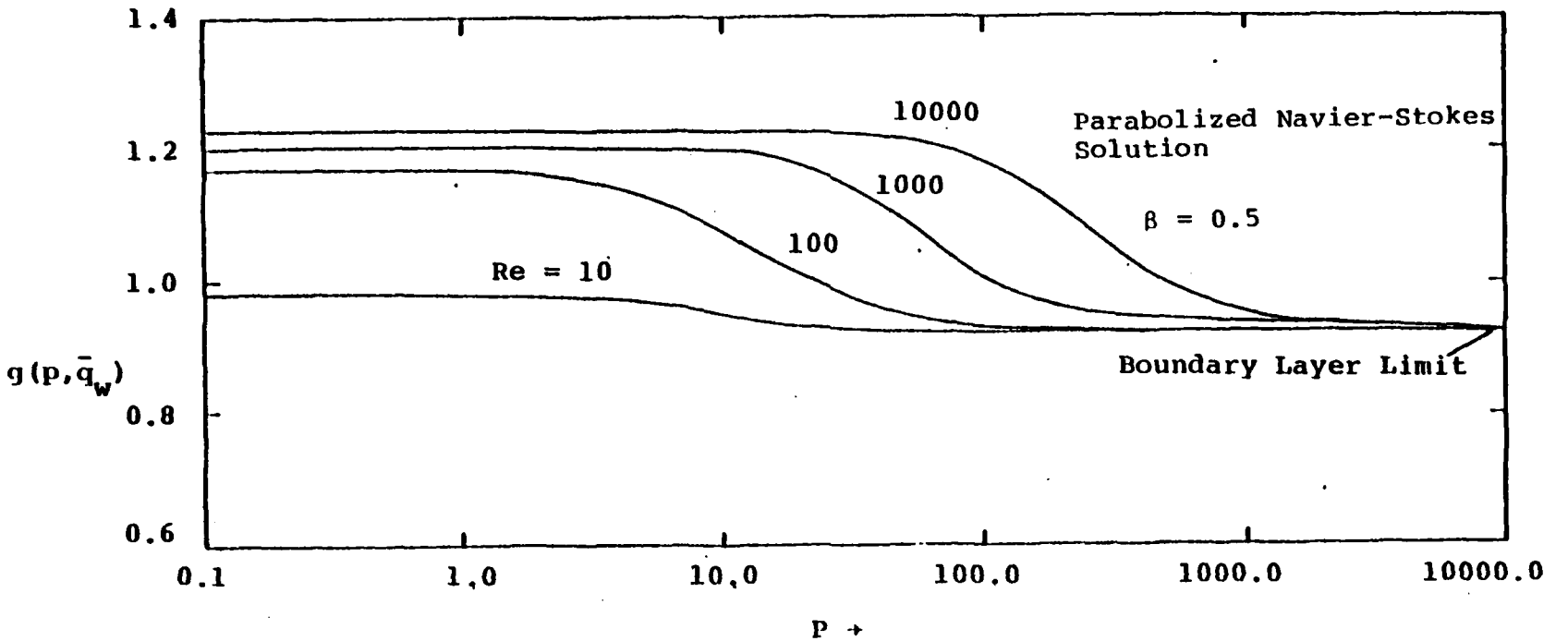

FIG. 27. SKIN FRICTION DISTRIBUTIONS FOR BLUNTED WEDGE

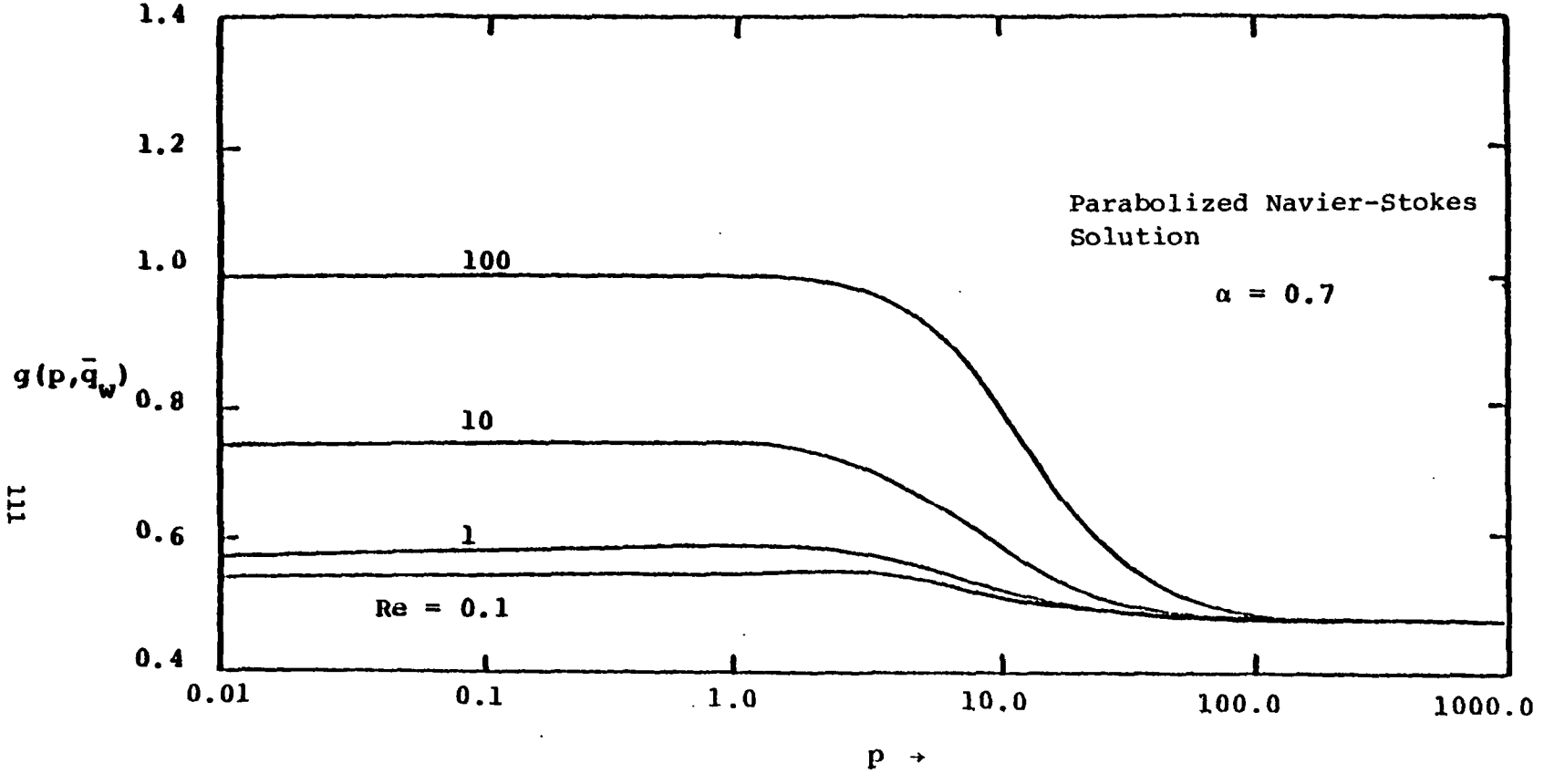

FIG. 28. SKIN FRICTION DISTRIBUTIONS FOR BLUNTED PLATE

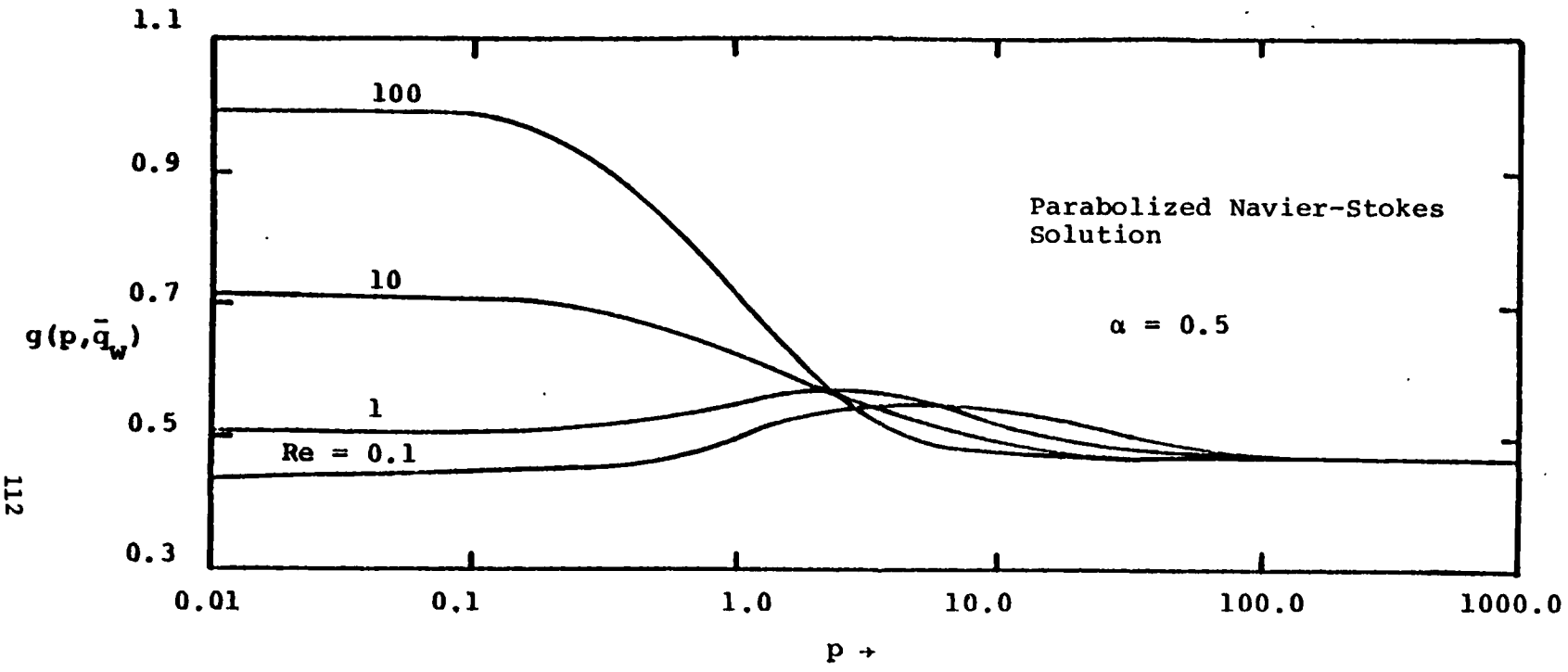

FIG. 29. SKIN FRICTION DISTRIBUTIONS FOR BLUNTED PLATE

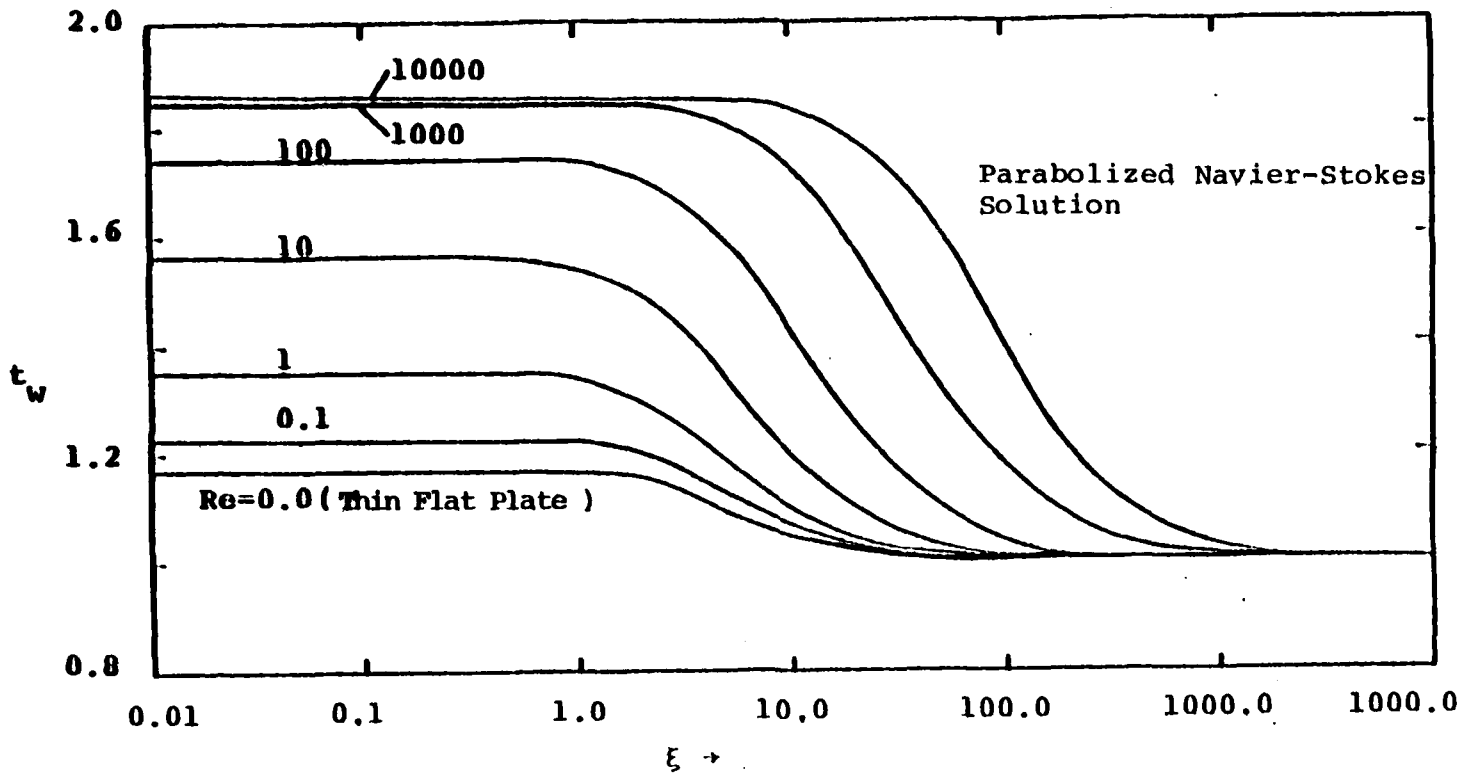

FIG. 30a. OPTIMAL COORDINATE FUNCTION DISTRIBUTIONS ON PARABOLIC CYLINDER SURFACE

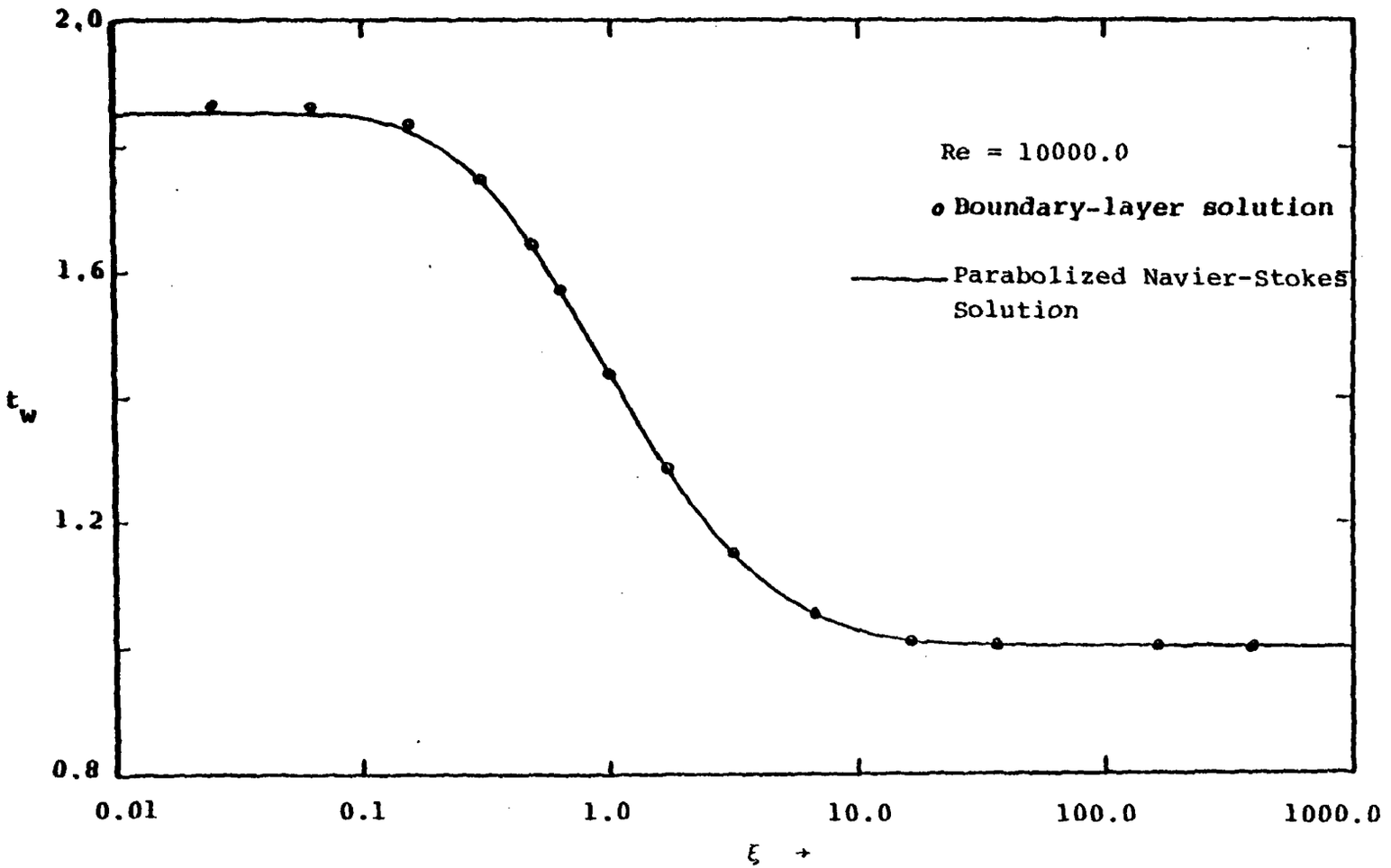

FIG. 30b. OPTIMAL COORDINATE FUNCTION DISTRIBUTION ON A PARABOLIC CYLINDER SURFACE

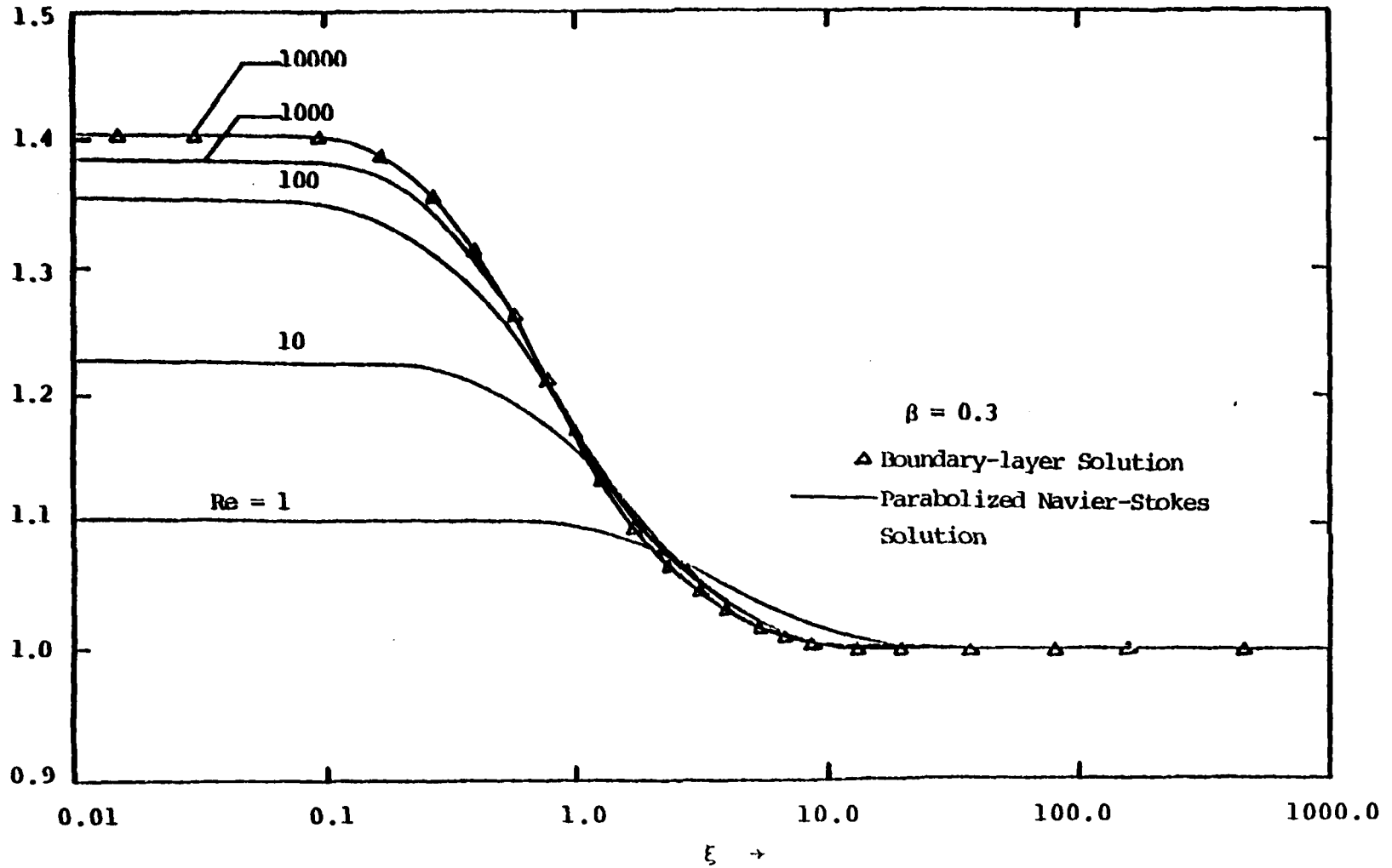

FIG. 31. OPTIMAL COORDINATE FUNCTION DISTRIBUTIONS ON BLUNTED WEDGE SURFACE

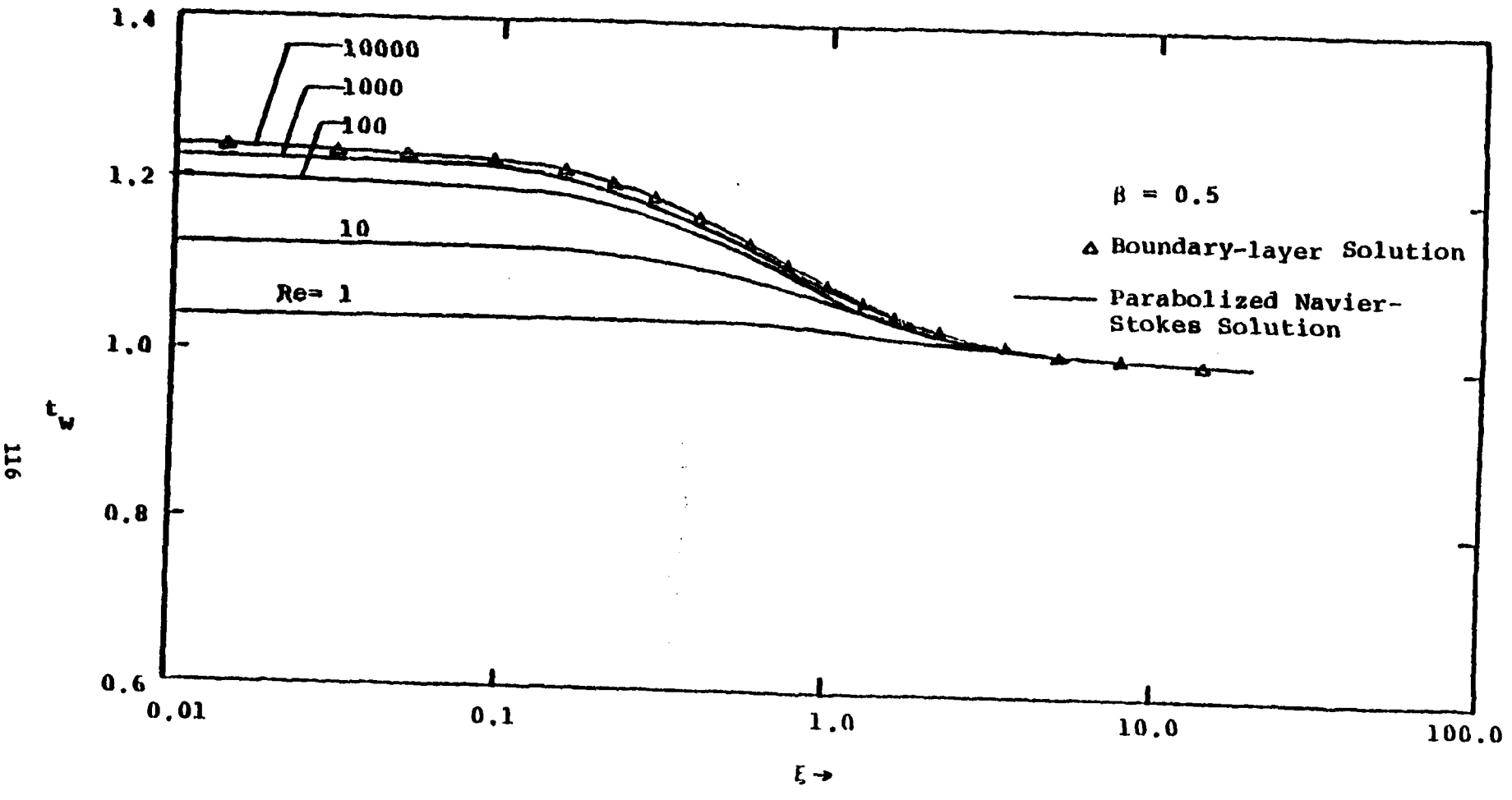

FIG. 32. OPTIMAL COORDINATE FUNCTION DISTRIBUTIONS ON BLUNTED WEDGE SURFACE

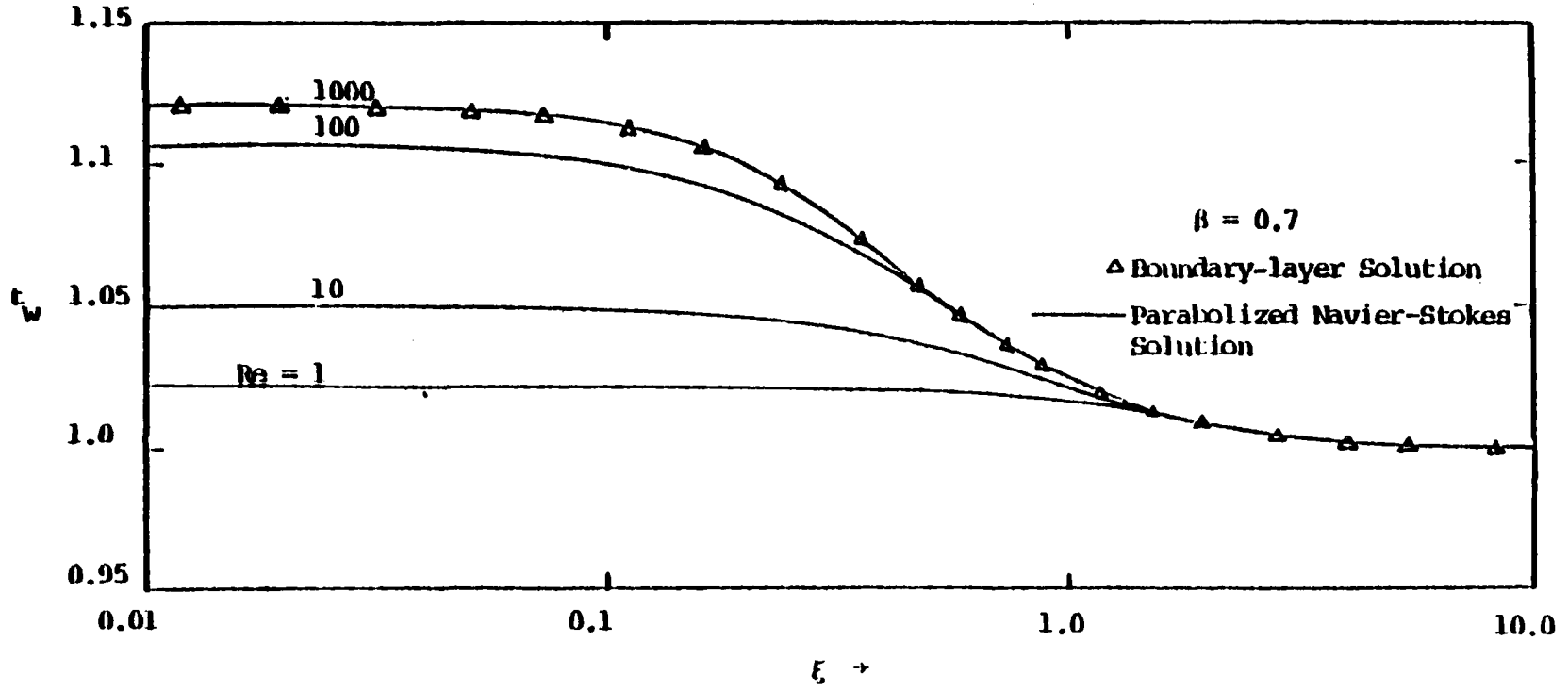

FIG. 33. OPTIMAL COORDINATE FUNCTION DISTRIBUTIONS ON BLUNTED WEDGE SURFACE

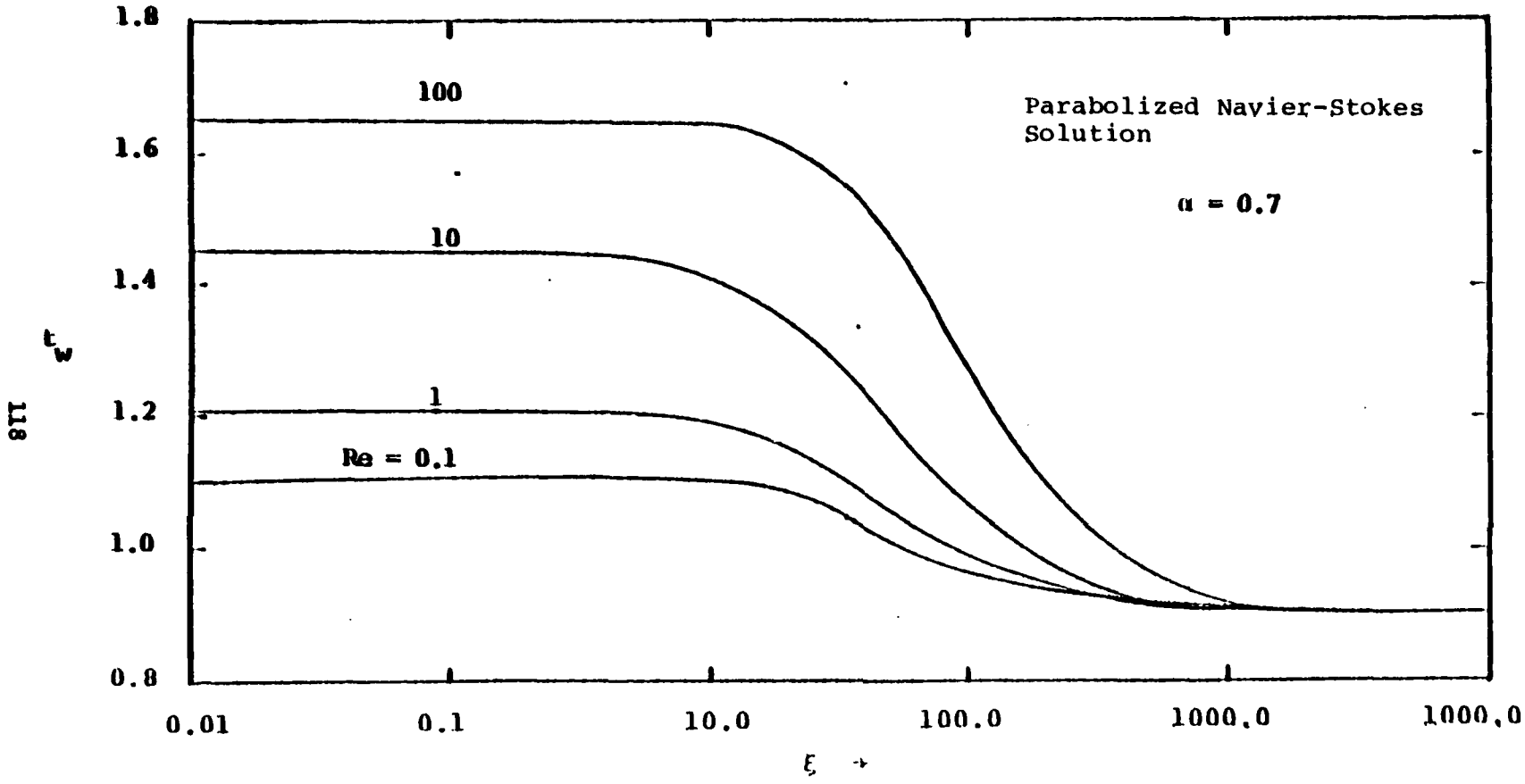

FIG. 34. OPTIMAL COORDINATE FUNCTION DISTRIBUTIONS ON BLUNTED PLATE SURFACE

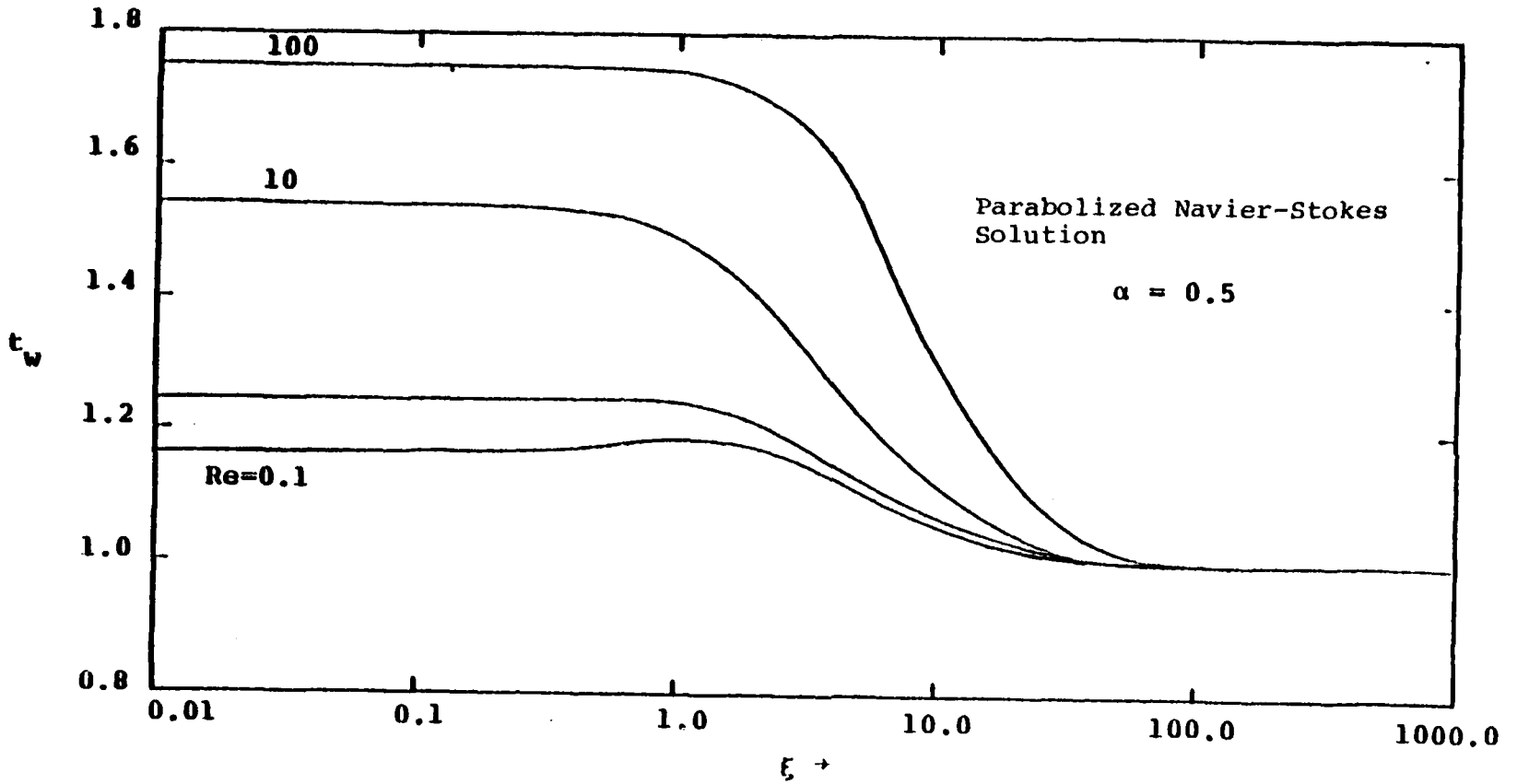

FIG 35. OPTIMAL COORDINATE FUNCTION DISTRIBUTIONS ON BLUNTED PLATE SURFACE

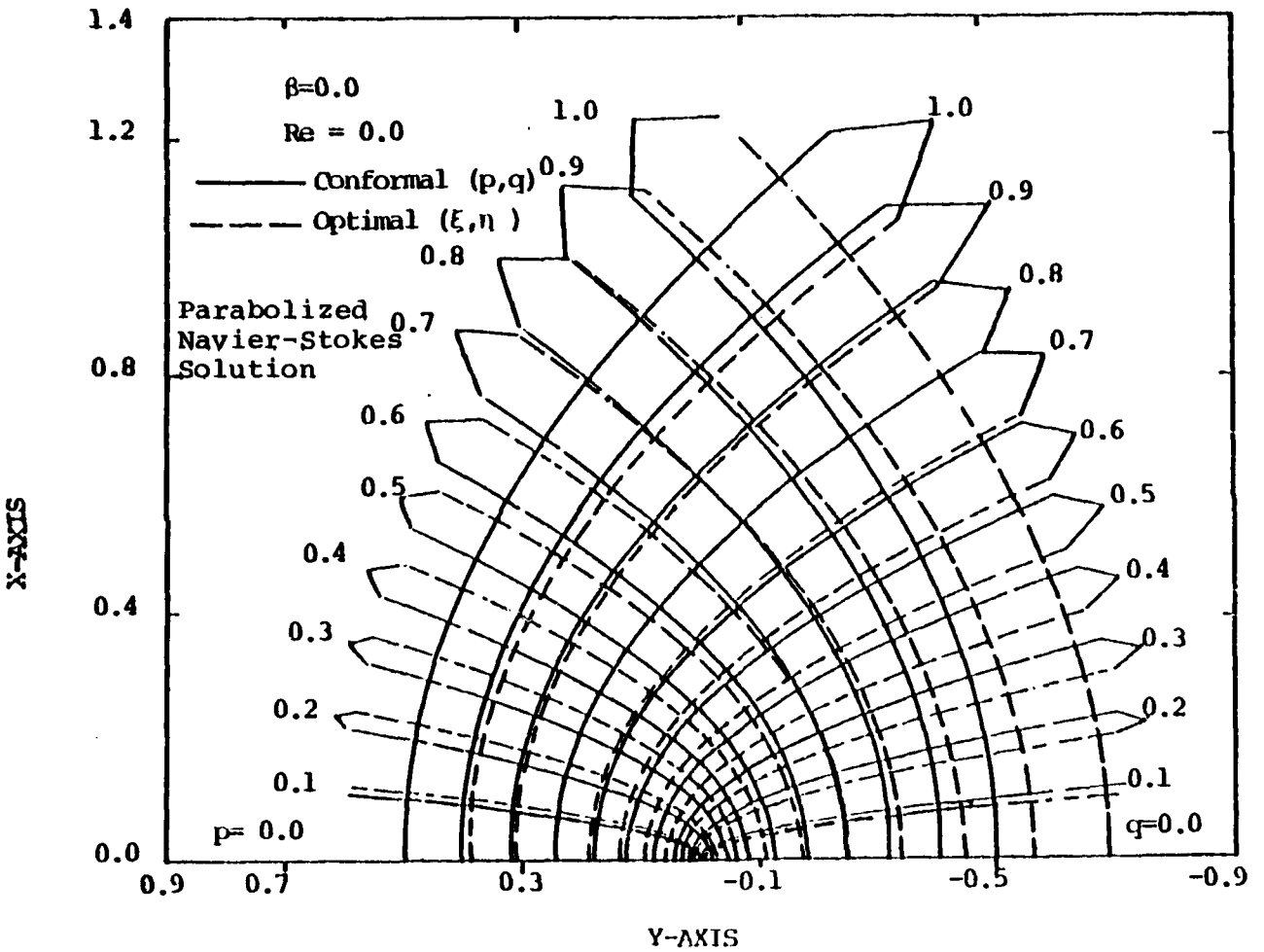

FIG. 36a. CONFORMAL AND OPTIMAL COORDINATES FOR SEMI-INFINITE THIN FLAT PLATE

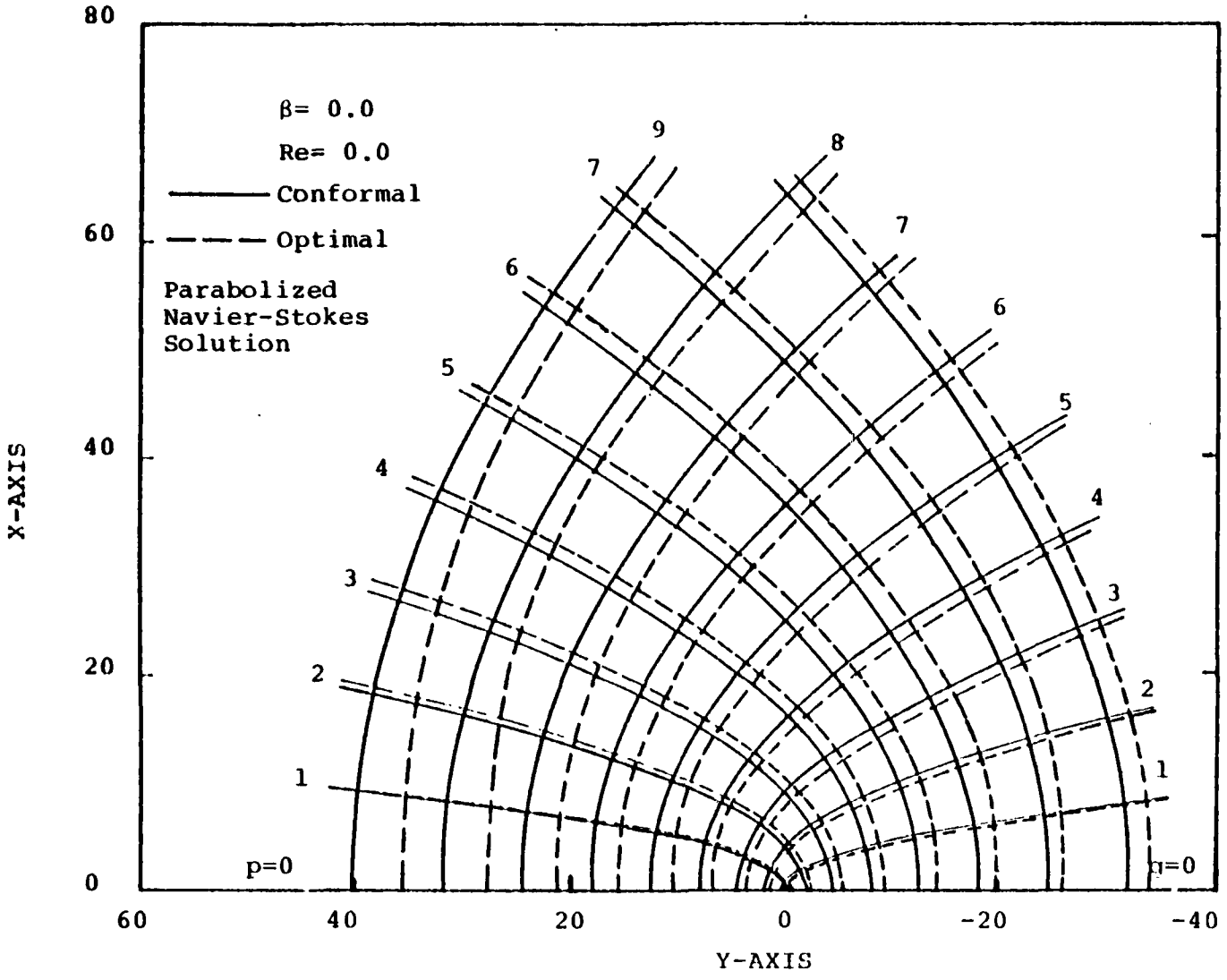

FIG. 36b. CONFORMAL AND OPTIMAL COORDINATES FOR SEMI-INFINITE THIN FLAT PLATE

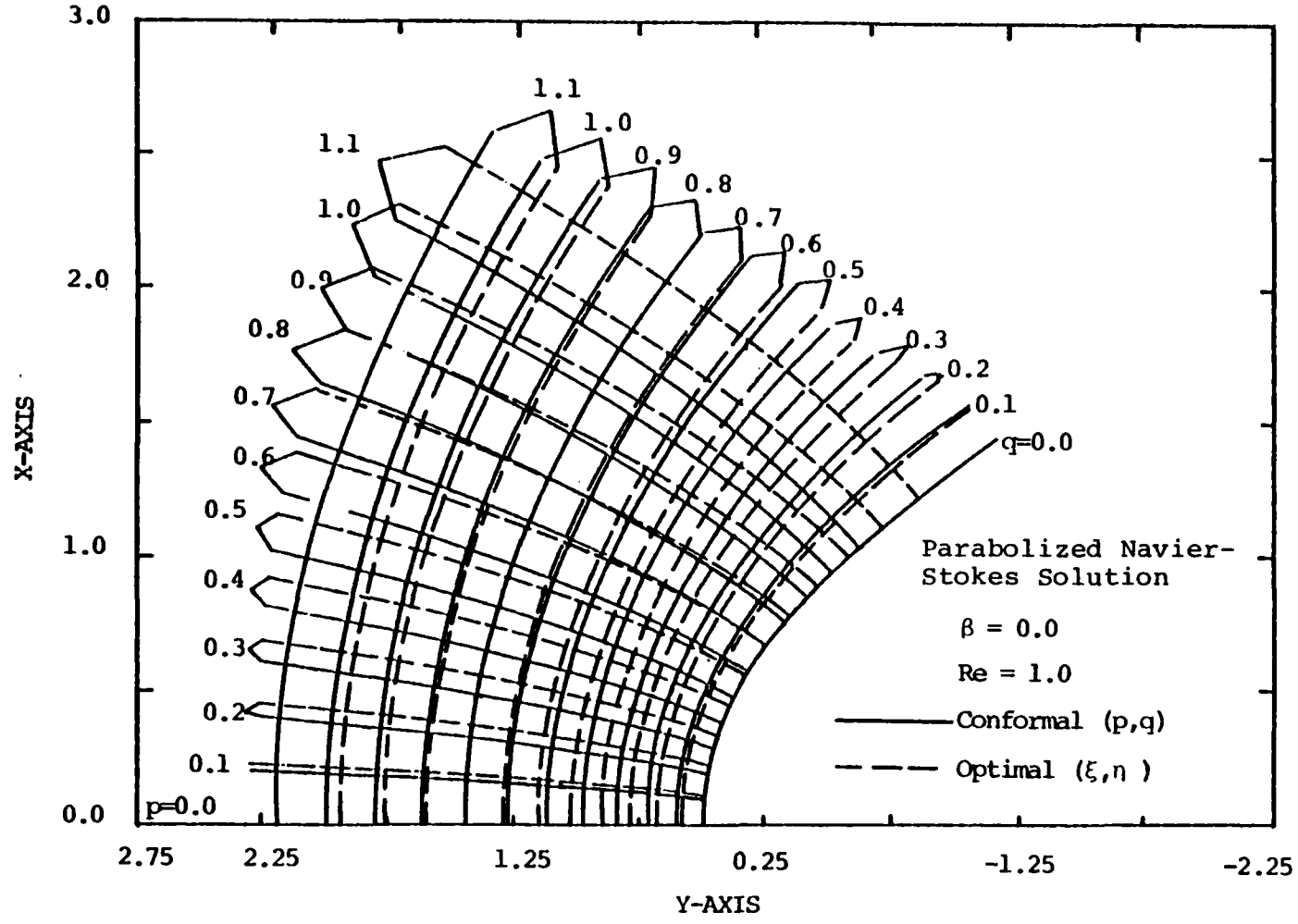

FIG. 37a. CONFORMAL AND OPTIMAL COORDINATES FOR A PARABOLA

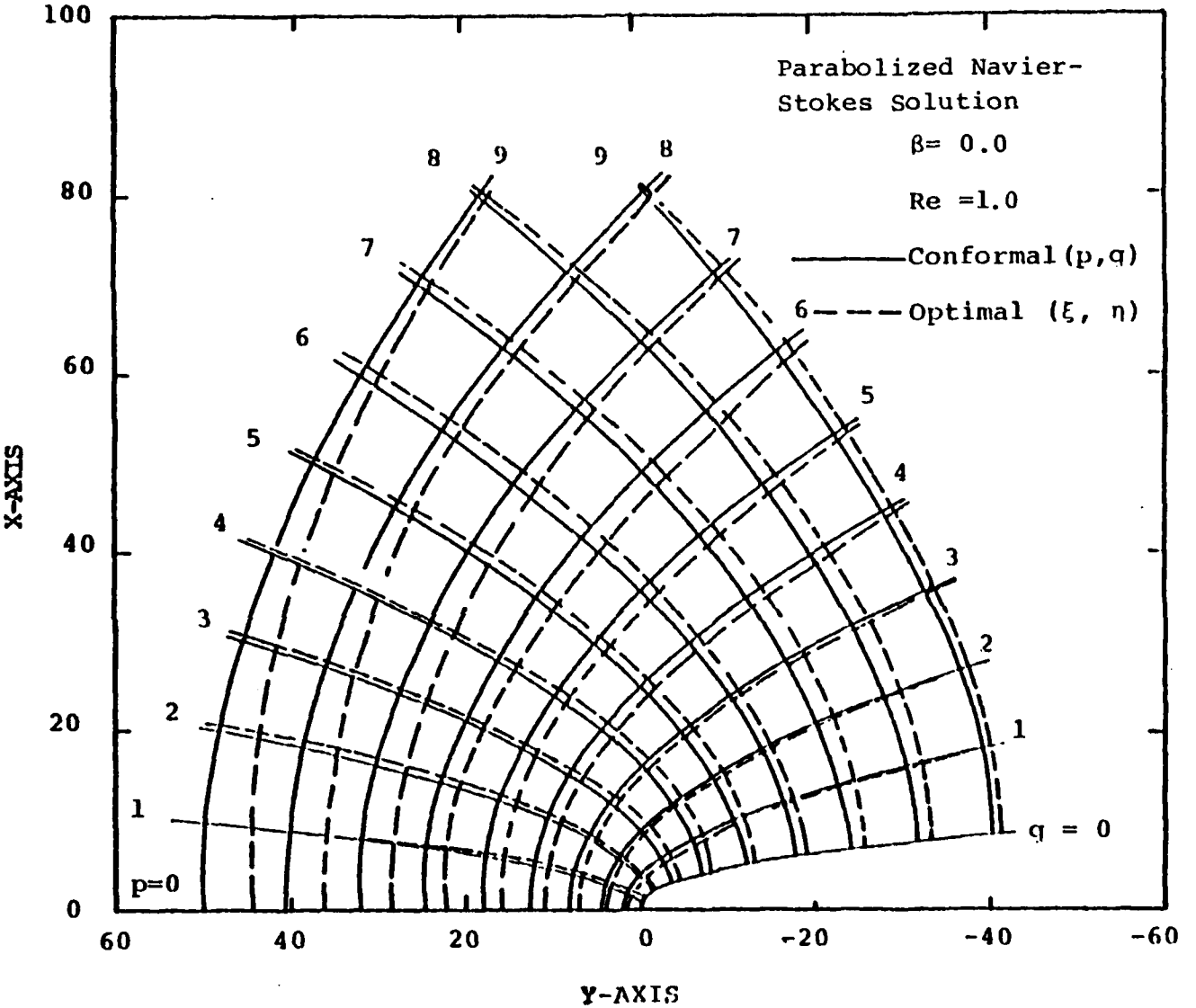

FIG. 37b. CONFORMAL AND OPTIMAL COORDINATES FOR A PARABOLA

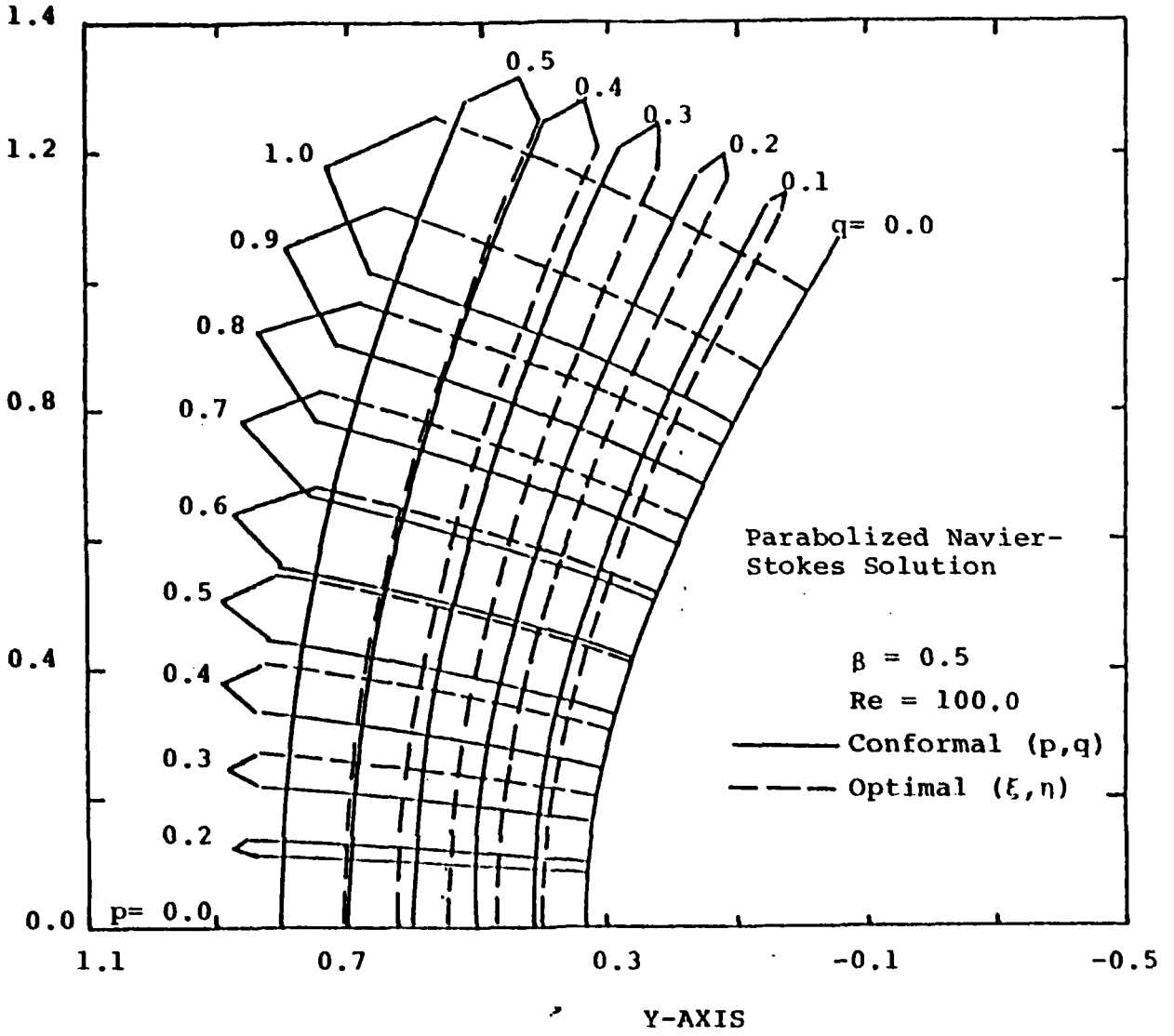

FIG. 38a. CONFORMAL AND OPTIMAL COORDINATES FOR BLUNTED WEDGE

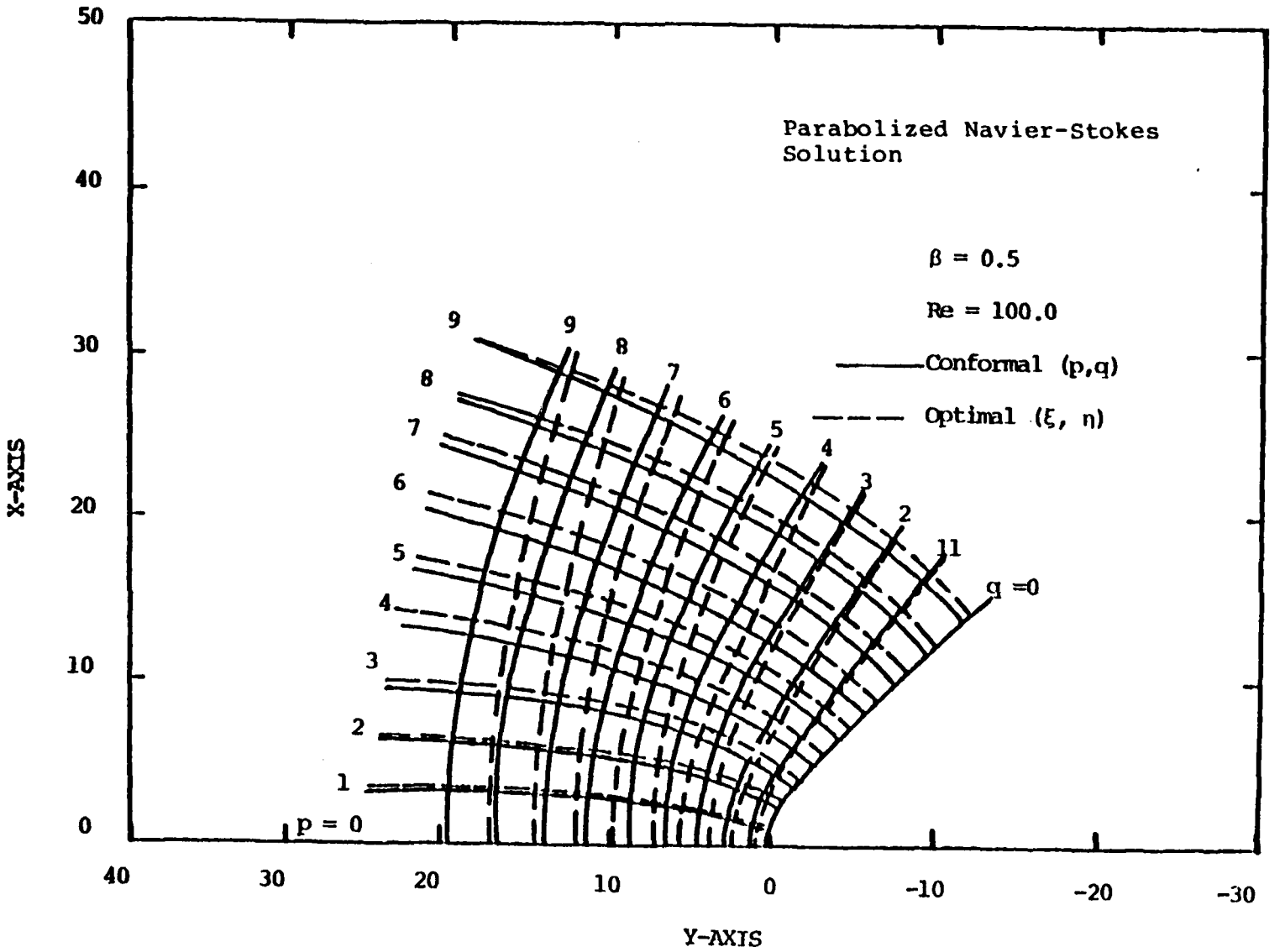

FIG. 38b. CONFORMAL AND OPTIMAL COORDINATES FOR BLUNTED WEDGE

Reynolds Number	Leading Edge Skin Friction $g(0, Re^{\frac{1}{2}})$	
Re	Present Results	Davis (1972) Full Navier-Stokes Results
0.0	0.529	0.533
0.1	0.562	0.563
0.3	0.583	0.586
1	0.628	0.629
3	0.694	0.694
10	0.793	0.793
30	0.899	0.899
100	1.009	1.009
300	1.083	1.089
1000	1.142	1.150
3000	1.182	1.186
10000	1.212	1.209

TABLE 1. COMPARISON WITH OTHER RESULTS.